NTNU
Norwegian University of Science and Technology
Department of Marine Technology

MASTER THESIS

Title:	Delivered:
Prediction of ice loads and response for an Arctic SPAR	14.06.2011
	Availability: Restricted until 14.06.2016
Student: Fredrik Røssel Larsen	**Number of pages:** Report: 86 Total: 116

Abstract:

Moored floating facilities in the Arctic region can be exposed to ice loads that far exceed those of waves, wind and current. Based on previous experience it has been found that a well-working ice management system can reduce the down time of the facility. The vessel should be able to reposition itself due to a change in ice drift direction, and also have the ability to disconnect riser and mooring systems in the event of extreme ice features. A conical shaped facility with a radially symmetric mooring system obtains an omnidirectional capability to resist ice actions.

Vertical structures experience much higher ice actions than sloping ones as the flexural strength of ice is less than the compressive strength. Vertical structures fail the ice by crushing whereas sloping structures fail the ice by bending and would be the preferred choice in waters with drift ice.

From model tests it has been found that both an increase in ice thickness and an increase in ice drift speed will increase the ice actions on a structure. An increase in ice thickness will increase the loads the most.

A numerical calculation model for estimating ice actions on a downward sloping structure based on Croasdale`s method have been compared to model test results. By implementing the actually achieved ice properties, breaking lengths and rubble geometries in the numerical model, correction factors were found from this comparison. The correction factors were implemented in the Matlab script, and ice actions were calculated for four interaction cases with both the corrected and the original script. From the deviations between the original and the corrected script, it was concluded that the numerical model might prove a valuable tool in an early design phase to obtain rough ice action estimates, but model tests should be performed to obtain the most accurate results.

Keyword:	Advisors:
Experience from operations in Arctic regions	Professor Jørgen Amdahl
Numerical ice action calculations	Professor Sveinung Løset
Model test analyse of ice actions	

Address:
NTNU
Department of Marine Technology
N-7491 Trondheim

Location
Marinteknisk Senter
O. Nielsens vei 10

Tel. +47 73 595501
Fax +47 73 595697

Problem text

MASTER THESIS 2011

for

Stud. Techn. Fredrik R. Larsen/Heidi Fjellvang

Prediction of ice loads and response for an Arctic SPAR

Beregning av islaster og respons for en arktisk SPAR

Field developments in the Arctic require specially designed offshore structures to facilitate drilling and production. In geographical areas where the occurrence of drifting ice coexists with a large water depth at the field's location, a robust floating structure, which can cope with both open water and ice loading, must be developed. This calls for research and development on different existing offshore structure concepts. This study will focus on the applicability of an Arctic SPAR in the above mentioned conditions.

The design load and requirements to motions of structures located in waters with drift ice conditions will often be governed by the local ice conditions. The determination of the global ice load and responses of the structure is a complex process which often includes many assumptions and uncertainties in the methods applied. Depending on the applied method and person performing the evaluations, different results will be obtained, often with large deviation between estimates.

As the ice conditions for structures located in Arctic regions most likely will govern the design conditions it is extremely important to be able to estimate the design load induced by these conditions in order to develop a safe and cost efficient platform concept for the field development.

Presently there exist many methods to determine iceinduced response on a floater for different structure geometries proposed for areas with drift ice; Analytical load models, Ice basin model testing, numerical analysis tool using analytical models as input and use of previous full scale measurements performed (scaling).

The following topics should be addressed:

Phase I (Proposed sections of report below):

Two structure models (one for each student) shall be used as base case for the proposed activities below, see Figure I and Figure . It is assumed that the Phase II activities will take approximately 2 months.

1. Literature study - previously experience from using moored floating structures in Arctic waters (with drift ice present)
    - Experience from moored floating structures applied in Arctic waters
        - Students shall perform a literature study and identify previously used floating moored units and describe the experience from operation of it
2. Literature study - Ice properties
    - The students shall perform a literature study and describe the properties (physical and mechanical, and their variability depending on time of the year) of both first-year/multi-year level ice and ice ridges
3. ISO load algorithm (ISO 19906)
    - The ISO load methodology for structures with a sloping geometry in the waterline shall be subject for study and description in detail with respect to (for the model chosen by the student):
        - Numerical comparison of ice load on sloping structure and load on vertical structure using ISO 19906 – justification of using sloping structures
        - Description/discussion of each term of the algorithm (physics behind and trigonometry) and how and where the load resultant from the term will act on the structure
        - Discussion of simultaneously appearance of the terms in the algorithm
        - Based on above findings:
            1. Prepare a Matlab script to perform time-domain analysis of the ice-structure interaction for the following cases (for both models)

Table I Level Ice Test Matrix (other properties will be provided)

	Level ice thickness [m]	Velocity [m/s]
Test 1	1	0.5
Test 2	1	1
Test 3	1.5	0.5
Test 4	1.5	1

4. Ice model test analysis (model test data and reports will be provided by AKSO when task 1- 3 completed):

An ice model test with models described in Figure I and Figure II tested in ice conditions described in Table I will be subject for analysis. The following activities shall be performed.

- Students shall describe the model test set-up and ice preparation/measurement methods

- Students shall plot the model test results and compare results from testing with various thickness and velocity
    - Compare with respect to obtained ice properties, ice failure period
- Students shall perform analysis of the model test:
    - Describe geometry of ice rubble accumulation and ice transport for the tests
    - Identify and compare ice breaking/failure period for the tests
    - Describe and use statistical measures that may be used to describe the measured ice load for the tests

- Based on above activities
- Compare the developed Matlab script with the measured loads for all tests
    - Describe deviation between script and measurements for:
        1. Measured loads
        2. Observed ice rubble behaviour
        3. Measured ice properties
- Propose and discuss method for correction of Matlab script towards the measured results
- Correct the Matlab script for observations and measured ice properties and compare results

Phase II:

- Analysis of ice ridge test

- Analysis of model test with moored set-up

Scope of Work (SoW) to be defined after phase I

(*Phase II activities were not commenced as Phase I proved very time consuming*)

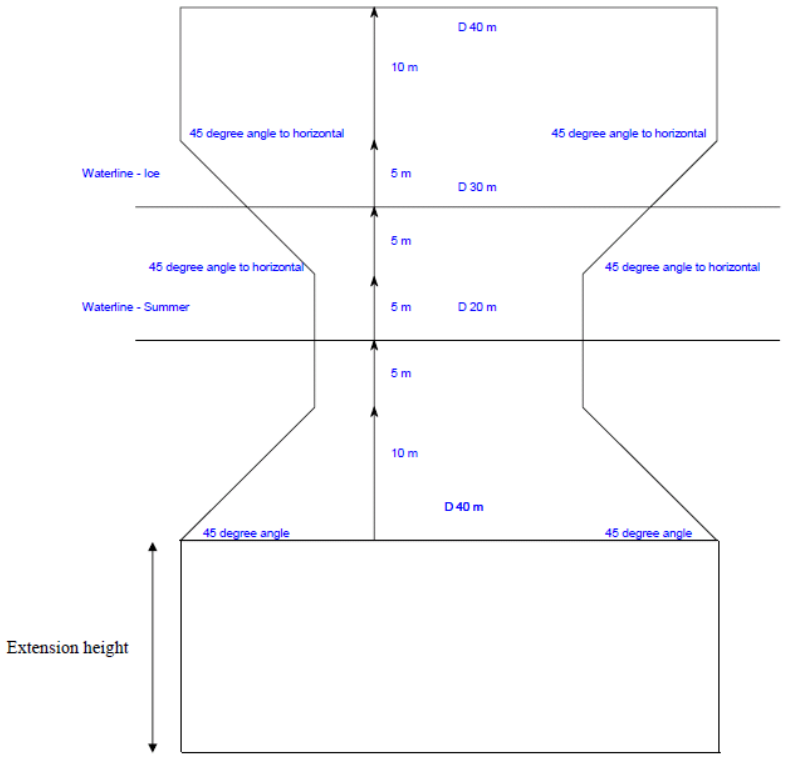

Figure I Model A

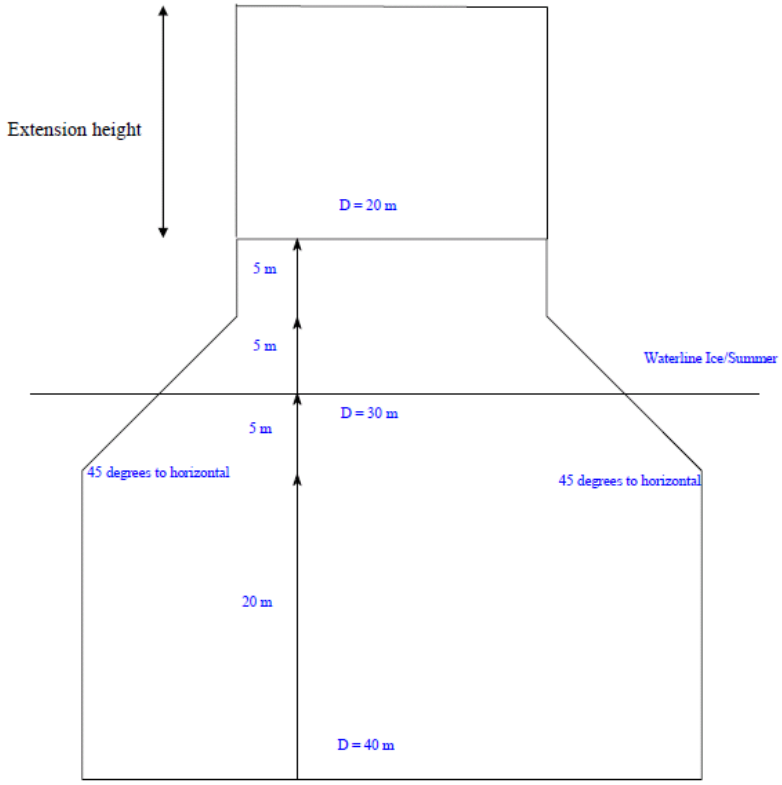

Figure II Model B

Preface

This report is the result of my Master Thesis during the last semester of my Master of Technology studies within Marine Technology. The thesis counts for 30.0 credits and has been completed during the first six months of 2011.

I would firstly like to thank my main supervisor Professor Jørgen Amdahl for very helpful guidance throughout the Master Thesis work. In addition I would like to thank my supervisor representing Aker Solutions, Per Kristian Bruun, who has given a very detailed and easy to understand scope of work and has proven very available and helpful with all problems that have occurred.

In addition, my gratitude goes to Aker Solutions ASA who has agreed to release model test data in accordance with this thesis. The model test data have given the opportunity to compare numerical calculations to real-life values, which has raised the level of this thesis substantially. This data has also helped making the Master Thesis work a very interesting and learning experience.

It should be noted that this thesis is confidential for five years from the delivery date, ref. confidentiality agreement of 22nd of March, 2011.

Trondheim, June 14th, 2011

_____

Fredrik Røssel Larsen

Summary

Moored floating facilities deployed in Arctic regions faces the threat of ice intrusions that might induce loads exceeding those of waves, wind and current. As a result, the hull of the facility need to be ice strengthened locally (to resist local ice loads and global ice pressure) and the mooring lines need to be designed to withstand the predicted ice loads. A well working ice management system may reduce the down time of a facility and might consist of vessels for breaking of large ice features and towing away approaching icebergs.

The Terra Nova FPSO was deployed at the Terra Nova field in the Grand Banks region in 2002. The riser and mooring systems were attached to a disconnectable turret, which gave the possibility to quickly move off location if extreme ice features occurred. The mooring line arrangement also gave the possibility to reposition the vessel due to change in ice drift direction. Both the riser and mooring system was protected from direct contact with ice. The Terra Nova FPSO was designed to withstand an impact with a 100 000 tonne iceberg [Lever, G. et.al. 2001] and according to [Wright, B. et.al. 2000] the mooring system could resist load levels in excess of 2000 tonnes. The Terra Nova FPSO`s ice management system consists of an ice tracking radar as well as a standby vessel for towing of icebergs.

In the Beaufort Sea, drilling operations commenced as early as 1976 with Canmar`s drilships. The mooring arrangement on these ships consisted of an eight point spread moored mooring system (four bow and four aft) which came off the deck and through the waterline. Due to this mooring arrangement, the ships were not able to reposition, but the mooring lines were equipped with remote anchor releases allowing the drillships to quickly disconnect and move off location if needed. The drillships were supported with two or more ice breakers for ice management which gave the ability for the drillships to stationkeep in difficult ice conditions. The drillships themselves were able to withstand global ice loads of about 100 tonnes.

In 1983 a conical shaped drilling unit named the Kulluk entered the Beaufort Sea with a purpose of extending the drilling season compared to Canmar`s drillships. Due to the conical shape in the waterline and radially symmetric mooring system it obtained an omnidirectional capability to resist ice actions. The mooring lines were designed to tolerate global loads of 750 tonnes in a drilling mode with maximum individual line tension of 260 tonnes (50% of their 520 tonne breaking strength). In a survival mode they were designed to tolerate global loads of 1000 tonnes with the risers disconnected, which gave a line tension of 75% of their breaking strength. Ice and performance monitoring programs were used to provide real time support for Kulluk stationkeeping, which gave an extensive data base consisting of mooring loads in different ice conditions and the effectiveness of ice management. [Wright, B. et.al. 2000] have collected and displayed the main results from this data base, and found that the loads on the vessel were substantially decreased when ice management was used. The global loads were found to decrease from about 450 tonnes to 100 tonnes for 2.0m pack ice in an unmanaged and managed scenario respectively.

[ISO 199906:2010] displays two methods for calculating level-ice actions on sloping structures, and one for vertical structures. The two different methods for sloping structures are Ralston`s method (based on plasticity theory) and Croasdale`s method (based on an elastic beam on an elastic

foundation). From static calculations of ice actions on a downward breaking structure, an upward breaking structure and a vertical structure it has been found that the vertical structure experiences loads that far exceed the sloping ones. On a vertical structure the main failure mode of ice is crushing, whereas bending of ice governs the failing against a sloping structure. Since the flexural strength of ice is much less than the compressive strength, sloping structures are preferred when ice is present. For an upward breaking structure the resultant load from ice actions points downward, whereas the resultant load point upwards for a downward breaking structure. The downward breaking structure experiences lower ice actions than the upward breaking structure and might seem the best option for a floating facility. In addition, the upward breaking structure might be submerged for high ice actions due to the direction of the resultant load. For a gravity based structure an upward breaking structure might be preferred as the resultant load points downwards into the ground and increases the stability. On a downward breaking structure the resultant load points upwards, which might reduce the stability by creating an overturning moment.

A numerical calculation model based on Croasdale`s method has been established in Matlab to calculate ice actions from an ice-structure interaction with a downward sloping structure in the time domain. The script produced is based on assumptions on how different load components will contribute and vary over time during an interaction process. When an ice sheet hits a sloping structure, it will be bent downwards and broken off from the oncoming sheet. A breaking load has been computed to occur with a period determined by the assumed breaking length of the ice and the ice drift velocity. After an ice block has been broken off, a new force component is needed to push the block down the slope of the structure until it reaches the vertical part of the submerged structure. This load component is assumed to contribute when the first block of ice is broken off, and increases over time as the block is pushed further down the slope. When the first block has reached the end of the sloping side, this component is assumed constant throughout the interaction process due to a continuous breaking of ice. When the first block of ice has reached the end of the sloping side it has to be turned to a vertical orientation by a new load component. This turning force obtains its maximum when the ice block first hit the vertical face, and decreases towards zero as the block is turned to vertical. The angle describing the orientation of the ice block is the time varying part of this load component. The process of turning ice blocks is assumed to repeat itself throughout the interaction process. After the first block of ice has been turned to vertical it is assumed to fall back onto the oncoming ice sheet and start to accumulate a volume of rubble in front of the structure. Three load components in Croasdale`s method is defined by the volume of rubble in front of the structure, and are assumed to start contributing when rubble starts to build up. These components will vary over time as the angle the rubble volume makes with the horizontal (θ) is assumed to be time dependent. When the rubble volume has reached a certain size determined by this angle, it is assumed constant due to rubble transportation around the structure. Because of this constant rubble volume, the load components determined by the rubble volume are assumed constant throughout the interaction scenario.

Four ice-structure interaction cases with the downward breaking structure were analyzed with the numerical calculation model with varying level ice thickness (h) and varying ice drift speed (v). The assumed rubble ride-down heights (h_r) and the assumed breaking lengths of the ice (l_c) were found from given formulas. The breaking period (T_B) was calculated from the assumed breaking lengths and the ice drift speed. These parameters as well as the average loads obtained are shown in Table II for the four interaction cases.

Table II Results from the Numerical Model for the different Interaction Cases with the Downward Breaking Structure

	v [m/s]	h [m]	h_r [m]	l_c [m]	T_B [s]	$F_{H,AVG}$ [MN]	$F_{V,AVG}$ [MN]	$F_{R,AVG}$ [MN]
Case 1	0.50	1.00	7.00	12.86	25.72	1.44	1.06	1.79
Case 2	1.00	1.00	7.00	12.86	12.86	1.44	1.07	1.80
Case 3	0.50	1.50	9.00	17.43	34.86	2.27	1.68	2.83
Case 4	1.00	1.50	9.00	17.43	17.43	2.29	1.69	2.84

The angle the rubble makes with the horizontal (θ) was assumed equal to 35 degrees for all the interaction cases. This value is given as the maximum angle the rubble volume can obtain in [ISO 199906:2010]. From the results it was found that the ice loads will increase for increased ice thickness. It is assumed that the average loads are of most interest from a numerical calculation model, as real life maximum and minimum loads might occur due to numerous factors not included in this script. The numerical model does not implement any speed effects, and gave no significant change in results when the ice drift speed was increased.

Four different model tests with the downward breaking structure were analyzed. The model tests correspond to the four interaction cases described above with regards to target ice thickness and ice drift speed. The model tests were performed by Aker Arctic over two days. The model was fixed to a towing carriage which towed the model through a stationary ice sheet. Loads on the model were measured through a six-component balance. The actually achieved physical and mechanical ice parameters (ice thickness h, flexural strength of ice σ_f, the modulus of elasticity E, and the density of ice ρ_i) were found to deviate from the target values for all cases. The target values and the actually achieved values are given for these parameters in Table III.

Table III Target and Actually Achieved Values for the Physical and Mechanical Ice Properties

	Target Values				Actual Values			
	h [m]	σ_f [kPa]	E [GPa]	ρ_i [kg/m^3]	h [m]	σ_f [kPa]	E [GPa]	ρ_i [kg/m^3]
Case 1	1.00	500.00	0.50	900.00	0.95	573.60	2.07	925.74
Case 2	1.00	500.00	0.50	900.00	0.97	726.30	2.07	925,74
Case 3	1.50	500.00	0.50	900.00	1.31	758.40	0.47	920.22
Case 4	1.50	500.00	0.50	900.00	1.42	680.10	0.47	920.22

Before the model tests were examined it was assumed that the loads would build up from the time when the model hit the ice due to rubble accumulation in front of the structure. The loads were assumed to reach a relatively constant value due to rubble transport around the structure. After the rubble had reached its constant volume, it was assumed to fail and build up again throughout the tests resulting in load maxima and minimums. From the analyze it was found that the loads did build up to a more or less constant value, but from the videos of the tests, no rubble failures and build ups were found. The average breaking lengths (br) of the ice as well as the average rubble geometry parameters (ride-down height h_r and the angle the rubble volume makes with the horizontal θ) were measured from the model test videos. These parameters and the calculated breaking period T_B is given together with the average load results in Table IV. The ice drift speed is also displayed.

Table IV Main Results from the Model Test Analyses

	v [m/s]	h_r [m]	θ [deg]	br [m]	T_B [s]	$F_{H,AVG}$ [MN]	$F_{V,AVG}$ [MN]	$F_{R,AVG}$ [MN]
Case 1	0.50	10.00	49.00	5.24	10.48	0.97	0.93	1.35
Case 2	1.00	13.00	57.00	3.34	3.34	1.44	0.77	1.64
Case 3	0.50	12.50	52.50	6.07	12.14	1.20	1.51	1.94
Case 4	1.00	13.75	63.50	4.38	4.38	1.93	1.24	2.31

Both an increase in ice thickness and ice drift speed gave higher resulting ice actions. As the vertical load components were reduced for increased ice drift speed due to more crushing of ice, the structure experienced a bigger increase in the resultant loads for increased ice thickness (Case 1 to Case 3 and Case 2 to Case 4) than for increased ice drift speed (Case 1 to Case 2 and Case 3 to Case 4). The horizontal load component increased the most when the ice drift speed was increased. From both Case 1 to Case 3 and from Case 2 to Case 4 (increased h, constant v at 0.5m/s and 1.0m/s respectively) the resultant load increased with approximately 40%. From both Case 1 to Case 2 and from Case 3 to Case 4 (increased v, constant h at 1.0m and 1.5m respectively) the resultant load increased with approximately 20%.

The developed numerical model was corrected by comparing the results obtained from calculations with those measured in the model tests. This correction was performed by first calculating ice actions for the four interaction cases with the actually achieved ice properties, the measured breaking lengths and the measured rubble geometry parameters. The measured θ values were greater than the sloping angle of the structure, which if implemented in Croasdale`s method will give a negative rubble volume and reduced loads. The measured rubble volume parameters implemented in the numerical calculations had to be transformed. This was done by setting the measured rubble angles equal to 35 degrees (as the assumed value) and calculate new ride-down heights. The assumed and measured values for the rubble geometry parameters and the breaking lengths are given in Table V. The transformed rubble geometry parameters are also given. The assumed breaking lengths are as before determined by the characteristic length l_c. The assumed breaking lengths in this part deviate from those given in Table II because l_c is a function of the modulus of elasticity E. The modulus of elasticity was set to 3GPa for the interaction cases displayed in Table II, whereas the target value of E was 0.50GPa in the model tests.

Table V Breaking Lengths and Rubble Geometry Parameters for the Model Tests

	Assumed Values			Measured Values			Transformed Values	
	h_r [m]	θ [deg]	br [m]	h_r [m]	θ [deg]	br [m]	h_r^* [m]	θ^* [deg]
Case 1	7.00	35.00	8.21	10.00	49.00	5.24	7.80	35.00
Case 2	7.00	35.00	8.21	13.00	57.00	3.34	8.77	35.00
Case 3	9.00	35.00	11.13	12.50	52.50	6.07	9.16	35.00
Case 4	9.00	35.00	11.13	13.75	63.50	4.38	8.12	35.00

By implementing the actually achieved ice properties as well as the breaking lengths and rubble geometry parameters measured from the videos the numerical calculation model should give the most accurate ice actions compared to the model test results. By comparing the calculated ice actions with the results measured in the model tests, correction factors for the horizontal and

vertical load components were found. The correction factors as well as the ice drift speed and the target ice thickness is given for each case in Table VI.

Table VI Correction Factors, Ice Drift Speed and Ice Thickness for all Interaction Cases

	Ice Properties		Correction Factors	
	v [m/s]	*h* [m]	$F_{H,AVG}$	$F_{V,AVG}$
Case 1	0.5	1.0	0.84	1.06
Case 2	1.0	1.0	1.04	0.59
Case 3	0.5	1.5	0.74	1.40
Case 4	1.0	1.5	1.25	0.71

From the correction factors it is found that the script overestimates the horizontal load component and underestimates the vertical load component when the ice drift speed is 0.5m/s. The numerical model underestimates the horizontal load components and overestimates the vertical load component when the ice drift speed is equal to 1.0m/s. It is also seen that the correction factors vary when the ice thickness is increased. From this, it can be concluded that the correction factors depends on both the ice drift speed and the ice thickness.

The correction factors were implemented in the numerical model, and ice actions were calculated for the target ice properties. The ice actions for the target ice properties were also calculated by using the original script. The main load statistics from both the original and the corrected script is given in Table VII together with the difference between the loads from the two calculations.

Table VII Ice Actions Calculated with both the Original and the Corrected Script

	Original Script [MN]			Corrected Script [MN]			Difference [%]		
	$F_{H,AVG}$	$F_{V,AVG}$	$F_{R,AVG}$	$F_{H,AVG}$	$F_{V,AVG}$	$F_{R,AVG}$	$F_{H,AVG}$	$F_{V,AVG}$	$F_{R,AVG}$
Case 1	1.17	1.06	1.58	1.11	1.06	1.53	-5.41	0.00	-3.27
Case 2	1.18	1.07	1.59	1.60	0.86	1.82	26.25	-24.42	12.64
Case 3	1.85	1.67	2.50	1.39	1.76	2.25	-33.09	5.11	-11.11
Case 4	1.87	1.69	2.52	2.13	1.36	2.53	12.21	-24.26	0.40

From the differences between the original and the corrected script, it is found that the original script is able to predict all ice actions within a deviation of approximately ±30% for all four cases. The original script might be used in an early design phase to give rough estimates of ice actions on different structures, but to obtain the most accurate results, model testing has to be performed. The original script might be used to cut down on the number of model tests needed which saves both time and money.

Contents

List of Figures

List of Tables

Nomenclature

An attempt has been made to explain all symbols when they first appear. Here is a list explaining the most important symbols and abbreviations.

Latin Symbols

A_N	Nominal contact area
c	Cohesion of rubble
C_R	Ice strength coefficient
D	Waterline diameter or width of construction
D_T	Diameter at end of sloping surface
e	Porosity of ice
E	Modulus of elasticity
E_1	Complete elliptical integral of first kind
E_2	Complete elliptical integral of second kind
F_G	Global ice action normal to a surface
F_H	Total horizontal load component
F_R	Resultant load component
F_V	Total vertical load component
g	Acceleration due to gravity
h	Ice thickness
h_r	Rubble ride-up/down height
H_B	Force needed to fail the ice sheet by flexure bending
H_L	Force needed to lift and shear the ice rubble on top of a sloping surface
H_P	Force needed to push ice sheet through rubble on top of the ice sheet
H_R	Force needed to push ice blocks from ice sheet failure through the rubble
H_T	Force needed to turn ice blocks due to interaction with the neck of the structure
l_c	Characteristic length an ice beam
M_0	Bending moment capacity

N	Normal load component
p_G	Global ice pressure
v	Velocity
w_C	total length of the circumferential crack
Y	Yield parameter

Greek Symbols

α	Sloping angle of inclination from horizontal
β	Characteristic length of an ice beam
δ	Deflection
θ	Angle rubble volume makes with the horizontal (angle of repose)
θ_{att}	Angle of attack of the resultant force
λ	Scaling factor
μ	Ice-structure friction coefficient
μ_i	Ice-to-ice friction coefficient
ν	Poisson`s ratio
ρ_i	Density of ice
ρ_w	Density of sea water
σ_c	Compressive strength of ice
σ_f	Flexural strength of ice
ϕ	Friction angle of rubble

Abbreviations

2-D	Two Dimensional
3-D	Three Dimensional
DP	Dynamic Positioning
FGX	Type of model ice, *F*=fine, *G*=grained, *X*=containing fresh water layers
FPSO	Floating Production Storage and Offloading vessel
FPU	Floating Production Unit

FY	First-Year
GBS	Gravity Based Structure
hpz	High Pressure Zone
MARC	Masa-Yards Arctic Research Centre
MY	Multi-Year
PSD	Power Spectral Density
TAPMS	Thruster Assisted Position Mooring System
ULS	Ultimate Limit Strength
YRP	Year Return Period

1 Introduction

As the known and currently producing oil and gas reservoirs are emptying out throughout the world, new technology can push barriers to extract hydrocarbons in deeper waters and more harsh conditions. The Arctic region is an area of great interest due to its already found oil and gas reservoirs, and the potential reservoirs hiding beneath the seabed of the ice covered waters. Oil and gas development and exploration in Arctic regions call for development of offshore structures that can operate efficiently in such conditions. Some of these regions experience seas free of ice during the summer months and intrusion of drift ice as well as icebergs during the winter. As a result, facilities in these waters need to be able to withstand environmental loads from waves, winds and current, as well as actions from ice features. Due to the deep waters in most of the Arctic regions, floating facilities might prove to be the preferred choice over gravity based structures. Icebergs pose a major threat to offshore installations, and collisions can be prevented by changing their drift direction by towing. This might be found impossible for the largest icebergs, and facilities should have the possibility to disconnect riser and mooring systems and move off location to avoid unmanageable ice features. Due to the low air and sea temperatures in these regions, winterization of facilities is also needed. The oil and gas fields in this region are far from infrastructure. The facilities therefore need to be constructed in such a way that evacuation is the last resort. As a result, the facilities should be able to withstand all ice features expected in the region or be able to move off location to avoid the most extreme ice features.

Throughout this thesis a numerical calculation model has been developed to estimate level-ice actions on a SPAR buoy from level ice. The estimated loads are compared to results from model tests to find the validity of performing numerical calculations compared to performing model tests. A correction of the developed calculation model has been performed based on the deviations between the predicted loads and the loads measured in the model tests. This thesis has been produced in accordance with the problem text displayed on page II. Task 2 has been performed by Stud. Techn. Heidi Fjellvang and is not presented in this report. As Phase I proved quite time consuming, Phase II activities were not commenced. As a result, the tasks described in Phase I could be performed more thoroughly.

Thesis Outline

Chapter 2: A review of existing experience of moored floaters in Arctic regions has been performed. The areas for operation, which ice conditions were encountered and a general discussion of the structures used, including their mooring systems, are given.

Chapter 3: A review of ice load formulas as given in [ISO 19906:2010] is presented. The methodologies for estimating level-ice actions on sloping structures (both Croasdale`s and Ralston`s method) as well as the methodology for estimating ice actions on vertical structures are described. A brief review on different ice action scenarios is also given in this section.

Chapter 4: Static and time domain analyses of ice-structure interaction have been performed. For the static calculations, an analysis of the differences in magnitude between ice actions on a vertical structure, a downward sloping structure and an upward sloping structure have been examined. In the time domain part, calculations of ice actions on a downward sloping structure have been examined based on Croasdale`s calculation method. Assumptions have been made on how the ice actions will vary over time for this kind of ice-structure interaction. Results are presented for four different scenarios where ice drift speed and ice thickness is varied.

Chapter 5: This section contains an analysis of performed model tests for four different ice-structure interaction scenarios corresponding to the four scenarios described in section 4. The model test program and the measured ice properties are described in this section. When examining the model tests, videos are used for visual analyze of the interaction process. The most important ice action statistics from the model tests are presented.

Chapter 6: In this section the developed numerical calculation model is corrected by comparing the results obtained with those measured in the model tests. Ice actions calculated for the target ice properties are developed from both the corrected and the original script. By comparing the results from the corrected and the original script, a discussion about the validity of performing numerical calculations compared to performing ice model testing is given.

Chapter 7: This section presents the most important conclusions drawn throughout the work on this thesis.

Chapter 8: This section describes the recommendations for further work on the tasks performed throughout this thesis.

2 Existing Experience from Moored Floaters in Arctic Regions

The Arctic region has received great interest over the past years due to its potentially extensive oil and gas reserves. To extract hydrocarbons from this region a great amount of new challenges occur, and the biggest challenge is the presence of ice. Ice might inflict loads on structures that far exceed those of waves, winds and currents which potentially can result in disastrous scenarios for facilities in these areas, e.g. moored floaters. Due to the deep waters in the region, floating production units (FPU) might stand out as the natural choice over gravity based structures (GBS). This section will highlight some of the projects executed in the Arctic region with moored floating facilities. The main objective of this chapter is to describe the structures used and the experience obtained from these.

Several projects have been executed in the Grand Banks region which lies off the east coast of Newfoundland. The first production in the area commenced in 1997 at the Hibernia field by the use of a fixed gravity based structure (GBS). The next major Grand Banks development was at the Terra Nova field where production started in 2002. The first ever floating production, storage and offloading (FPSO) vessel to operate in the harsh conditions in the Northern Atlantic was built in accordance with this development, the Terra Nova FPSO (Figure 1). There has also been produced oil from the White Rose and Hebron field in the Grand Banks region.

Figure 1 The Terra Nova FPSO [www.hydro.com]

The Terra Nova FPSO was the first FPSO with a fully-automated quick disconnectable turret and riser system, and its ice strengthened hull was designed to withstand an impact with a 100 000 tonne iceberg. It also had the first application of open glory holes for protection of subsea equipment from scouring icebergs [Lever, G. et.al. 2001]. At the Terra Nova field the incursion of sea ice is a seasonal event beginning in mid-February and can extend into March. The expected ice cover in the region is

3/10ths with maximum cover reaching 9/10ths. The ice thickness varies from 0.3m to a maximum of 1.5m. The Terra Nova FPSO was designed to operate in sea ice greater than that anticipated in the region.

The key feature of the Terra Nova FPSO is its turret. The turret can be disconnected from its risers and mooring lines enabling the FPSO to move off location in the event of an iceberg encroachment. In an emergency situation the FPSO is able to leave its location in approximately 20 minutes [Lever, G. et.al. 2001]. The turret arrangement is shown in Figure 2. Disconnecting the turret is a last resort solution as this lead to a production stop. The Terra Nova FPSO has a comprehensive ice management system to detect, monitor and deflect oncoming icebergs. The vessel is equipped with a high-resolution ice-tracking radar, and if a collision with an iceberg is likely a standby vessel will tow the iceberg away from the FPSO [www.oilpubs.com/oso].

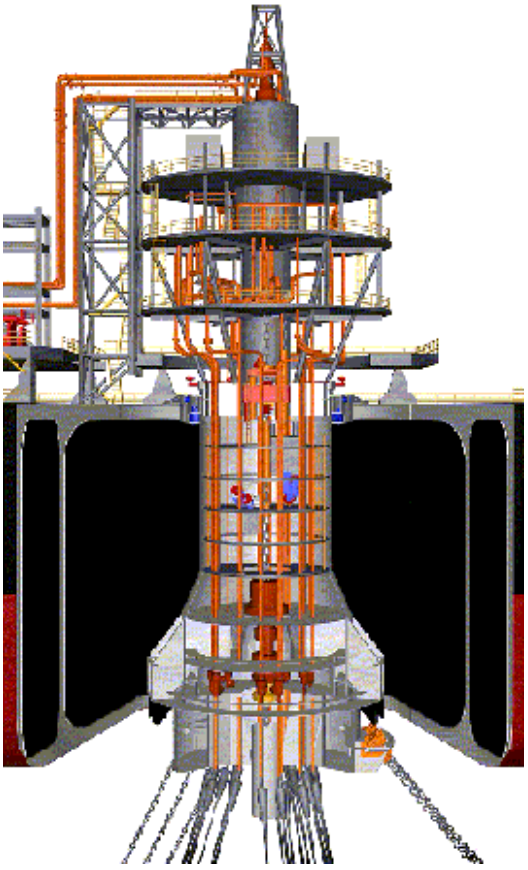

Figure 2 Turret General Arrangement [G.V. Lever et.al. 2001]

The FPSO utilizes an active station keeping system based on a Thruster Assisted Position Mooring System (TAPMS) which consists of 9 mooring legs, five retractable azimuth thrusters and a TAPMS dynamic positioning (DP) system [Lever, G. et.al. 2001]. The mooring lines are grouped in three groups consisting of three mooring lines each, spaced 120 degrees apart attached to the turret (see Figure 3).

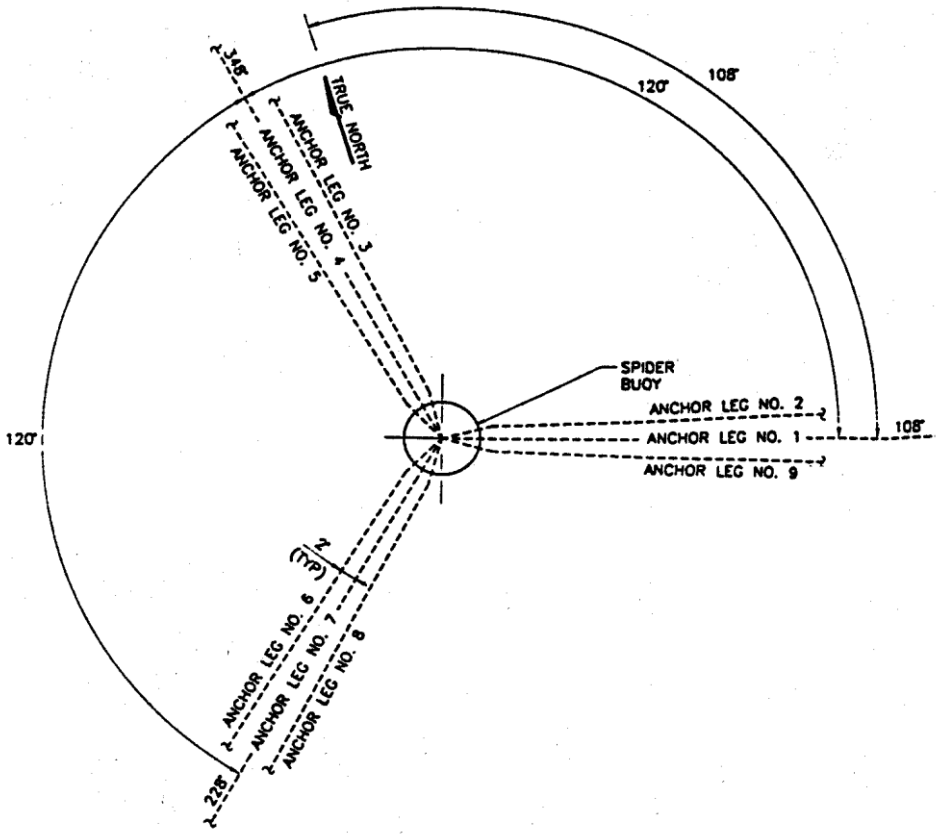

Figure 3 Mooring Lines Arrangement [Paterson, R. et.al. 2000]

The mooring system is not equipped with any instrumentation to measure the mooring line tension or the angle of inclination, but Figure 4 shows the total restoring force of the mooring system for offset direction aligned with mooring line 1 and offset direction bisecting the angle between lines 1 and 4. These results are obtained through a mooring system calculation model [Paterson, R. et.al. 2000].

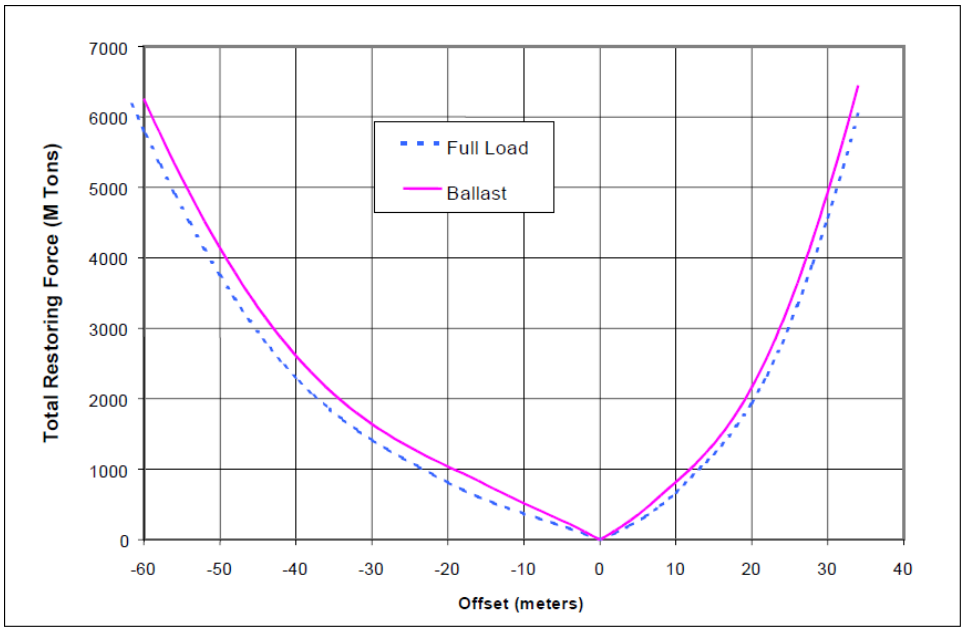

Figure 4 Mooring Line Loads on the Terra Nova FPSO [Paterson, R. et.al. 2000]

As an example given in [Paterson, R. et.al. 2000] the total load on the mooring system obtained from model tests with a 100% cover of pack ice of thickness 1.0m is 1500 tonnes. According to [Wright, B. et.al. 2000] the mooring system on the Terra Nova FPSO can resist load levels in excess of 2000 tonnes.

The Terra Nova FPSO encountered a series of mechanical problems which began in 2004, some leading to oil spill and others to production halts. There are no records of ice causing any of these problems.

Another area that has received the interest of the oil and gas industry is the Beaufort Sea which lies off the coast of Northern Alaska. Exploration drilling started in 1976 with Canmar`s drillships operating in depths of about 20-80m. These drillships were ice-strengthened for seasonal operations, and each ship was deployed with an eight point spread moored mooring system (four bow and four aft) that came off the deck and through the waterline. One of the ships had underwater fairleads for protection against ice. The mooring lines were equipped with remote anchor releases that allowed the drillships to quickly disconnect and move off location should difficult ice or storm conditions occur. The mooring system was capable of resisting global ice loads of about 100 tonnes. Due to the mooring arrangement the drillships were aligned in a fixed direction and could not reposition themselves in response to changing ice drift directions. The drillships were supported with two or more icebreakers for ice management.

Figure 5 Canmar`s Drillship Explorer 4 with Ice Management Support Vessel [Wright, B. et.al. 1999]

Canmar`s drillships experienced first year (FY) ice floes of 0.3-1.5m thickness and FY pack ice 0.3-0.5m thick. It was found that the drillships were able to stationkeep in most conditions due to the ice management system used. All of the ice breaking needed was done by the support vessels which gave relatively low ice actions on the drillships themselves. Large rough ice floes (rubble fields, multi-year (MY) floes) that could not be managed, high drift rates of pack ice and ice drift direction perpendicular to the long axis of the ships gave the most challenging situations and lead to downtime. It was also a problem with the mooring lines coming off the deck and through the

waterline as this impeded ice clearance and increased the mooring line tension. The most important finding with Canmar`s drillships were that even though the mooring lines could not withstand high ice loads, the ships were able to stationkeep in difficult conditions due to a well-established ice management system [Wright, B. et.al. 1999].

In 1983 a conical shaped drilling unit named the Kulluk entered the Beaufort Sea with a purpose of extending the drilling season from the spring break-up period to the early winter. The Kulluk therefore operated in a much wider and more difficult range of pack ice than Canmar`s drillships. During its operations, in-ice performance information was systematically obtained, providing the best source of full scale data for most considerations related to moored vessel stationkeeping operations in various pack ice conditions. [Wright, B. et.al. 1999] and [Wright, B. et.al. 2000] have collected and displayed the main results from this data base. This work was meant to collect in-situ experience obtained by the Kulluk to provide helpful information for moored floaters in pack ice conditions, and was written in accordance with the Grand Banks development. There is no record of any other full scale data base for floaters in pack ice, which makes this a unique and very useful guide for all Arctic development.

Due to the Kulluks conical shape and radially symmetric mooring system it obtained an omnidirectional capability to resist ice actions. The hull had a downward sloping form at the waterline which failed the ice in bending and an outward flare near its bottom to ensure that broken ice pieces cleared around it and did not enter the moonpool or got tangled in the submerged mooring lines. The mooring system was comprised of twelve 3 ½ inch wire lines and was designed to withstand the load from 1.2m of level unbroken ice, when the vessel was operating in a stationkeeping mode, with no ice management support. The mooring lines were designed to tolerate global loads of 750 tonnes in a drilling mode with maximum individual line tension of 260 tonnes (50% of their 520 tonne breaking strength). In a survival mode they were designed to tolerate global loads of 1000 tonnes with the risers disconnected, which gave a line tension of 75% of their breaking strength.

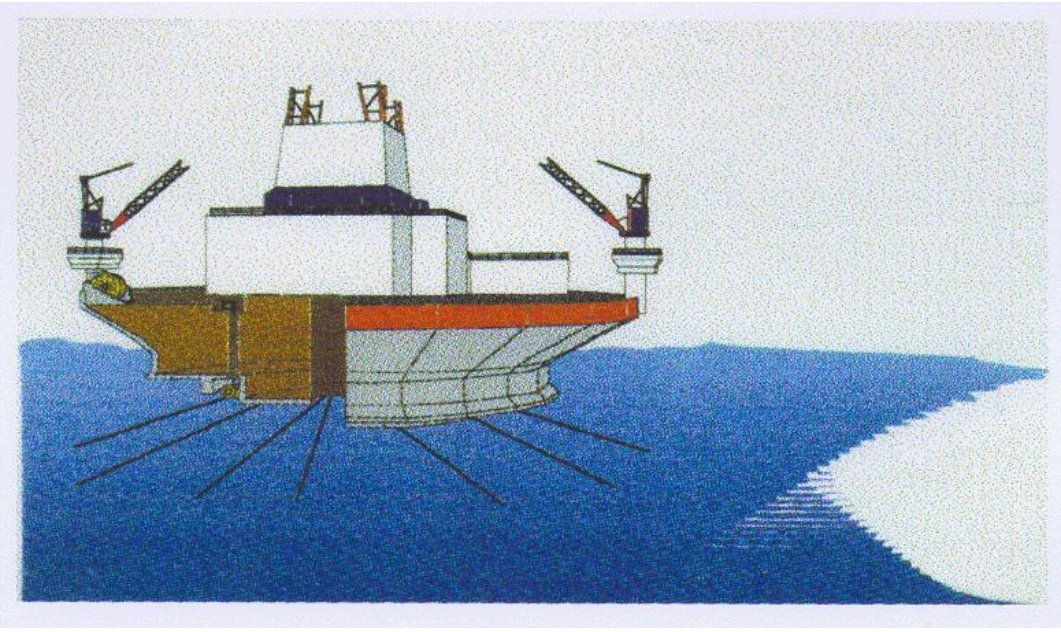

Figure 6 Schematic Illustration of the Kulluk [Wright, B. et.al. 1999]

Good ice management was an important factor in enhancing stationkeeping, and Kulluk was supported by between two to four icebreakers during its operations in heavy pack ice conditions. Large expanses of level ice are relatively rare in the Beaufort Sea and ice management was required to fragment ridges, rough ice areas and thicker old floes that are more commonly experienced. Due to a well-established ice management system the Kulluk was able to operate from late May until late December. Between 1983 and 1989, Kulluk experienced an operating efficiency of more than 90%.

Ice and performance monitoring programs were used to provide real time support for Kulluk stationkeeping which gave an extensive data base on the mooring loads and motions experienced by the vessel in different pack ice conditions, and the effectiveness of the ice management methods used. [Wright, B. et.al. 2000] have gathered this information to an extensive report describing ice actions in a series of different ice conditions. Figure 7 shows the ice loads experienced by the Kulluk in different ice conditions, and the load reduction due to ice management. This is only but a fraction of the results obtained.

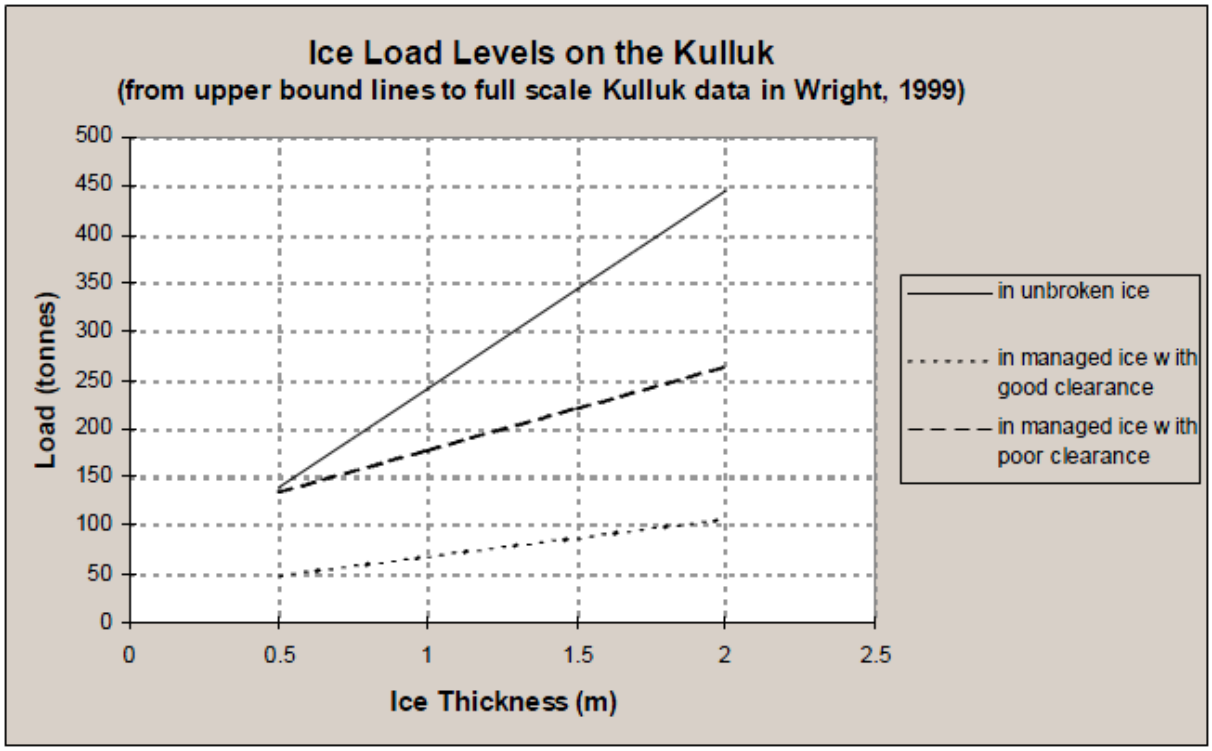

Figure 7 Loads on the Kulluk for Varying Ice Thickness With or Without Ice Management [Wright, B. et.al.2000]

The data base obtained from the Kulluk is quite unique regarding ice actions on a moored floating facility. There are currently many different ongoing projects for oil and gas extraction in ice infested waters which have resulted in many different studies and model tests of floating facilities in ice. One area that has been of interest for some years is the Shtokman field located 610 km from Murmansk in the Barents Sea. The Shtokman location is influenced by large inflow of relatively warm Atlantic water leading to an area mostly free of ice during the whole year, only with occasional sea ice and iceberg invasions. It is estimated that sea ice occurs approximately 3-4 out of 10 years. The sea is covered by ice about 6% of the total time, and during years with occurrence of ice it can be present from a few days to a few months. The ice mainly consists of FY ice that can be up to 2m thick with

ridges that can locally be 21m deep [Le Marechal, G. et.al. 2011]. The field also has a possibility of iceberg intrusion.

The current design concluded with after various conceptual studies for the Shtokman field is a floating ship shaped platform with a disconnectable moored turret. The production unit is designed to withstand independently almost all ice and iceberg actions expected. The ultimate limit state (ULS) of the mooring system includes head-on interaction with 100 year return period (YRP) ice ridge and 5 000 tonnes horizontal loads. The mooring system is also designed with a smaller offset capacity than the risers, meaning the mooring lines will fail before the risers. An emergency disconnection of the turret can be performed in 3 minutes and direct contact between mooring lines and icebergs is avoided [Liferov, P. et.al. 2009].

Ice management will be used to detect and mitigate sea ice and iceberg threats to minimize/avoid production downtime. Experience from the Grand Banks and the Beaufort Sea (e.g. the Kulluk) have been revised in accordance with ice management. It has been found that with a well working ice management system the production unit at the Shtokman field should be able to avoid disconnection due to sea ice. The challenge will be to obtain a reliable system that works in all conditions [Liferov, P. et.al. 2009].

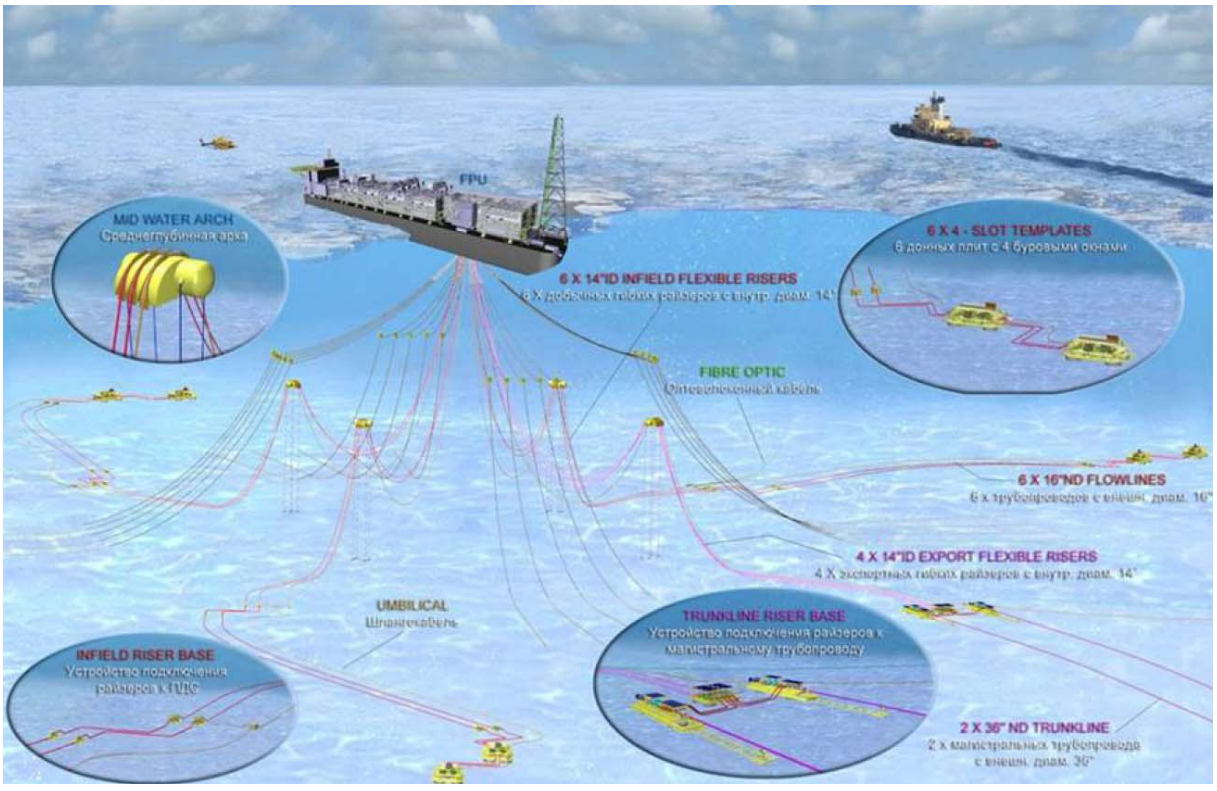

Figure 8 Illustration of Shtokman Phase 1 Development [Liferov, P. et.al. 2009]

3 Review of the Ice Load Formulas in ISO 19906:2010

Early work to predict ice forces on conical shaped structures has been undertaken since the mid-1960`s. In the late 1970`s, Croasdale developed an analytical model based on an elastic beam on an elastic foundation and later modified this model for three dimensional (3-D) effects. In the early 1980`s Ralston developed a full 3-D model based on plasticity theory. These models as well as a model developed to describe ice forces on a vertical structure has been revised and further developed several times, and [ISO 19906:2010] gives the latest proposed models.

This section will review the two models describing ice actions on sloping structures as well as the model for vertical structures as given in [ISO 19906:2010]. The one thing in common for the three models is that they are established for fixed, rigid constructions. A rigid structure is defined as one where the ice interaction process is not influenced by the deformation of the structure itself. As a brief introduction to this chapter, a discussion about different ice action scenarios as well as ice failure modes on different structure types will be given (with emphasis on vertical and sloping structures exposed to level ice).

3.1 Ice Action Scenarios

Ice actions are described as the result of an interaction between a given ice feature and a structure [ISO 19906:2010]. Different interaction scenarios can occur depending on the type of ice feature and the ice properties as well as the shape and size of the structure. Examples of ice features include level ice, ice ridges or icebergs, and ice properties include strength, porosity, drift speed and thickness. It is common to separate ice features in first-year (FY) ice and multi-year (MY) ice, where MY ice is features that have survived one or more summer periods. MY ice is typically colder and has a higher strength compared to FY ice as the salinity is lower in MY ice than in FY ice.

The mode of ice failure against the structure has a significant effect on the magnitude of the ice action. The most common failure modes of ice are given in Figure 9.

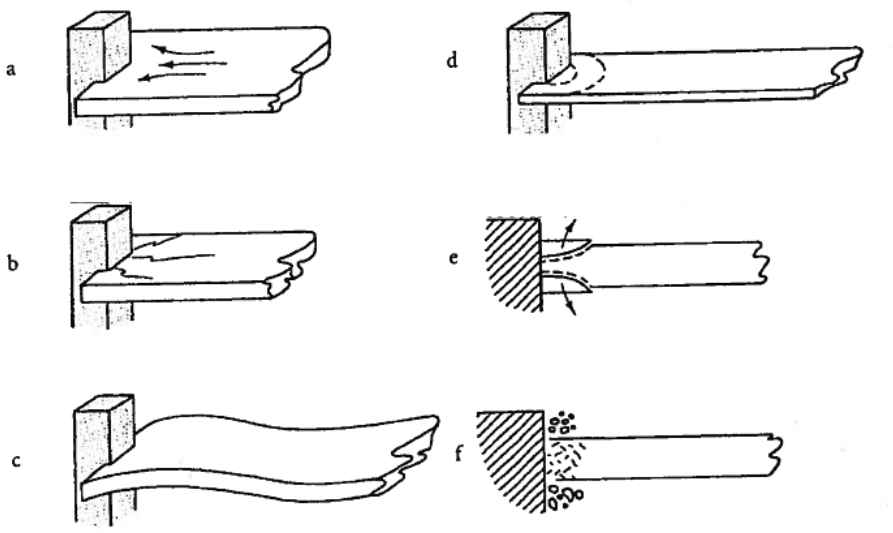

Figure 9 Principle Failure Mechanisms Observed during Laboratory Indentation Experiments [Løset, S. et. al. 2006]

The failure modes are described in the list below [Løset, S. et. al. 2006]. Aspect ratio is introduced to describe the failure modes, and is given as the structure width divided by the ice thickness.

a) Creep: develops continuously, and no cracks form in the ice. Ice velocity, aspect ratio and ice properties determine the probability of creep formation.
b) Radial cracking: develops above certain stress levels, and especially at high aspect ratios. The cracks may radiate from corners of rectangular structures, or as central and side cracks in front of a cylindrical structure.
c) Buckling: characteristic for thin ice and wide structures. This type of failure is often connected with radial or circumferential crack formation.
d) Circumferential cracks: will be formed as a result of elastic buckling or out-of-plane bending due to eccentric loading conditions.
e) Spalling: horizontal cracks grow away from the contact zone, and divide the ice sheet into layers. The lengths of the cracks are determined by the velocity of the ice, and the higher the velocity is the smaller are the crack lengths. The final stage of the spalling effect is formation of ice fragments at the top and bottom of the ice sheet.
f) Crushing: at high rates, ice is crushed against the structure. The ice is pulverized and escapes to the top and bottom of the ice sheet.

When level ice interacts with a vertical structure, crushing usually dominates the ice action scenario. For sloping structures, the ice sheet most often fail in buckling as it rides up or down the face of the structure. Other failure modes can occur depending on parameters like the ice drift speed and the ice thickness.

For many interaction scenarios, it is useful to consider limit stress, limit energy and limit force mechanisms. Each mechanism corresponds to the situation when one of the parameters reaches the utmost value [ISO 19906:2010].

Limit stress mechanism is when ice failure processes adjacent to the structure (compressive, shear, buckling, splitting) govern the ice action. The ice feature has sufficient driving force to fail the ice and completely envelop the structure.

Limit energy mechanism (limit momentum mechanism) occurs when the ice action is limited by the kinetic energy (or momentum) of the ice feature (e.g. iceberg impact). The ice feature will be insufficiently penetrated by the structure, and the feature will come to a halt.

Limit force mechanism develops if a strong ice field is brought to rest in front of a wide structure and transmits actions from surrounding ice features, wind and current to the structure.

3.2 Model for Vertical Structures

From observations of ice actions subjected on vertical structures, it has been found that the governing failure mode of ice is crushing. The term crushing refers to a complex compressive failure process, involving the development of a damaged layer as well as sequential development of flakes or spalls, and horizontal splits or cleavage cracks [ISO 19906:2010].

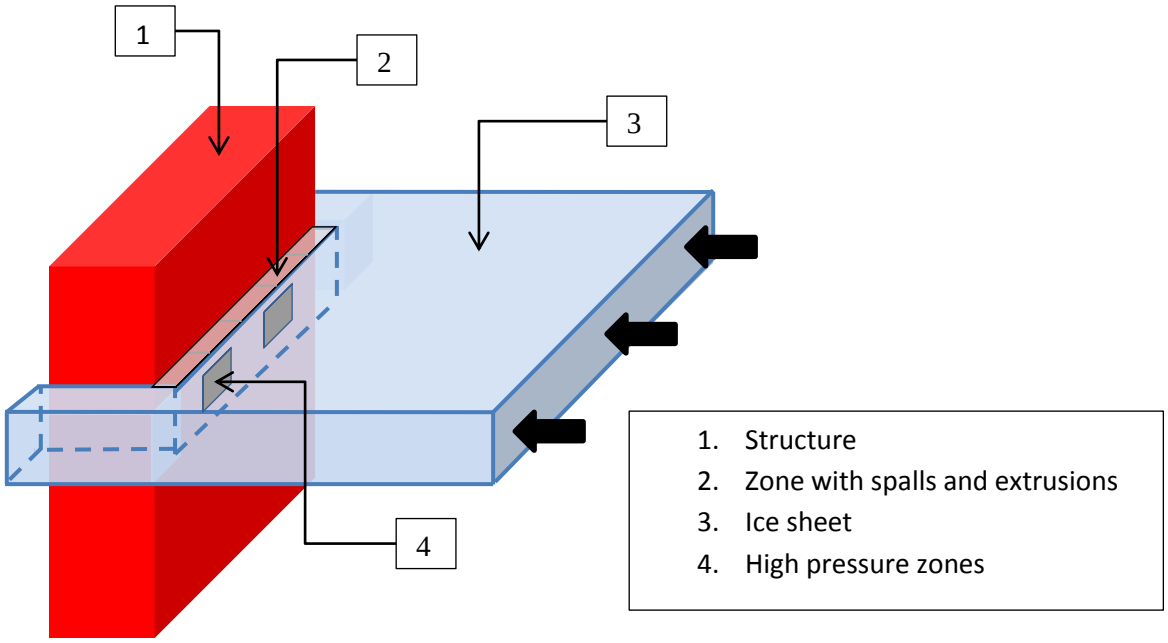

Figure 10 Crushing of Ice against a Vertical Structure

At higher ice movement rates than 1 mm/s fractures and spalls occur, resulting in the formation of high pressure zones (hpz`s) in the contact area between the ice and the structure. Also, fracturing of large ice pieces results in areas of little or no pressure. The result is that some small patches or narrow line-like areas are subjected to high pressures and others to little or no pressure (see Figure 10).

When ice crushing occurs against a vertical structure, the global ice action normal to the surface, F_G, can be expressed as follows.

$$F_G = p_G A_N \tag{3.1}$$

A_N and p_G is the nominal contact area (the projected area of the intact ice feature on the structure) and the global ice pressure respectively. The global ice pressure is the pressure averaged over the nominal contact area associated with the global ice action. For level ice the nominal contact area is equal to the ice thickness (h) multiplied by the width (D) of the structure, and equation (3.1) can be rewritten to the following.

$$F_G = p_G h D \tag{3.2}$$

The global ice pressure is influenced by numerous factors like ice temperature, shape or aspect ratio of the contact area and displacements between ice and structure. To determine upper bound ice pressure values, full-scale data from Cook Inlet, the Beaufort Sea, Baltic Sea and Bohai Bay have been used [ISO 19906:2010]. Based on these studies the global ice pressure can be determined as follows.

$$p_G = C_R \left(\frac{h}{h_1}\right)^n \left(\frac{D}{h}\right)^m \tag{3.3}$$

The coefficients in equation (3.3) are given as follows.

- p_G is the global average ice pressure [MPa]
- D is the projected width of the structure [m]
- h is the ice sheet thickness [m]
- h_1 is a reference thickness equal to 1m
- m is an empirical coefficient equal to -0.16
- n is an empirical coefficient equal to
  - -0.50+h/5 for h<1.0m
  - -0.30 for h≥1.0m
- C_R is the ice strength coefficient [MPa]

Equation (3.3) applies for rigid structures with aspect ratio D/h greater than 2. In Figure 11 the aspect ratio for structures with waterline diameter of 100m, 50m, 30m and 10m is plotted against level ice thickness varying from 0.5m to 3.0m. It is seen that the aspect ratio criteria is valid for a great variety of structures and ice thicknesses.

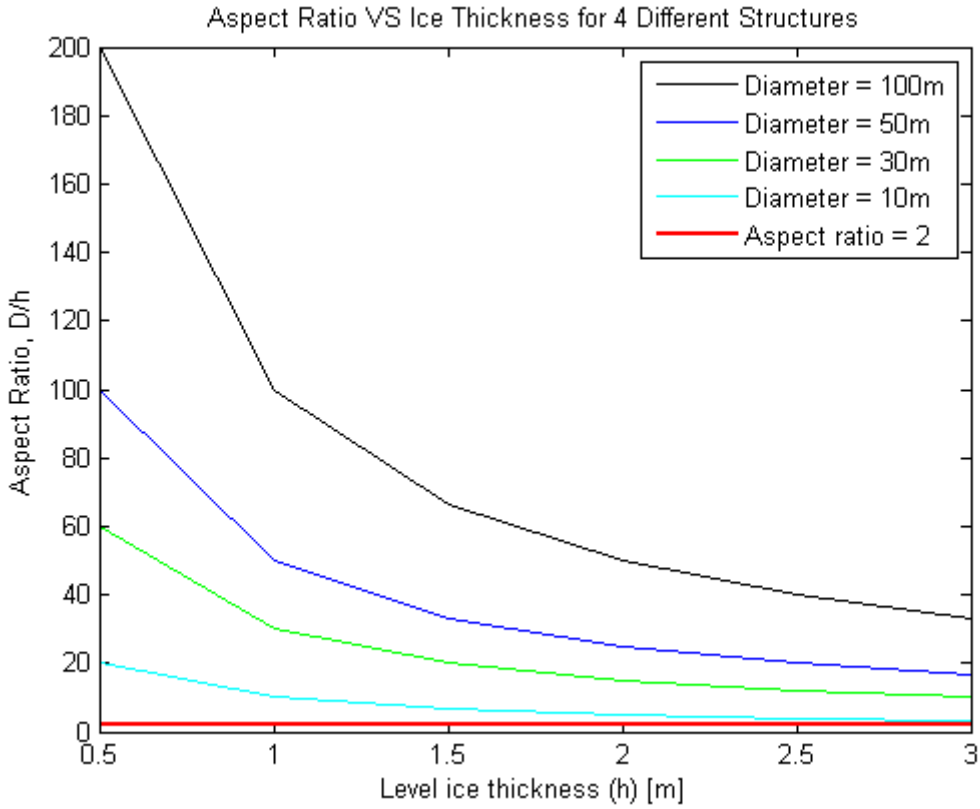

Figure 11 Aspect Ratio VS Ice Thickness for Different Structures

The strength parameter can be assumed as C_R=2.8, based on first-year and multi-year ice data from the Beaufort Sea [Blanchet, D. 1998], [Timco, G. et.al. 2004] and [Wright, B. 1998]. This value can be conservative as it potentially includes some magnification due to the compliance of the structure in the referenced data from the Beaufort Sea [Jefferies, M. et.al. 2008].

From data obtained in the Baltic Sea [Kärnä, T. et.al. 2006], the strength parameter has been obtained as C_R=1.8. Here, the ice drift velocity was higher than 0.1m/s and the maximum waterline

displacements, in the direction of ice action, of the structure were about 0.4% of the ice thickness. Under these conditions, the strength parameter does not exhibit magnification due to the compliance of the structure.

According to [ISO 19906:2010], the strength parameter can vary in different geographical areas due to the absence of multi-year ice. This will not be addressed in this paper, and for calculations performed later in the report the conservative value of C_R=2.8 will be used (this is given in [ISO 19906:2010] as the recommended value for Arctic areas).

3.3 Models for Sloping Structures

As sheet ice interacts with a sloping structure, the main failure mode of ice is bending (see Figure 12a). This will generally result in reduced ice actions compared to crushing failure mode as the flexural strength of ice is less than its compressive strength. The failure mode of ice against a sloping structure can vary depending on several parameters e.g. the ice density, the flexural strength of ice and the ice drift speed.

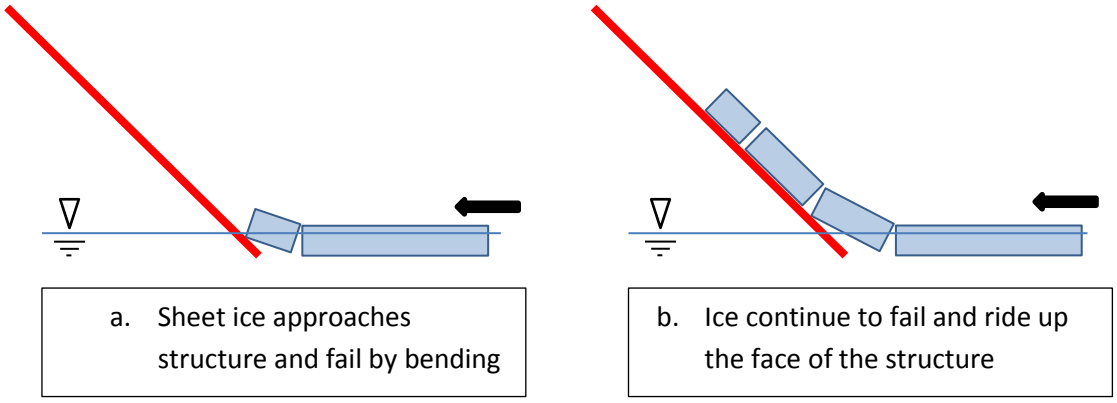

Figure 12 Ice Failing in Bending Against a Sloping Structure

As the ice sheet continues to move against the structure ice blocks are continued to be broken off from the ice sheet and are starting to ride up the sloping surface (see Figure 12b). In the following two sections a review has been done on two different methods to calculate ice loads against a sloping structure. The starting point of both methods have been to develop equations for ice loads from bending failure and ride-up along the slope, but as will be addressed in the following, one of the methods are further developed to include also other ice-structure interaction load components.

For a two-dimensional (2-D) interaction between a sloping structure and sheet ice the horizontal and vertical load component can be expressed as given in equation (3.4) and shown in Figure 13.

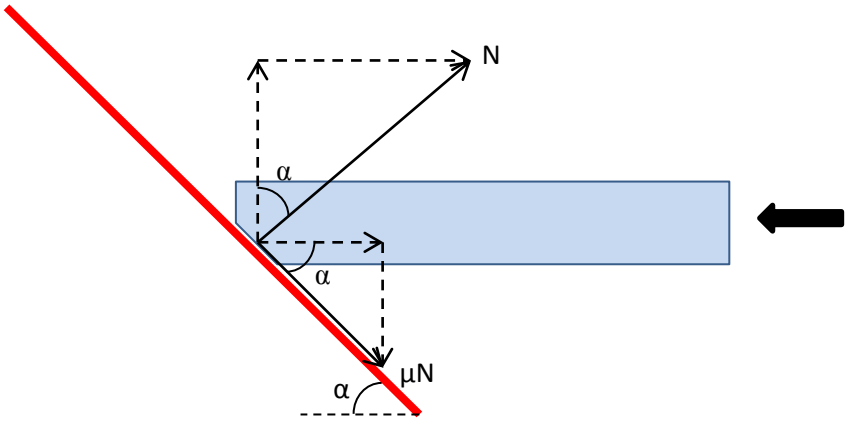

Figure 13 Relationship between Horizontal and Vertical Load Component

$$F_H = N sin\alpha + \mu N cos\alpha$$
$$F_V = N cos\alpha - \mu N sin\alpha \quad (3.4)$$

The relationship between the horizontal and vertical load component can further be written as follows.

$$F_V = F_H \frac{cos\alpha - \mu sin\alpha}{sin\alpha + \mu cos\alpha} = F_H \frac{\xi_2}{\xi_1} = \frac{F_H}{\xi} \quad (3.5)$$

where

$$\xi = \frac{\xi_1}{\xi_2}$$

The coefficients in equation (3.4) and equation (3.5) are defined as follows.

- F_H Horizontal component of ice action
- F_V Vertical component of ice action
- N Normal component of reaction to ice action on structure
- μ Ice-structure friction coefficient
- α Sloping angle from horizontal

The two methods to calculate ice actions on a sloping structure given in [ISO 19906:2010] are hereinafter described as Ralston`s method and Croasdale`s method.

3.3.1 Ralston`s Method

[Ralston, T.D. 1977] considered a floating ice sheet to be an elastic-plastic plate resting on an elastic-plastic foundation, and through plastic limit analysis developed a mathematical model for both sheet ice failure and ride-up on a conical structure (see Figure 12). This model includes the effects of cone angle, waterline diameter, exposed conical surface, ice-structure friction, ice flexural strength and ice sheet thickness. In his analysis a pure bending failure criterion is used by assuming that the ice bending moment capacity, M_0, is isotropic in the plane of the ice sheet, and that the upward and downward bending strengths are equal. As the flexural strength, σ_f, of the ice sheet is the most common way to display the strength of the ice and M_0 is the relevant parameter in this analysis,

Ralston uses the relationship between σ_f and M_0 given in equation (3.6) to express the equations through σ_f.

$$\sigma_f = \frac{6M_0}{h^2} \tag{3.6}$$

h is the thickness of the ice sheet. Ralston uses the technique of plastic limit analysis which consists of constructing a velocity field for the ice sheet and setting the rate of work done by the boundary forces equal to the rate of energy dissipation that results from the assumed motions. [ISO 19906:2010] and [Ralston, T.D. 1977] presents the resulting equations with some differences, and the equations given in this report are taken from [ISO 19906:2010].

The horizontal and vertical load components are found to be as follows.

$$H_R = W\frac{\tan(\alpha) + \mu E_2 - \mu f g_r \cos(\alpha)}{1 - \mu g_r} \tag{3.7}$$

$$V_R = W cos(\alpha)\left(\frac{\pi}{2}\cos(\alpha) - \mu\alpha - f h_v\right) + H_R h_v \tag{3.8}$$

$$H_B = \frac{\sigma_f h^2}{3}\frac{\tan(\alpha)}{1 - \mu g_r}\left(\frac{1 + Yxln(x)}{x - 1} + G(x-1)(x+2)\right) \tag{3.9}$$

$$V_B = H_B h_v \tag{3.10}$$

H_R and V_R are the horizontal and vertical load component due to ride-up effects on the structure, and H_B and V_B are the horizontal and vertical load component due to flexural failure of the ice sheet. The functions used in the equations are given as follows.

$$f = \sin(\alpha) + \mu E_1 \cos(\alpha)$$

$$g_r = \frac{\sin(\alpha) + {}^{\alpha}/_{\cos(\alpha)}}{\frac{\pi}{2}\sin^2(\alpha) + 2\mu\alpha\cos(\alpha)}$$

$$h_v = \frac{f\cos(\alpha) - \mu E_2}{\frac{\pi}{4}\sin^2(\alpha) + \mu\alpha\cos(\alpha)} \tag{3.11}$$

$$W = \rho_i g h_r \frac{D^2 - D_T^2}{4\cos(\alpha)}$$

$$G = \frac{\rho_i g D^2}{4\sigma_f h}$$

$$x = 1 + \left(3G + \frac{Y}{2}\right)^{-0.5}$$

Y=2.711 for Tresca yielding or *Y=3.422* for Johansen yielding. E_1 and E_2 are the complete elliptical integrals of the first and second kind given in equation (3.12).

$$E_1 = \int_0^{\pi/2} (1 - \sin^2(\alpha)\sin^2(\eta))^{-0.5} d\eta$$
$$E_1 = \int_0^{\pi/2} (1 - \sin^2(\alpha)\sin^2(\eta))^{0.5} d\eta \tag{3.12}$$

The total horizontal and vertical force from the ice loads are given as follows.

$$F_H = H_B + H_R$$
$$F_V = V_B + V_R \tag{3.13}$$

The parameters used in equation (3.7) to equation (3.11) are given as follows.

- h_r ride-up height of ice blocks
- ρ_i density of ice
- ρ_w density of sea-water
- D waterline diameter of the structure
- D_T diameter at end of sloping surface
- g acceleration due to gravity

[Ralston, T.D. 1977] defines the functions *W* and *x* given in equation (3.11) with some differences from [ISO 19906:2010].

$$W_{RALSTON} = 0.9\rho_w g h \frac{D^2 - D_T^2}{4\cos(\alpha)} \tag{3.14}$$

It is found that the two expressions for *W* gives approximately the same value for $h=h_r$. The expression for *x* in [Ralston, T.D. 1977] is given as the solution of equation (3.15).

$$x - \ln x + 0.0830(2x+1)(x-1)^2\left(\frac{\rho_w g D^2}{\sigma_f h}\right) = 1.369 \tag{3.15}$$

Ralston`s method, as displayed in this report, is established for an upward breaking structure, but is valid for a downward breaking structure if the dry weight of ice in air is replaced with ice buoyancy in water ($\rho_i g$ replaced by $(\rho_w - \rho_i)g$).

3.3.2 Croasdales Method

[Croasdale, K.R. 1980] proposed a two dimensional (2-D) ice action model where the force needed to fail the ice sheet by bending and the force needed to push the ice blocks up the slope were taken into account. The model was also expanded to consider (3-D) effects by extending the zone of ice failure wider than the structure. [Croasdale, K.R. et al. 1994] further developed this calculation method to include rubble effects and in-plane compression. The equation for the total horizontal load component as given in [ISO 19906:2010] is as follows.

$$F_{H=}\frac{H_B + H_P + H_R + H_L + H_T}{1 - \frac{H_B}{\sigma_f w_c h}} \tag{3.16}$$

The factors included in the horizontal load component are defined as follows.

- H_B force needed to fail the ice sheet by flexure bending
- H_P force needed to push the ice sheet through the rubble on the ice sheet
- H_R force needed to push ice blocks from ice sheet failure through the rubble
- H_L force needed to lift and shear the ice rubble on top of the sloping surface
- H_T force needed to turn ice blocks due to interaction with the neck of the structure
- w_C total length of the circumferential crack

Equation (3.16) gives the maximum static horizontal ice load on a sloping structure, and the vertical component can be found by using equation (3.5). [ISO 19906:2010] presents these loads as valid for an upward sloping structure, but expresses that the equations can be modified to be valid for a downward breaking structure by replacing ice weight in air by ice buoyancy in water (i.e. in the same way as described in Ralston`s method).

In the following a review of each term in equation (3.16), as well as its denominator, will be given as they are presented in [ISO 19906:2010].

3.3.2.1 Breaking force H_B

The basic 2-D model for ice action on a sloping structure is based on simple mechanics and uses the theory for the bending of a beam on an elastic foundation. The vertical load required to fail the sheet ice by bending will be limited by the strength of the ice sheet with an edge loading. If the ice sheet is represented by a beam or an elastic foundation and its strength is limited by its bending moment capacity, M_0, the beams flexural strength (σ_f) can be expressed as follows.

$$\sigma_f = \frac{6M_0}{bh^2} \tag{3.17}$$

b is given as the width of the beam. For a semi-infinite beam on an elastic foundation it can be shown [Hetenyi, M. 1946] that the maximum bending moment due to an edge load (*V*) is given by:

$$M_0 = \frac{V}{\beta e^{\pi/4}}\sin(\pi/4) \tag{3.18}$$

where $1/\beta$ is a characteristic length, defined as follows.

$$\beta = \left(\frac{K}{4EI}\right)^{0.25} \tag{3.19}$$

K is the foundation constant equal to $\rho_w g b$ for a floating beam and *I* is the second moment of area of the cross section equal to $bh^3/12$.

By combining equation (3.17), (3.18) and (3.19) we can obtain the vertical load required to fail the sheet ice by bending, *V*, and the horizontal component, *H* is found by using equation (3.5). The result is a (2-D) horizontal bending load.

$$V = 0.68\sigma_f b\left(\frac{\rho_w g h^5}{E}\right)^{0.25}$$
$$H = H_{B(2D)} = 0.68\xi\sigma_f b\left(\frac{\rho_w g h^5}{E}\right)^{0.25} \tag{3.20}$$

Due to 3-D effects, the zone of ice broken by the structure extends wider than the waterline diameter. To account for this increased width of failure, the 2-D load is multiplied by the ratio of the length of the circumferential crack to the structure width (see Figure 14) [Croasdale, K.R. 1980].

l_c is the characteristic length given as follows.

$$l_c = \left(\frac{Eh^3}{12\rho_w g(1-\nu^2)}\right)^{0.25} \tag{3.21}$$

Where

- *E* Modulus of elasticity
- ν Poisson`s ratio

As the distance to the first crack is about $(\pi^2/4)l_c$ [Croasdale, K.R. 1980], the 3-D breaking term is given as follows.

$$H_{B(3D)} = H_{B(2D)}\left(\frac{D + (\pi^2/4)l_c}{D}\right) \tag{3.22}$$

For a given structure with diameter *D*, *b=D* in equation (3.20). This gives the breaking term as displayed in [ISO 19906:2010].

$$H_B = 0.68\xi\sigma_f\left(\frac{\rho_w g h^5}{E}\right)^{0.25}\left(D + \frac{\pi^2 l_c}{4}\right) \tag{3.23}$$

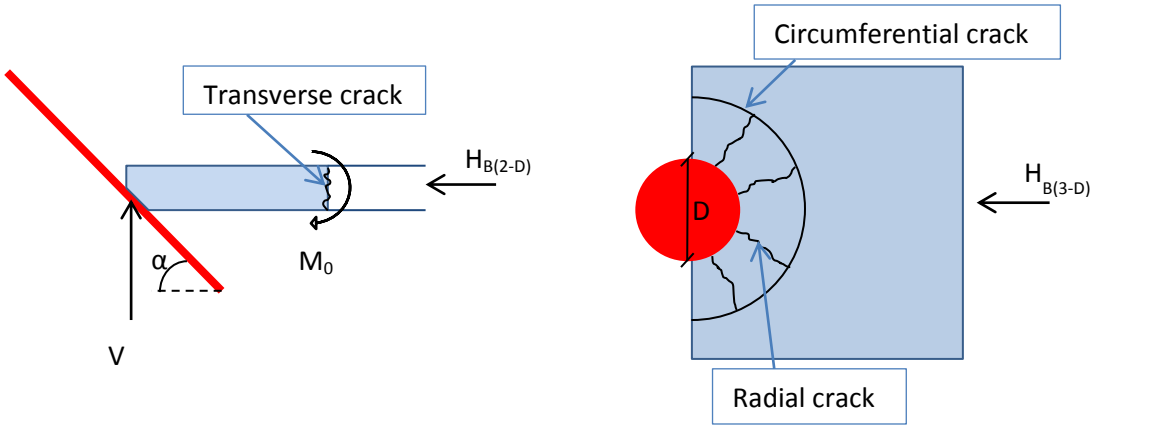

2-D Interaction	3-D Interaction
Length of transverse crack equal to width of structure	Length of circumferential crack greater than width (*D*) of structure

Figure 14 2-D VS 3-D Interaction for Bending Term

3.3.2.2 *Turning Force H_T*

After the sheet ice has been broken off and pushed up the slope, ice blocks will reach the end of the sloping side. A turning force is required to rotate the ice blocks to a vertical orientation (see Figure 15).

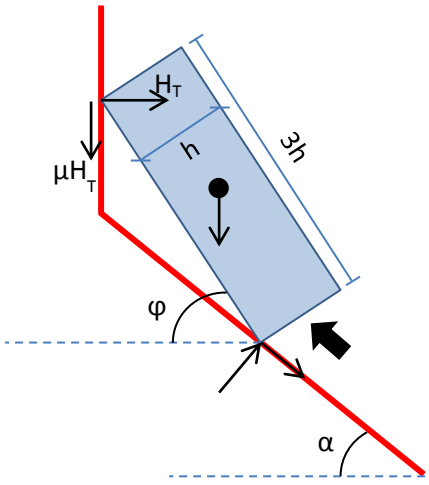

Figure 15 Forces Involved in Turning an Ice Block at end of Slope

It is assumed that secondary failures of the ice have reduced the block size to three times it thickness [Croasdale, K.R. 1980], which through equilibrium gives the turning force to be as follows.

$$H_T = 1.5h^2\rho_i g D\left(\frac{\cos\varphi}{\sin\varphi - \mu\cos\varphi}\right) \tag{3.24}$$

The maximum turning force is obtained when φ is equal to α (the sloping angle of the structure), and the turning force given in [ISO 19906:2010] is expressed with α.

3.3.2.3 Rubble Dependent Terms

As ice blocks are broken off from the oncoming level ice sheet continuously and pushed to the top of the slope, ice pieces will fall back and start to accumulate on the slope and in front of the structure. The ice pieces will be broken into smaller pieces as this process continues and a pile of rubble forms in front of the structure (see Figure 16).

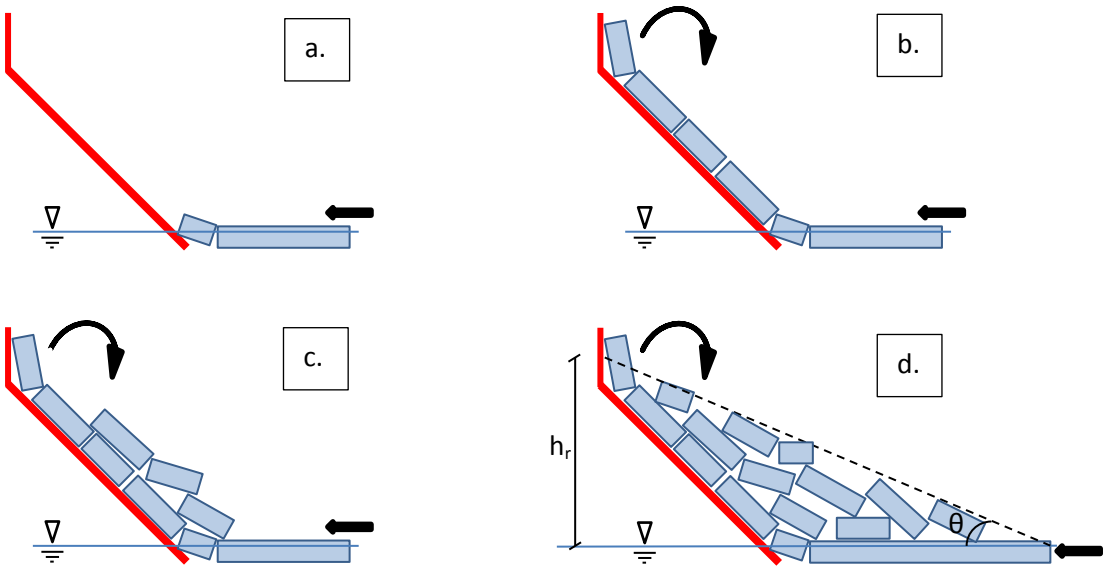

Figure 16 Rubble Accumulation in front of Structure

As shown in Figure 16, sheet ice is pushed against the structure before failing in bending and pushed up the sloping side (a). As the ice blocks reach the top of the sloping side they are turned and fall back in front of the structure (b). This process continues (c) until a volume of rubble has been formed in front of the structure (d). h_r is the rubble height and θ is the angle the rubble makes with the horizontal (the angle of repose). It should be noted that an angle of repose equal to the sloping angle ($\theta=\alpha$) implies a single layer of ice riding up the slope. Angles of repose steeper than the slope angle cannot be accounted for in this model because this leads to a negative amount of ice rubble on the slope and a reduction of the loads.

The three remaining terms in equation (3.16) (H_R, H_P and H_L) takes into account the additional forces on the structure due to rubble accumulation. They all depend on the volume of rubble accumulated in front of the structure, and are calculated in [ISO 19906:2010] from the theoretical maximum rubble volume obtained. The rubble height h_r depends on the slope angle, the width of the structure and frictional effects. The angle of repose, θ, should not be less than the slope angle minus 10 degrees. Both parameters are difficult to establish analytically and are best found based on experience and observations from actual structures or model tests [ISO 19906:2010]. The volume of ice rubble is assumed to reach a more or less constant volume defined by h_r and θ due to transportation of ice around the structure (see Figure 17).

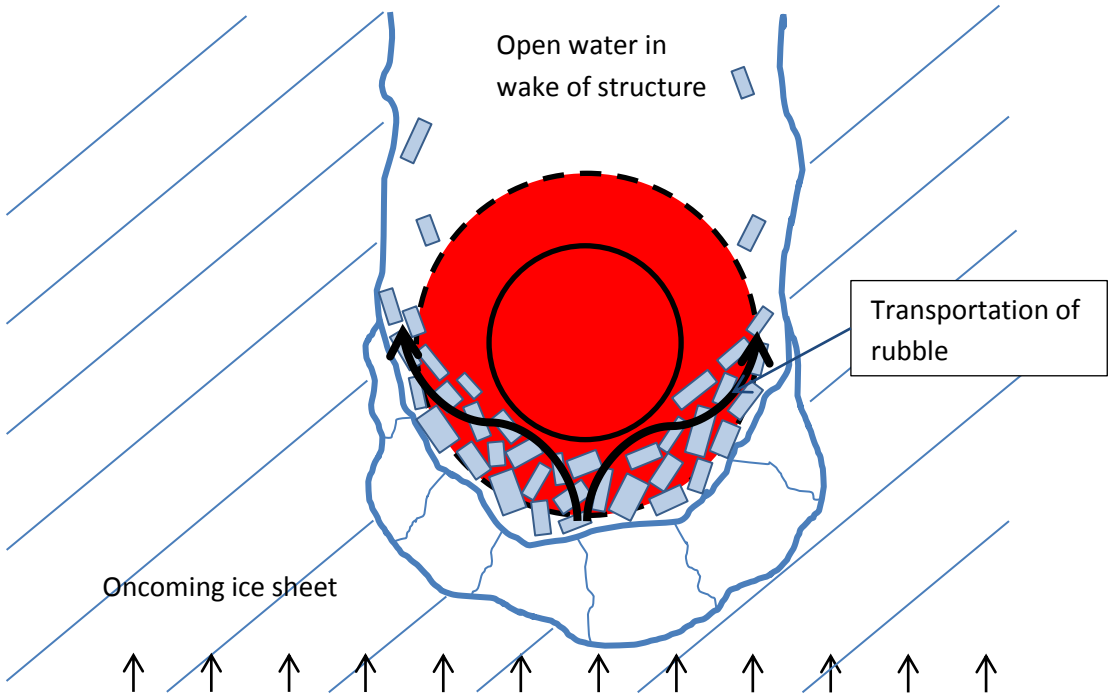

Figure 17 Top View of Transportation of Rubble around a Conical Structure

H_R is the force required to push ice blocks up the slope through ice rubble as shown in Figure 18 and given in equation (3.25).

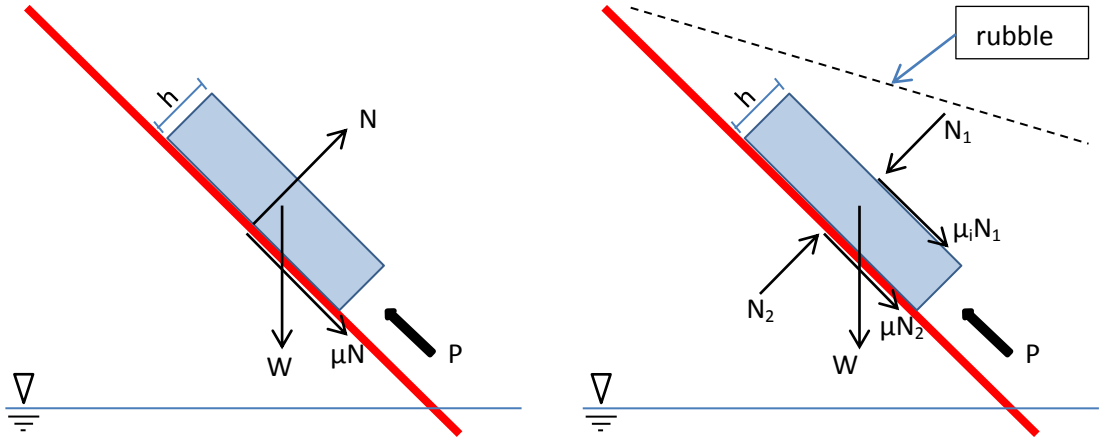

a. Load *P* when no rubble is present on the slope

b. Load *P* when rubble is present on the slope

Figure 18 Load Component Required to Push Ice Blocks up the Slope

$$H_R = DP\frac{1}{\cos(\alpha) - \mu\sin(\alpha)} \tag{3.25}$$

The function *P* is defined as:

$$P = 0.5\mu_i(\mu_i - \mu)\rho_i g(1-\mathrm{e})h_r^2 \sin(\alpha)\left(\frac{1}{\tan(\theta)} - \frac{1}{\tan(\alpha)}\right)\left(1 - \frac{\tan(\theta)}{\tan(\alpha)}\right)$$
$$+ 0.5(\mu_i - \mu)\rho_i g(1-\mathrm{e})h_r^2 \frac{\cos(\alpha)}{\tan(\alpha)}\left(1 - \frac{\tan(\theta)}{\tan(\alpha)}\right) \quad (3.26)$$
$$+ h_r h \rho_i g \frac{\sin(\alpha) + \mu\cos(\alpha)}{\sin(\alpha)}$$

Where

- μ_i Ice to ice friction coefficient
- e Porosity of ice

P in equation (3.26) is the load component in the direction of the slope per unit length (see Figure 18). The first two terms in equation (3.26) takes into account the additional friction forces due to rubble weight on the slope (Figure 18 b), and the last term is the load required to push the ice blocks up the slope when no rubble is present (Figure 18 a).

H_P is the additional force required to push the oncoming sheet ice through the rubble and is found from the weight of the rubble on top of the sheet ice (see Figure 19).

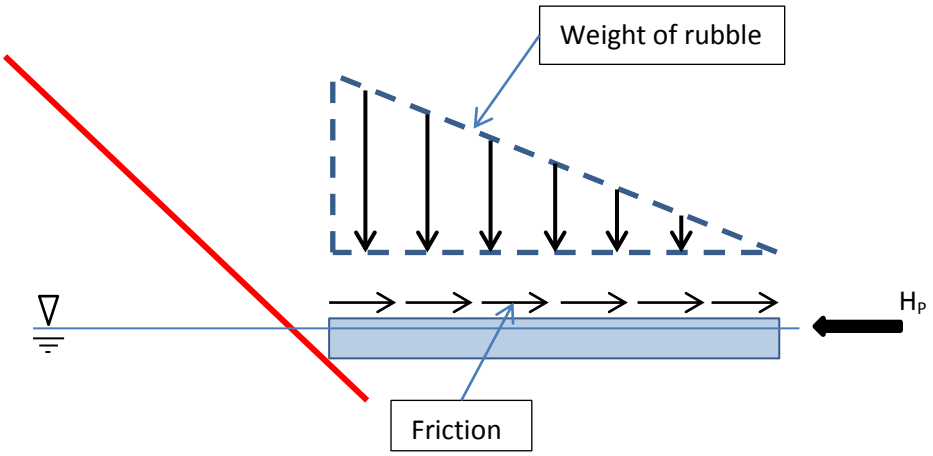

Figure 19 Load Component Required to push Advancing Ice Sheet through the Ice Rubble

The load component H_P is given as follows.

$$H_P = Dh_r^2\mu_i\rho_i g(1-\mathrm{e})\left(1 - \frac{\tan(\theta)}{\tan(\alpha)}\right)^2 \frac{1}{2\tan(\theta)} \quad (3.27)$$

H_L is the additional force required to lift and shear the ice rubble on top of the ice sheet prior to failing it by bending (see Figure 20).

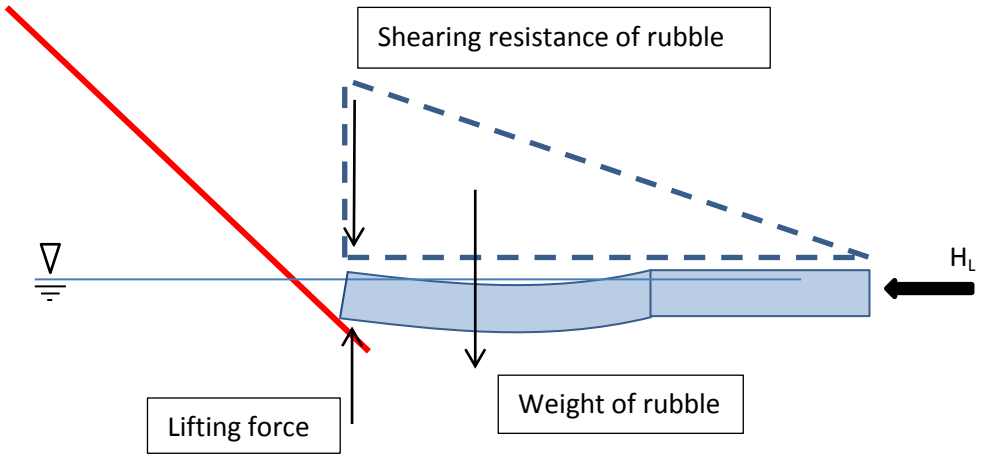

Figure 20 Load Component Required to Lift and Shear the Rubble on top of the Ice Sheet

The load component H_L is given as follows:

$$H_L = 0.5Dh_r^2\rho_i g(1-\mathrm{e})\xi\left(\frac{1}{\tan(\theta)}-\frac{1}{\tan(\alpha)}\right)\left(1-\frac{\tan(\theta)}{\tan(\alpha)}\right) + 0.5Dh_r^2\rho_i g(1-\mathrm{e})\xi\tan(\phi)\left(1-\frac{\tan(\theta)}{\tan(\alpha)}\right)^2 + \xi \mathrm{c}Dh_r\left(1-\frac{\tan(\theta)}{\tan(\alpha)}\right) \quad (3.28)$$

where c and ϕ are the cohesion and the friction angle of the ice rubble respectively.

3.3.2.4 Modification for in-plane Compression

The total horizontal force acting on the structure is given in equation (3.29) as a sum of the load components described throughout section 0.

$$F_H = H_B + H_P + H_R + H_L + H_T \quad (3.29)$$

F_H acts both on the structure and within the ice sheet, which creates a compressive stress in the ice. Due to this compression the effective flexural strength of the ice sheet increases because it has to be overcome before a tensile crack can be initiated. The effective flexural strength is given in equation (3.30).

$$\sigma_f^1 = \frac{F_H}{w_c h} + \sigma_f \quad (3.30)$$

w_c is the total length of the circumferential crack, given as follows.

$$w_c = D + \frac{\pi^2}{4} l_c \quad (3.31)$$

The increase in the flexural strength will increase the breaking term H_B, and also the total horizontal force. This increase is accounted for in the expression for the total horizontal load by the denominator in equation (3.16).

4 Static and Time Domain Analysis of Ice-Structure Interaction

For this project there has been developed two Matlab scripts to calculate level ice loads on different structures. This chapter will give a brief explanation of each script, the assumptions behind the calculations as well as the results obtained. The two scripts are given on the enclosed CD in Appendix E.

4.1 Vertical VS Sloping Geometry in the Waterline

In this section, static load estimations have been performed in Matlab to compare ice actions on a vertical structure with a downward breaking and an upward breaking structure. Schematics of the structures with the most important full scale (f. sc.) measures are given in Figure 21. More detailed schematics of the structures are given in Appendix A.

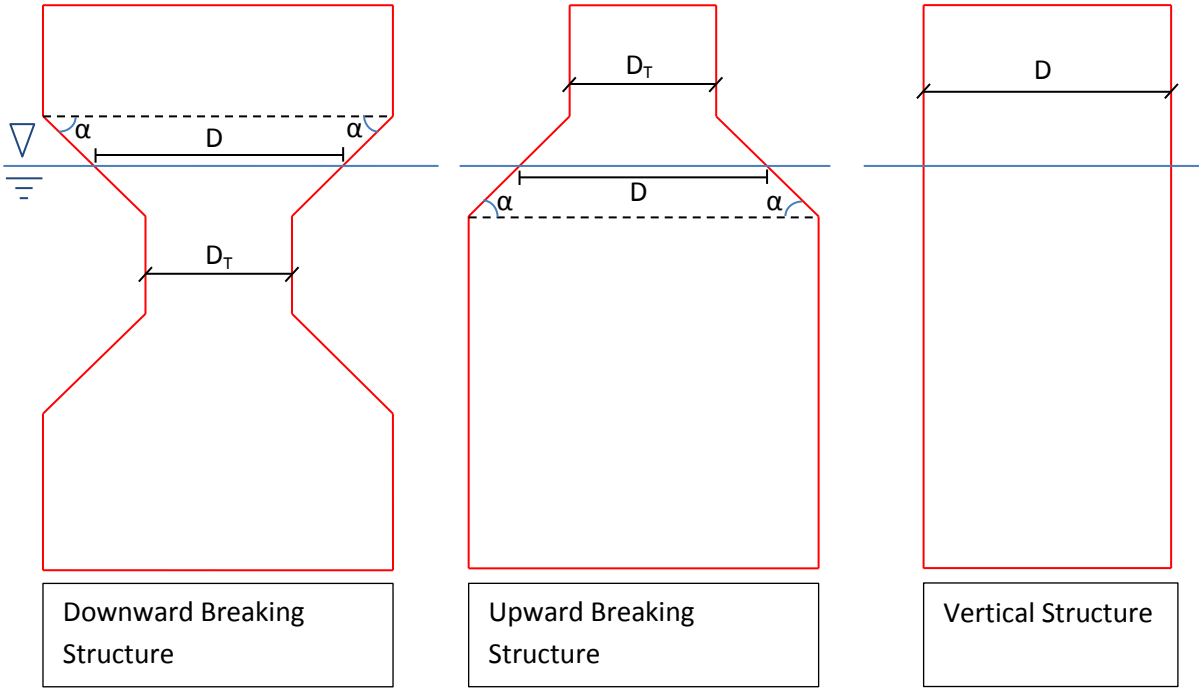

Figure 21 Schematics of the Downward Breaking Structure, the Upward Breaking Structure and the Vertical Structure

D is the waterline diameter, D_T is the diameter at the end of the sloping side and α is the sloping angle of the structure. The parameters have the following values for all the structures.

- D 30m
- D_T 20m
- α 45deg

The formulas used for the load calculations are given in Chapter 3. For the vertical structure equation (3.2) has been used, and for the sloping structures both equation (3.13) (Ralston`s method) and equation (3.16) (Croasdale`s method) have been used. To obtain the vertical load component from

Croasdale`s method, equation (3.5) have been used. The ice data used in the comparison are given in Table 1.

Table 1 Ice Data for Comparison of Vertical VS Sloping Structure

h	σ_f	ρ_i	μ	ν	E	c	ϕ	e	h_r	θ	μ_i
[m]	[MPa]	[kg/m3]	[-]	[-]	[GPa]	[kPa]	[deg]	[-]	[m]	[deg]	[-]
1.00	0.50	900.00	0.15	0.30	3.00	8.00	35.00	0.30	1.00	35.00	0.03

The parameters in Table 1 are defined as follows.

- h Ice thickness
- σ_f Flexural strength of ice
- ρ_i Density of ice
- μ Ice-structure friction coefficient
- ν Poisson`s ratio
- E The elastic modulus
- c Cohesion
- ϕ Friction angle of the ice rubble
- e Porosity
- h_r Rubble ride-up/down height
- θ Angle of repose of the rubble volume
- μ_i Ice-to-ice friction coefficient

The rubble ride-up/down height is assumed to be equal to one ice thickness for simplicity in the calculations done in this section. The angle of repose of the rubble volume is the angle the rubble volume makes with the horizontal (see Figure 16) and is given in [ISO 19906:2010] to be 10 degrees less than the sloping angle at maximum. The ice-to-ice friction is the kinetic friction given in [Serway, R.A. 4th edition].

4.1.1 Results

The results are divided into two parts to separate between which method that has been used to calculate the ice actions on the two sloping structures. In the first part Ralston`s method has been used and in the second, Croasdale`s method has been used. In both parts a comparison have been performed to analyze differences in the magnitude of ice actions between a downward breaking structure, an upward breaking structure and a vertical structure. The horizontal force (F_H), the vertical force (F_V), the resultant force (F_R) and the angle of attack of the resultant force (θ_{att}) have been calculated. The angle of attack is defined as positive from horizontal and upwards for the upward breaking structure and from the horizontal and down for the downward breaking structure (see Figure 22).

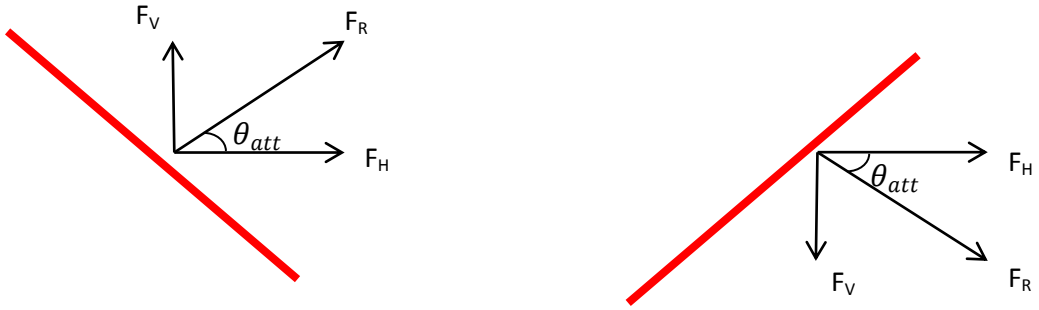

Figure 22 Load Components and the Angle of Attack for the Resultant Force

4.1.1.1 Results from Ralston`s Method

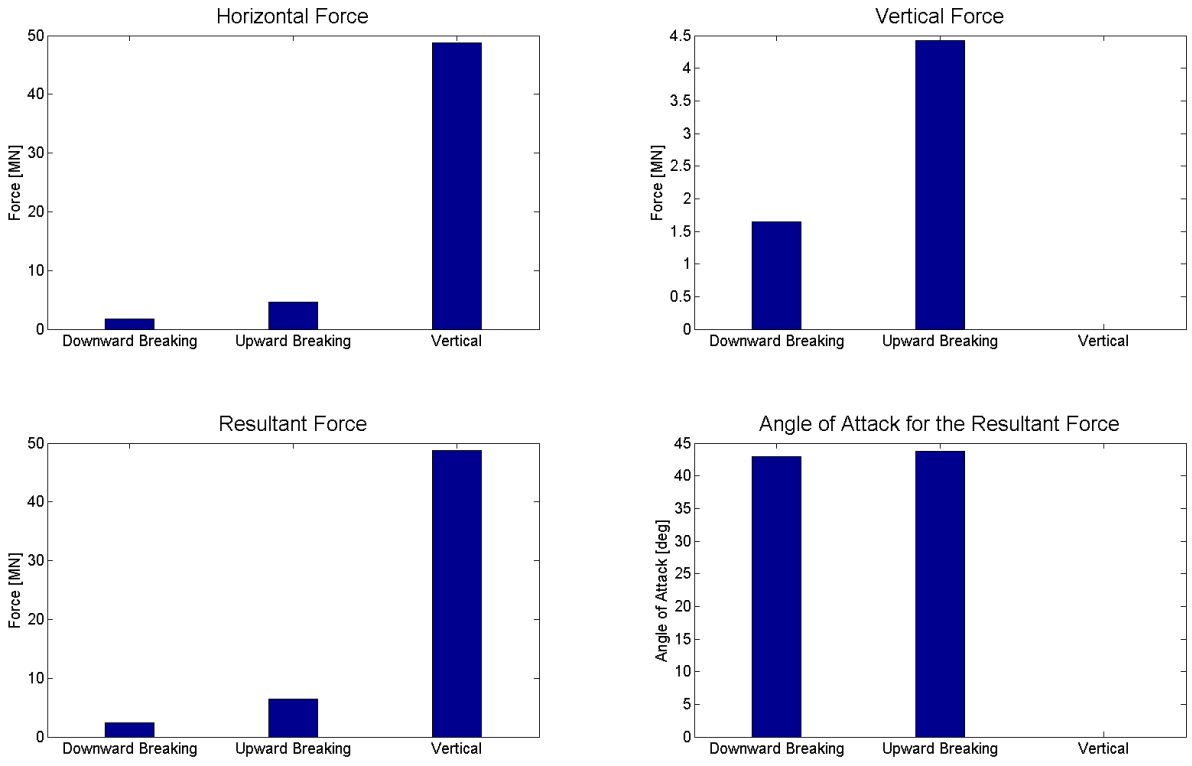

Figure 23 Vertical VS Sloping Structure, Ralston`s Method

Table 2 Vertical VS Sloping Structure, Ralston`s Method

	Downward Breaking	Upward Breaking	Vertical Structure
F_H [MN]	1.77	4.63	48.75
F_V [MN]	1.65	4.42	0.00
F_R [MN]	2.42	6.40	48.75
θ_{att}[deg]	43.00	43.71	0.00

4.1.1.2 Results from Croasdale`s Method

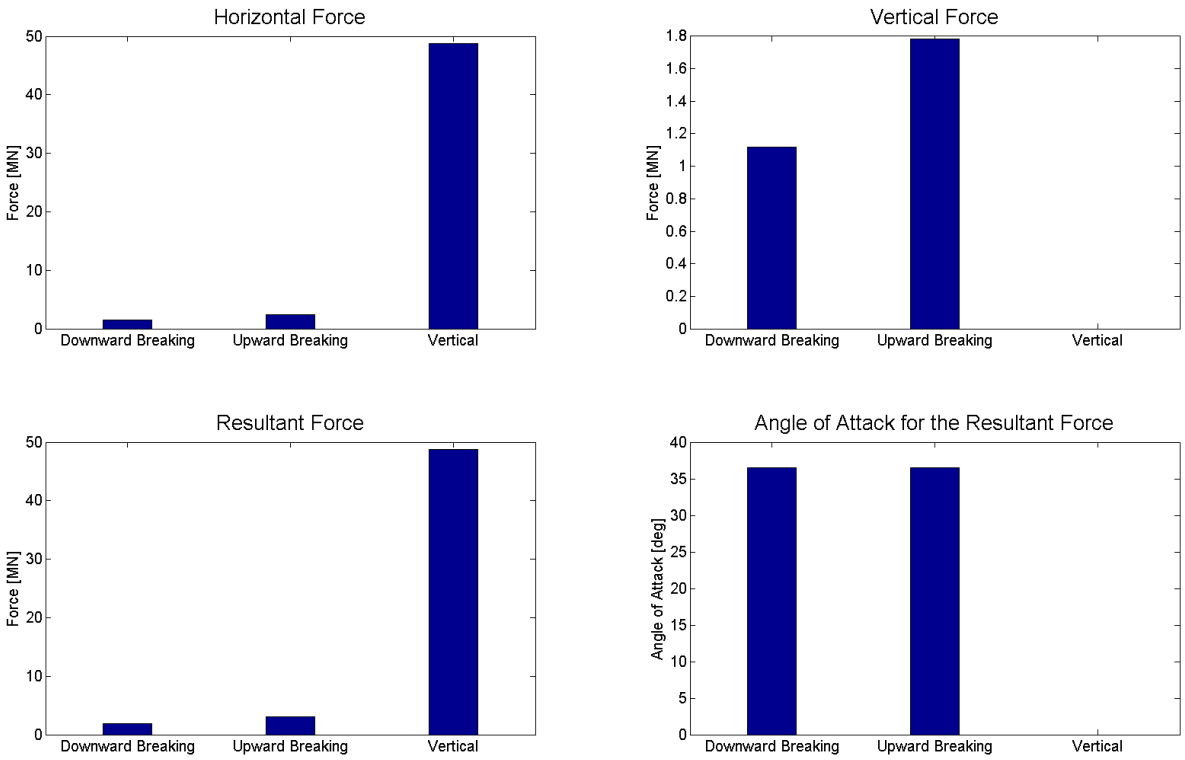

Figure 24 Vertical VS Sloping Structure, Croasdale`s Method

Table 3 Vertical VS Sloping Structure, Croasdale`s Method

	Downward Breaking	Upward Breaking	Vertical Structure
F_H [MN]	1.51	2.41	48.75
F_V [MN]	1.12	1.78	0.00
F_R [MN]	1.88	3.00	48.75
θ_{att}[deg]	36.47	36.47	0.00

4.1.2 Discussion of results

The results from Ralston`s method clearly shows that the vertical structure will experience the highest ice actions with ten to twenty times higher loads than the sloping structures. It is also seen that the upward breaking structure will experience loads more than twice as high compared to the downward breaking structure for both the horizontal, vertical and resultant load component. The resulting load components are approximately normal to the sloping sides for both the sloping structures.

From Croasdale`s method it is found that all the load components for the sloping structures are reduced compared to Ralston`s method, but the downward breaking structure experiences lower loads compared to the upward breaking one for both methods. Also, Croasdale`s method gives smaller differences between the loads on the two sloping structures compared to Ralston`s method.

From the results it is seen that a sloping geometry in the waterline is preferred when ice is present compared to a vertical geometry. A vertical geometry will experience crushing of ice which again results in much higher ice loads. For a floating facility high ice actions might exceed the mooring line capacity, which can result in disastrous situations. It would be recommended to use a sloping geometry over a vertical geometry due to the substantial difference in the magnitude of the ice actions for construction of floating facilities. To further be able to choose between the two sloping structures a response analyzes should be performed to see which structure that obtains the best motion characteristics. From the static load estimates performed here, a downward breaking structure seems to be the best option as it experiences the lowest ice loads. Also, the resultant load points downwards for an upward breaking structure, which might submerge the structure for high ice loads.

For a gravity based structure (GBS) the vertical structure would again seem to be the least appropriate choice due to its high ice loads. In this case an upward breaking structure might be the better choice of the two sloping structures as the resultant load points downward into the ground which will increase the structure`s stability. A downward breaking structure with a resultant load upwards will create an overturning moment that results in reduced stability (see Figure 25).

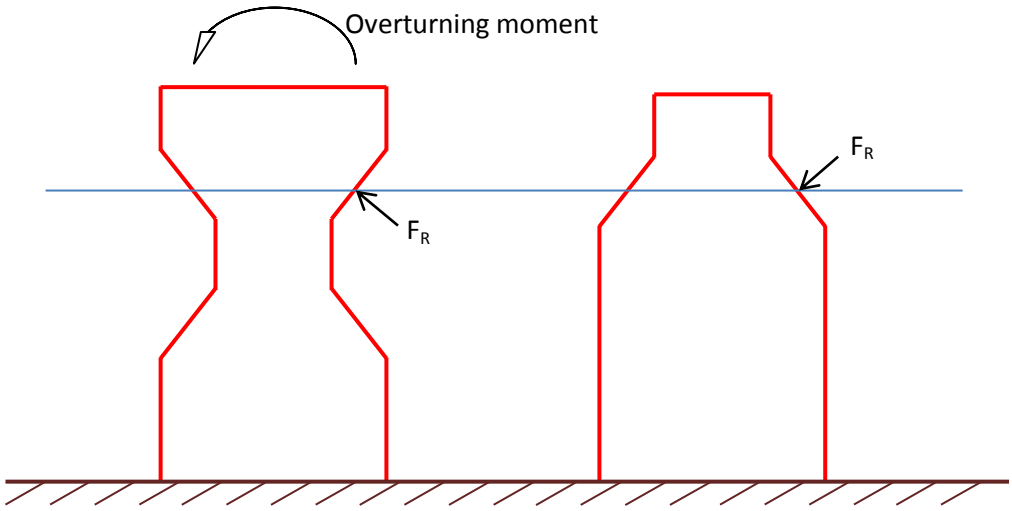

Figure 25 Overturning moment on a downward sloping GBS

4.2 Time Domain Simulation of Ice-Structure Interaction

In this section a Matlab script has been developed to calculate time varying ice actions on the downward breaking structure shown in Figure 21 using Croasdale`s method. The script is based on assumptions about how the different load contributions in equation (3.16) will vary over time due to the ice failure process and rubble accumulation. The script is given on the enclosed CD in Appendix E.

4.2.1 Theory behind the script

The ice failure process is shown in Figure 16. As the ice sheet comes in contact with the structure, a vertical force will build up until the ice sheet fails by bending. The horizontal contribution to create this vertical force is given in equation (3.23) as H_B. This bending force will occur with a period determined by the breaking length and the ice drift velocity (v). The breaking length has been assumed equal to l_c given in equation (3.21), which means that the breaking period (T_B) can be found as follows.

$$T_B = \frac{l_c}{v} \tag{4.1}$$

In this section, the time it takes for the breaking force H_B to obtain the value needed to fail the ice sheet by bending is assumed to be 0.22s. This value is obtained from a simplified deflection analysis shown in Appendix B, and is used to introduce H_B as a time varying load rather than an impulse load. It will be verified through model test videos if this is a good approximation or not. This means that H_B is assumed to use 0.22 seconds to build up to its value, and H_B will occur in the time domain with a period defined by T_B.

The ice block broken off from the ice sheet is then pushed down the slope by a force P (Figure 18 a). This force is given per unit length as the last term in equation (3.26). If the rubble ride-down height h_r in this equation is described through a varying height z this load term can be given as follows.

$$P = zh\rho_i g \frac{\sin(\alpha) + \mu\cos(\alpha)}{\sin(\alpha)} \tag{4.2}$$

$z/\sin(\alpha)$ describes the length in the sloping direction the ice block has been pushed, and is the time-varying part of this load. The time it takes to reach the end of the sloping surface is then found directly from this length and the speed of the ice sheet. Equation (4.2) can be written in the following manner to be time-dependent.

$$P = vth\rho_i g(\sin(\alpha) + \mu\cos(\alpha)) \tag{4.3}$$

As P is the load per unit length in the sloping direction it has to be multiplied with the waterline diameter, D, of the structure. To obtain the horizontal component of P, it has to be divided by $\cos(\alpha) - \mu\sin(\alpha)$ (see equation (3.5). This gives the load P as implemented in the Matlab script (equation (4.4).

$$P = vth\rho_i gD \frac{\sin(\alpha) + \mu\cos(\alpha)}{\cos(\alpha) - \mu\sin(\alpha)} \tag{4.4}$$

The load *P* in the script start from *t=0* just after the breaking load H_B has reached its maximum value, and is increasing until *z* has reached the height of the sloping structure, after which time *P* is assumed constant.

The next load component to come into action is the turning load H_T given in equation (3.24) which starts to contribute as the ice blocks have reached the end of the sloping side (see Figure 15). This load component can be made time varying by introducing a time varying angle as H_T will obtain maximum value for φ equal to the sloping angle, and is equal to zero as the ice block has reached a vertical orientation (φ=90 degrees). It has been assumed that the time the ice blocks use to obtain a vertical orientation can be found from the ice drift speed and the fact that the ice blocks are assumed to be of a length equal to 3*h* when reaching the end of the sloping side [ISO 19906:2010]. In the script this load component comes into action when the ice blocks have been pushed to the end of the sloping side with its maximum value and is decreased until the ice block is turned to vertical. It has been assumed that this process will repeat itself throughout the ice-structure interaction.

Further it has been assumed that at once after the first H_T period, rubble will start to build up in front of the structure. This means that the three remaining load components in equation (3.16), H_R, H_P and H_L will start to contribute. It has been found that these terms all depend upon the volume of ice rubble in front of the structure which is determined by the rubble ride-down height h_r and the angle of repose θ (see Figure 16 d). For these load components the ride-down height is estimated according to [Løset, S. et.al 2006]. [Løset, S. et.al 2006] describes the following two equations for estimating the ride-down height.

$$h_r = 3 + 4h \tag{4.5}$$

$$h_r = 7.6h^{0.64} \tag{4.6}$$

As the two equations give approximately the same results [Løset, S. et.al 2006], equation (4.5) has been chosen used in this section. For the rubble dependent terms this h_r value is assumed constant after the turning load has obtained a vertical orientation for the first broken off ice block. This means that the only time varying parameter for the rubble dependent terms is the angle θ. The rubble volume is found to be zero as θ is equal to the sloping angle (which gives zero load contribution from these terms), and is increasing for a *decreasing* θ. This gives an increasing load contribution for a decreasing θ. According to [ISO 19906:2010] the rubble angle θ is said to be 10 degrees less than the sloping angle at its maximum, and the script is developed so that this angle will decrease over a given time period from the sloping angle to 10 degrees less than the sloping angle. When these load components come into action the load *P* given in equation (4.4) is set equal to zero, as the load component H_R includes this load (see equation (3.26) describing the load *P* for both rubble present on the slope and no rubble present on the slope). The load components H_R, H_P and H_L are given in equations (3.25), (3.27) and (3.28) respectively.

Due to rubble transport around the structure it is difficult to determine the time it takes for the rubble volume to reach this maximum volume, but it has been assumed to take 100s in the script. This will later be analyzed in model test videos. After the rubble angle has reached its minimum value (giving the maximum rubble volume), all rubble dependent load components are assumed constant.

This means that the rubble volume in front of the structure is assumed constant due to transportation of rubble around the structure.

4.2.2 Results from four interaction cases

Based on the assumptions in section 4.2.1 a Matlab script has been developed to obtain a time varying load history for four different ice-structure interaction cases with the downward breaking structure shown in Figure 21, using Croasdale`s method. The ice drift speed (v) and the ice thickness (h) is varied in the four interaction cases. The Matlab script is found on the enclosed CD in Appendix E. The ride-down heights (h_r) for the rubble dependent terms are found from equation (4.5), the assumed breaking lengths (l_c) are determined from equation (3.21) and the corresponding breaking periods T_B are calculated from equation (4.1). All parameters are given in Table 4. The remaining ice properties of these cases are the same as for the comparison between vertical and sloping structures given in Table 1.

Table 4 Properties of the Four Interaction Cases

	v [m/s]	h [m]	h_r [m]	l_c [m]	T_B [s]
Case 1	0.50	1.00	7.00	12.86	25.72
Case 2	1.00	1.00	7.00	12.86	12.86
Case 3	0.50	1.50	9.00	17.43	34.86
Case 4	1.00	1.50	9.00	17.43	17.43

In the following, results from each case are given with plots of the total horizontal load, vertical load and resultant load. A table describing the main statistics of the loads is also given. The horizontal load component is calculated from equation (3.16) and the vertical load component from equation (3.5). The resultant load and the angle of attack of the resultant load are calculated by using the sentence of Pythagoras. Since the vertical load component is calculated as a function of the horizontal load component, the angle of attack will be constant over the entire time domain. The angle of attack of the resultant force is given for each case. All statistics are calculated after the signal has stabilized itself, i.e. from t=150s to t=500s. A brief discussion of the results will be given in section 4.2.3 to compare the different cases. A more thorough analyze of the results will be given in section 6 where the results from the Matlab script will be compared to actually achieved model test results.

4.2.2.1 Results from Case 1

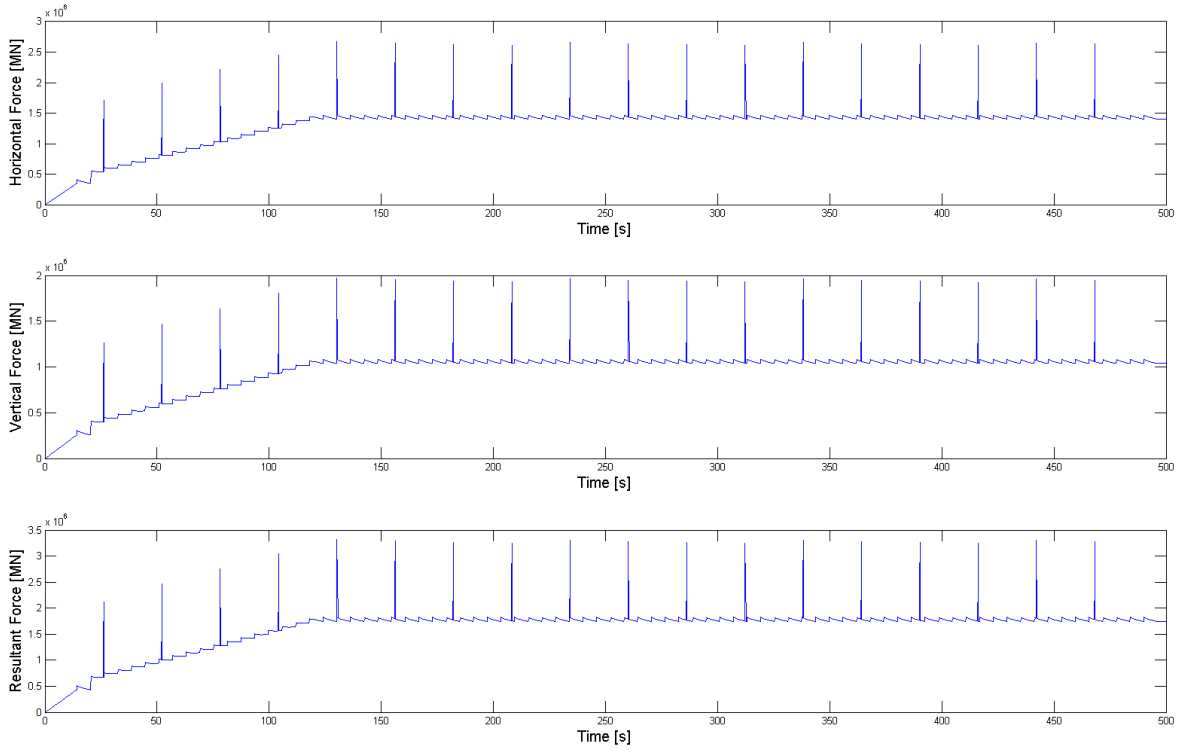

Figure 26 Time-Domain Results from Case 1

Table 5 Load Statistics from Case 1

	F_H [MN]	F_V [MN]	F_R [MN]
Max	2.67	1.97	3.31
Min	1.40	1.04	1.75
Average	1.44	1.06	1.79
Standard Deviation	0.08	0.06	0.10

The angle of attack of the resultant force was found to be 36.50 degrees.

4.2.2.2 Results from Case 2

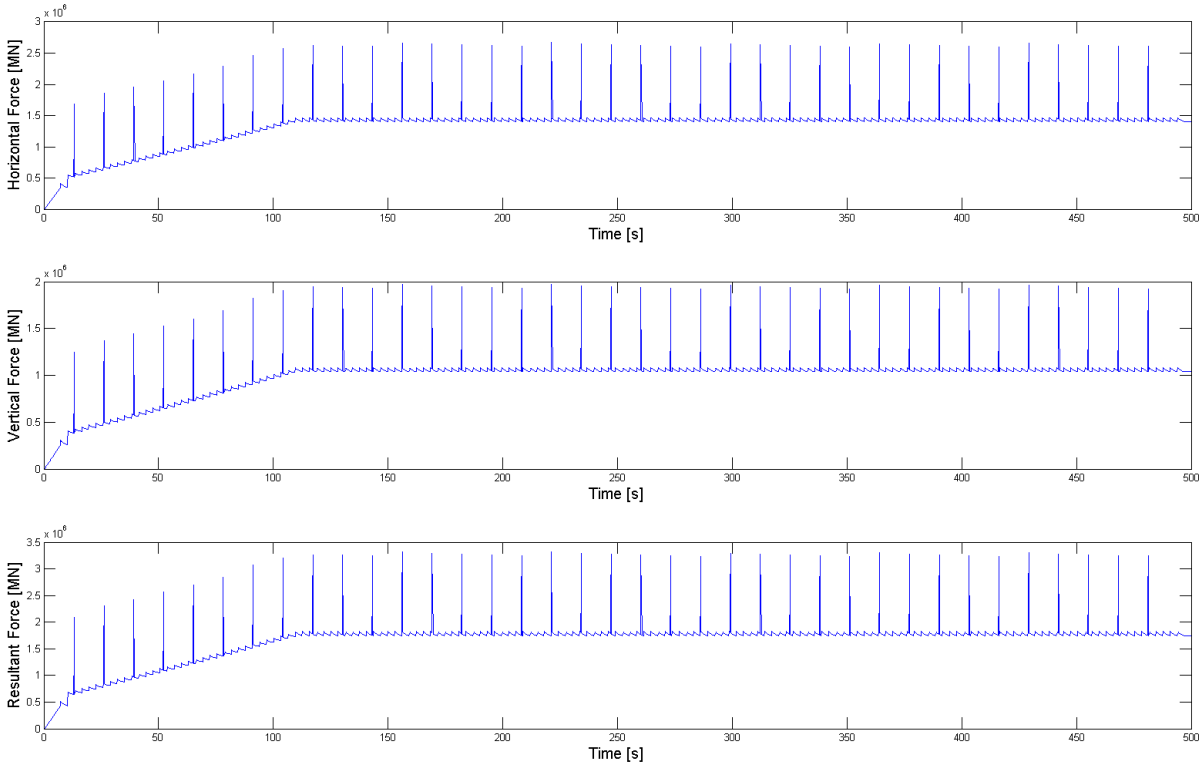

Figure 27 Time-Domain Results from Case 2

Table 6 Load Statistics from Case 2

	F_H [MN]	F_V [MN]	F_R [MN]
Max	2.67	1.97	3.32
Min	1.40	1.04	1.75
Average	1.44	1.07	1.80
Standard Deviation	0.12	0.09	0.14

The angle of attack of the resultant force was found to be 36.50 degrees.

4.2.2.3 Results from Case 3

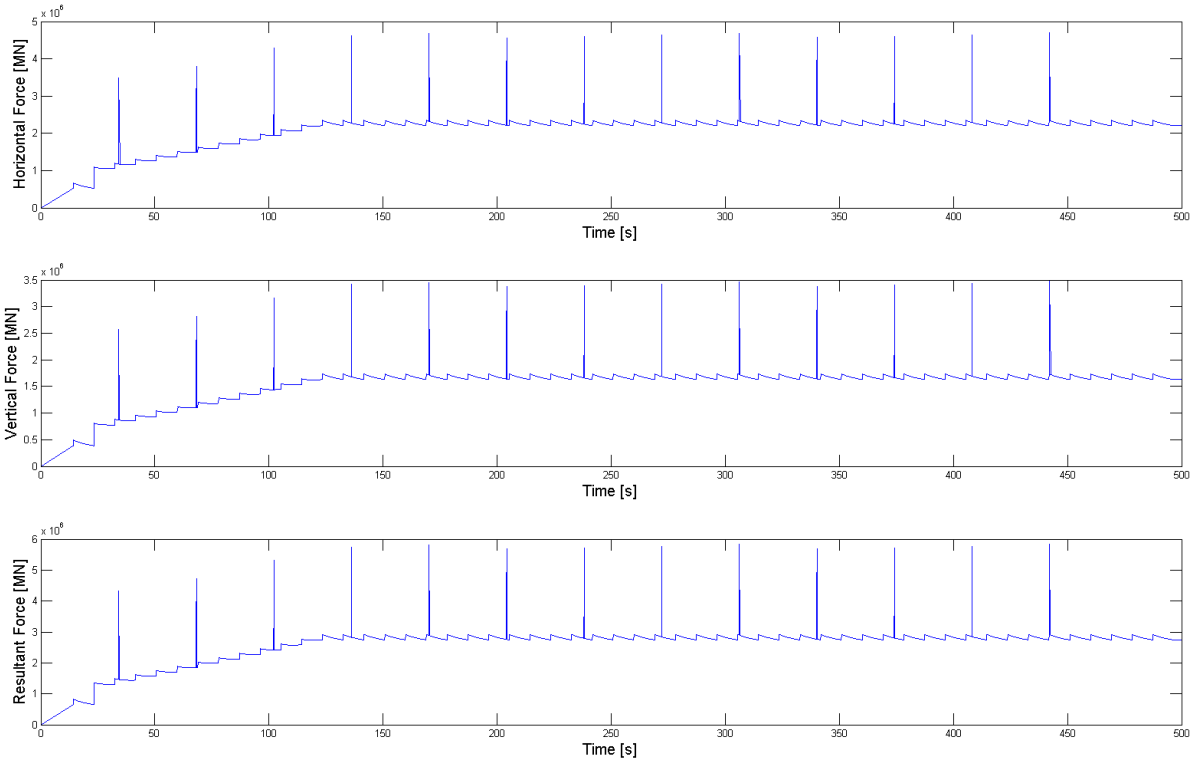

Figure 28 Time-Domain Results from Case 3

Table 7 Load Statistics from Case 3

	F_H [MN]	F_V [MN]	F_R [MN]
Max	4.70	3.47	5.84
Min	2.21	1.63	2.74
Average	2.27	1.68	2.83
Standard Deviation	0.14	0.10	0.17

The angle of attack of the resultant force was found to be 36.50 degrees.

4.2.2.4 Results from Case 4

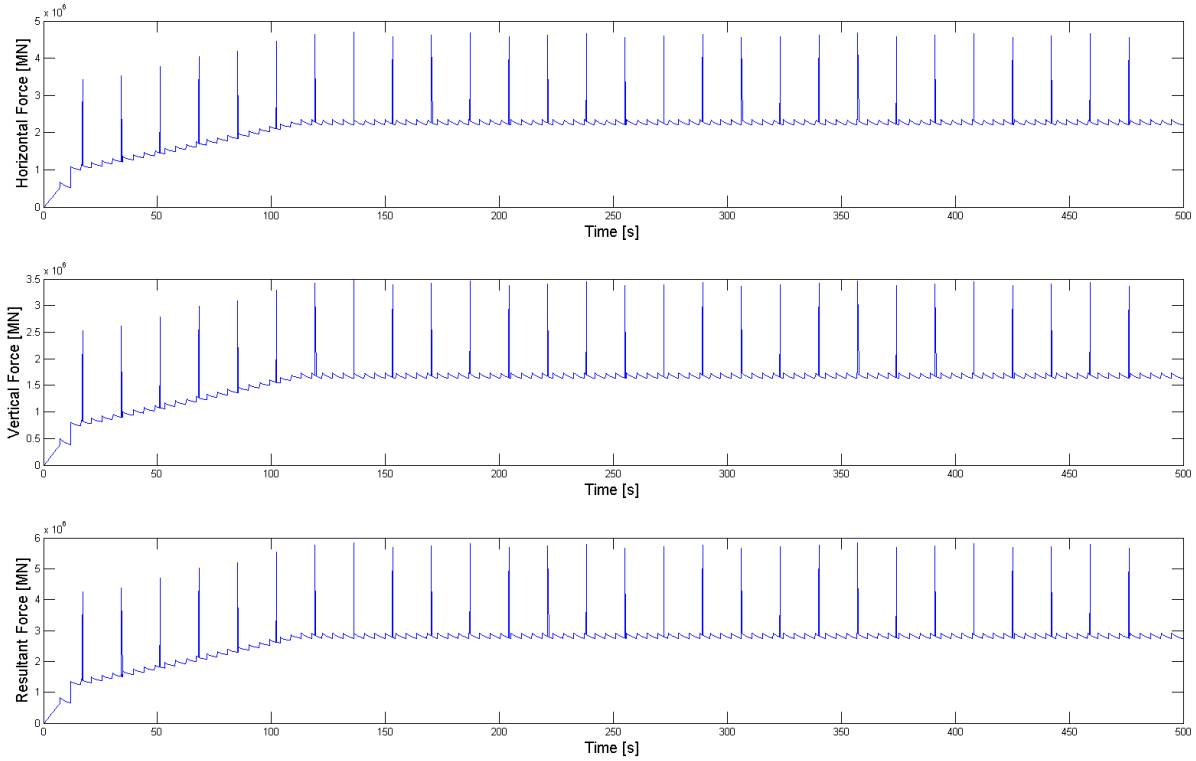

Figure 29 Time-Domain Results from Case 4

Table 8 Load Statistics from Case 4

	F_H [MN]	F_V [MN]	F_R [MN]
Max	4.69	3.47	5.83
Min	2.21	1.63	2.74
Average	2.29	1.69	2.84
Standard Deviation	0.20	0.15	0.25

The angle of attack of the resultant force was found to be 36.50 degrees.

4.2.3 Comparison of the Four Interaction Scenarios

The results from the four interaction cases are given in Table 9.

Table 9 Load Statistics from the Four Interaction Cases

	F_H [MN]				F_V [MN]				F_R [MN]			
	Max	Min	Avg	Std	Max	Min	Avg	Std	Max	Min	Avg	Std
Case1	2.67	1.40	1.44	0.08	1.97	1.04	1.06	0.06	3.31	1.75	1.79	0.10
Case2	2.67	1.40	1.44	0.12	1.97	1.04	1.07	0.09	3.32	1.75	1.80	0.14
Case3	4.70	2.21	2.27	0.14	3.47	1.63	1.68	0.10	5.84	2.74	2.83	0.17
Case4	4.69	2.21	2.29	0.20	3.47	1.63	1.69	0.15	5.83	2.74	2.84	0.25

From the results it is found that the loads are unchanged in the first two cases and also in the last two cases. From Case 1 to Case 2 the speed is increased from 0.5m/s to 1.0m/s but all other parameters are kept constant. The same is done between Case 3 and Case 4. Since the script is based purely on Croasdale`s method where no speed effects are considered in the different load components, the maximum and minimum loads will not be changed for a drift speed change. The slight differences in some of the load statistics between these cases might be due to difference in simultaneously occurrence of the different load components.

The peaks observed throughout the time series is due to the breaking load component H_B. When the speed is increased the ice will break with a shorter period (see Table 4) resulting in more frequent peaks in the time-domain. The breaking period also depend upon the characteristic length l_c (given in equation (3.21)) which will increase when the ice thickness is increased, resulting in a longer breaking period. Due to the short duration of the breaking load this component affect the average loads very slightly even when it occurs more frequent. It does however affect the standard deviation some, with a larger standard deviation of the loads for increased speed. In Croasdale`s method the total static ice action is found when all the different load components contribute. This means that by using Croasdale`s method directly, the calculated maximum value given in Table 9 would be the value obtained for the different interaction cases. Under the assumption that the breaking load component only will contribute over a very short time period as explained in section 4.2.1, the average loads are much lower than the maximum loads. For a numerical calculation tool it might be of most interest to establish an estimate of the average loads, and then by implementing a safety factor, maximum loads can be accounted for. The ice actions calculated with this model will be compared to model test results in section 6, where the average loads obtained from the model tests will be examined. It will then be found if the average loads from the numerical calculations will be within an acceptable range of the average loads measured from the model tests, even though the breaking component does not influence the average loads significantly in the numerical model.

When comparing Case 1 with Case 3 and Case 2 with Case 4 (drift speed kept constant, ice thickness increased) a great load increase is observed. When the ice thickness is increased the rubble ride-down height is increased which results in an increase of all the load components in Croasdale`s method.

It is assumed that an increase in drift speed will increase the loads due to more crushing of ice in the failure process. The script does not implement any load increase due to an increase in the drift speed, and it will be discussed in section 6 if this creates great deviations from the model test results or not.

5 Ice Model Test Analysis

To verify the calculation method established in section 4.2, a comparison with model test data from similar tests will be performed. In 2007 Aker Solutions executed a project on behalf of Chevron Norway to perform ice model tests on the two sloping structures shown in Figure 21. In this thesis model tests performed with the downward breaking structure will be analyzed. The four interaction cases described in section 4.2 have the same ice properties as four model tests performed with this downward breaking structure. In this section an analysis of these model tests will be performed, containing a description of the model test set-up and which ice parameters that were measured. This section is based on the report produced in accordance with the model tests, [Mattsson, T. 2007], and the report describing the model test facility [MARC Report 2001]. In section 6 a comparison between the measured loads from the model tests and the results from the calculation model will be performed. The script will also be corrected for the deviations achieved.

5.1 Model Test Set-up and Measurement Analysis

The model tests were executed at Masa-Yards Arctic Research Centre (MARC) by Aker Arctic. The total length of the test basin is 76m where the total test length is 60m. The width of the basin is 6.5m and the depth is 2.3m. There is also a shallow water section of the basin with a length of 26m and a depth varying from 0.0m to 0.8m. For the tests performed in 2007 a towing carriage was used to tow the structure through a stationary model ice field, where the ice properties were carefully measured to obtain the desired target values.

The main goals for the tests performed were to establish the global forces acting on the model as well as visually see how rubble accumulate in front of the structure for different towing speeds and ice thicknesses. The structure was attached to the towing carriage through a six-component balance used to measure the forces acting on the structure. Three transducers measure the vertical forces, and three transducers measure the vertical forces [MARC Report 2001] (see Figure 30).

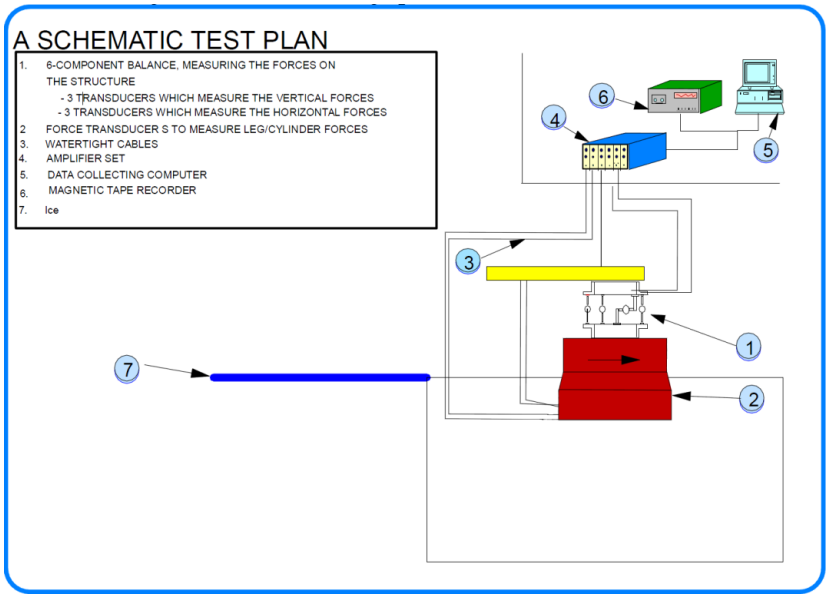

Figure 30 Schematics of the Test Set-Up [MARC Report 2001]

The six-component balance consists of two relatively stiff rings placed above one another. The rings are interconnected through six force transducers, three of which being in vertical position and three placed horizontally. The connecting points lie on a division circle of 0.7m in diameter. The middle points of the transducers are balanced and are placed at intervals of 60°, horizontal and vertical transducers in turn. The six-component balance is presented in more detail in Figure 31.

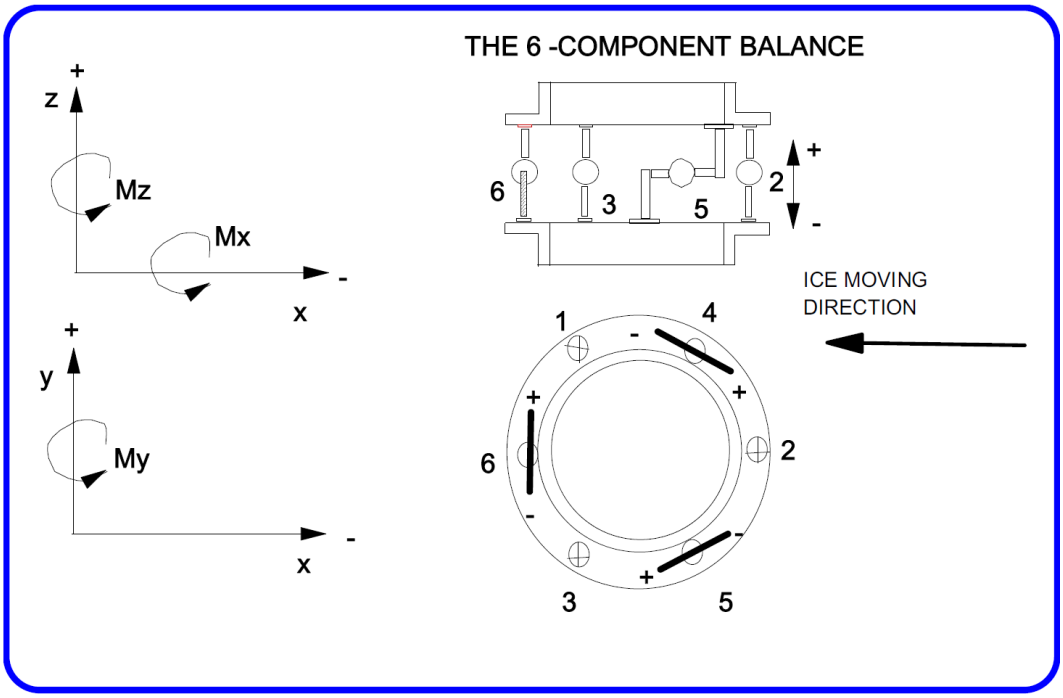

Figure 31 Six-Component Balance [MARC Report 2001]

Transducers 1, 2 and 3 in Figure 31 measure the vertical forces (described as F_{ver1}, F_{ver2} and F_{ver3}) and transducers 4, 5 and 6 measures the horizontal forces (F_{hor1}, F_{hor2} and F_{hor3}). The total forces and moments acting on the structure can be derived from these measured forces through the following equations.

$$F_x = -[F_{hor4}\sin 60° + F_{hor5}\sin 300° + F_{hor6}\sin 180°]$$

$$F_y = -[F_{hor4}\cos 60° + F_{hor5}\cos 300° + F_{hor6}\cos 180°]$$

$$F_z = -F_{ver1} - F_{ver2} - F_{ver3}$$

$$M_x = -rF_{ver1}\sin 120° - rF_{ver3}\sin 240° \quad (5.1)$$

$$M_y = rF_{ver1}\cos 120° + rF_{ver2}\cos 0° + rF_{ver3}\cos 240°$$

$$M_z = -r[F_{hor4} + F_{hor5} + F_{hor6}]$$

The parameters in equation (5.1) are defined as follows.

- F_x Total force in x-direction
- F_y Total force in y-direction
- F_z Total force in z-direction
- M_x Total moment around the x-axis
- M_y Total moment around the y-axis
- M_z Total moment around the z-axis
- r Radius of middle point of the transducers, in this case 0.35m

The coordinate system is shown in Figure 31. Note that the ice drift direction is in the positive x-direction.

In the MARC facility a well-recognized FGX (F=fine, G=grained, X=containing fresh water layers) model ice type is used. This model ice has a great ability to scale both the strength components and the elasticity together correctly. To manufacture a level ice sheet, the level ice thickness, its flexural strength and the scaling factor need to be given. Properties such as the compressive strength, the positions for the property measurements and possible special measurements that need to be conducted before or after the test run also have to be known before the ice sheet is manufactured.

Before the test both the flexural strength of the ice and its modulus of elasticity are measured by bending beams of ice downwards. After the test the ice thickness is measured throughout the longitudinal direction of the testing length for every 1m at both sides of the broken channel. The flexural strength is also control measured after the test. If desired it is possible to measure the density and crushing strength of the ice before the test, and the width of the broken channel after the test. The flexural strength of the ice is measured using in-situ cantilever beams through the following formula.

$$\sigma_f = \frac{6Fl}{bh^2} \tag{5.2}$$

F is the maximum loading force, l is the length of the beam, b is the width of the beam and h is the ice thickness. The elasticity modulus can be found from the beam test through the following formula.

$$E = \frac{Fl^3}{3\delta I} \tag{5.3}$$

δ is the deflection in the free end of the beam. The modulus of elasticity can also be determined by the infinite plate testing where the ice sheet is loaded with known weight and the deflection is measured.

$$E = \frac{3}{16}\frac{1-\nu^2}{kh^3}\left(\frac{F}{\delta}\right)^2 \tag{5.4}$$

Here, k is the modulus of foundation. The ice density is found based on the measurements of the buoyancy when the sawn ice plate is pushed under water from the following equation.

$$\rho_i = \rho_w - \frac{F}{g\pi\left(\frac{d}{2}\right)^2 h} \tag{5.5}$$

Where d is the diameter of the ice plate to be pushed under water. The compressive strength (σ_c) is measured by loading a cubic ice block cut out from the level ice sheet (sides equal to the ice thickness) both vertically and horizontally in an electric press. The compressive strength is found as follows.

$$\sigma_c = \frac{F}{h^2} \tag{5.6}$$

The crushing strength (σ_{cr}) is found from pushing an indenter with a diameter of 50mm against the level ice edge at a constant speed of 1, 10 and 20mm/s. The typical test length is 0.5-1.0m. The indenter is equipped with a force transducer for measuring the total load, and the crushing strength is found from the following formula.

$$\sigma_{cr} = \frac{F}{C_i mkbh} \tag{5.7}$$

m is the shape factor (here 0.9), b is the diameter of the indenter, k is the contact factor (0.4 … 0.7) and C_i is a factor depending on the b/h ratio.

Another important ice parameter that can be measured is the ice-structure friction coefficient. By varying the priming paint content to the lacquer layer applied last on the model surface the friction coefficient is controlled. Any friction coefficient between 0.02 and 0.20 can be achieved to an accuracy within a deviation of 0.01.

5.1.1 Model Test Program

The downward breaking model was built in a scale 1:30 giving a scaling factor λ equal to 30 (by using Froude scaling). This factor is used to scale all measured and calculated values from model scale (m. sc.) to full scale (f. sc.). Some important scaling rules are given below.

- Length $L_{fsc} = \lambda L_{msc}$
- Velocity $v_{fsc} = \sqrt{\lambda} v_{msc}$
- Time $t_{fsc} = \sqrt{\lambda} t_{msc}$
- Force $F_{fsc} = \lambda^3 F_{msc}$

The four model tests with similar ice properties as the four interaction cases described in this thesis were run over two days. The tests related to Case 1 and 2 were run the one day with a target level ice thickness of 33mm (1.0m f. sc.) and the tests related to Case 3 and 4 the other day with a target level ice thickness of 50mm (1.5m f. sc.). The ice sheet was divided into frames of length 1m. The model was pushed through the first 20 frames with a velocity of 0.5m/s (f. sc.) and through the next 10 frames with a velocity of 1.0m/s (f. sc.) both days.

5.1.2 Ice Properties Measured During the Model Tests

By inspecting Croasdale`s calculation method the ice parameters that influence the ice loads the most is the flexural strength of the ice, σ_f, the level ice thickness, h, and the ice-structure friction

coefficient, μ. Also the modulus of elasticity, E, and the density of ice, ρ_i, will to some extent influence the ice loads. The ice loads will be increased by increasing σ_f, h and μ or decreasing E and ρ_i.

The prepared ice sheet was divided into 60 frames of 1.0m length each. The two tests with speed 1.0m/s were run through the first 20 frames and the two tests with speed 1.5m/s through the next 10 frames. Other tests were run in the last 30 frames, but these will not be addressed in this thesis. The ice thickness h was measured in all frames at both the starboard and port side of the structure to control the ice thickness throughout the testing length. The flexural strength was measured in one frame within each testing length before the test run with two cantilever beam tests. The modulus of elasticity was measured in one frame outside both the level ice testing lengths and the density of the ice was only control measured in some of the ice sheets as the density of the FGX model ice is constant. The following target values were valid for all cases.

- μ kept constant at 0.05
- σ_f target value of 18kPa m. sc. (500kPa f. sc.)
- E/σ_f target value above 1000

In the following a description of the actual measured ice properties are given for each case. The measured ice properties are given in [Mattsson, T. 2007].

5.1.2.1 Case 1

The target value of the level ice thickness for this test was 33mm m. sc. (1.0m f. sc.). The test related to Case 1 was run through the first 20 frames of the modeled ice sheet. Figure 32 shows the variation in the level ice thickness over the testing length with starboard and port thickness values for each frame. In [Mattsson, T. 2007] there are no values for the thickness in the first 3 frames. Table 10 gives average values and standard deviation of the ice thickness over the testing length.

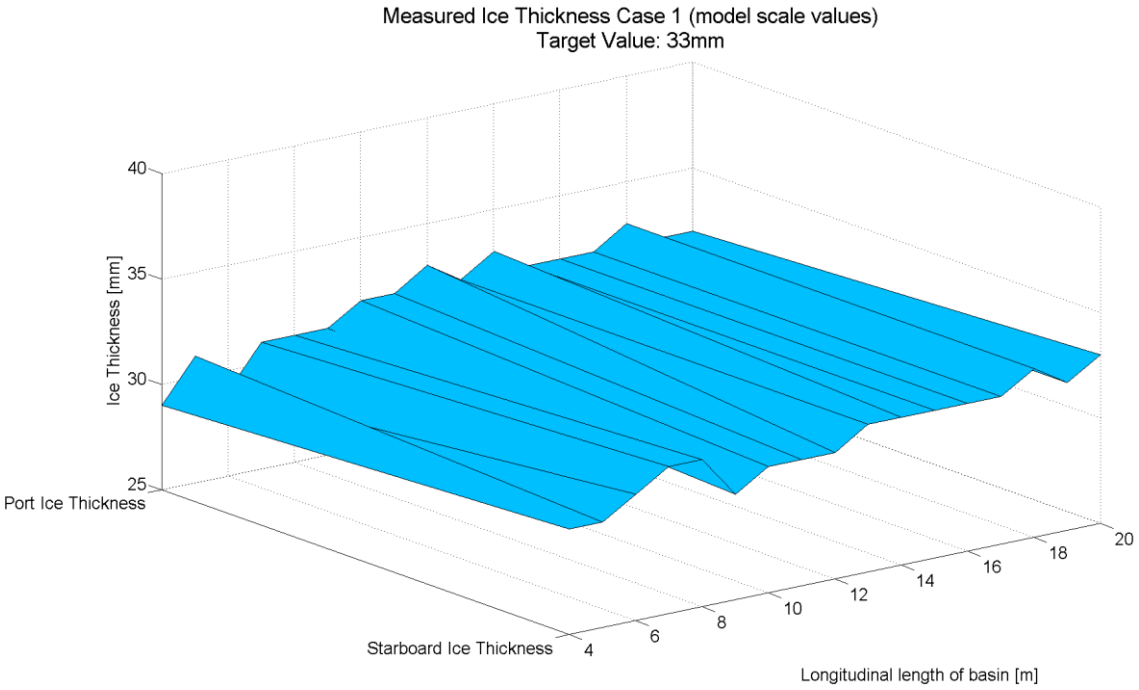

Figure 32 Measured Ice Thickness Case 1

Table 10 Statistics of the Ice Thickness Case 1

	Model Scale [mm]		Full Scale [m]	
	Starboard	Port	Starboard	Port
Average	31.53	31.59	0.95	0.95
Stdev	0.94	1.18	0.03	0.04
Stdev/avg	0.03	0.04	0.03	0.04
Diff. from target	-4.46%	-4.28%	-5.41%	-5.24%

The flexural strength was measured in frame 16 with two cantilever beam tests. The modulus of elasticity was measured with two infinite plate tests with different weights in frame 40. The density of ice was also control measured, and the values obtained are given in Table 11.

Table 11 Measured Ice Properties Case 1

		Model Scale	Full Scale
σ_f	[kPa]	19.12	573.60
E/σ_f	[-]	3605.00	3605.00
ρ_i	[kg/m^3]	925.74	925.74

5.1.2.2 Case 2

The target value of the level ice thickness for this test was 33mm m. sc. (1.0m f. sc.). The test related to Case 2 was run from frame 20 to frame 30 in the modeled ice sheet. Figure 33 shows the variation in the level ice thickness over the testing length with starboard and port thickness values for each frame. Table 12 gives average values and standard deviation of the ice thickness over the testing length.

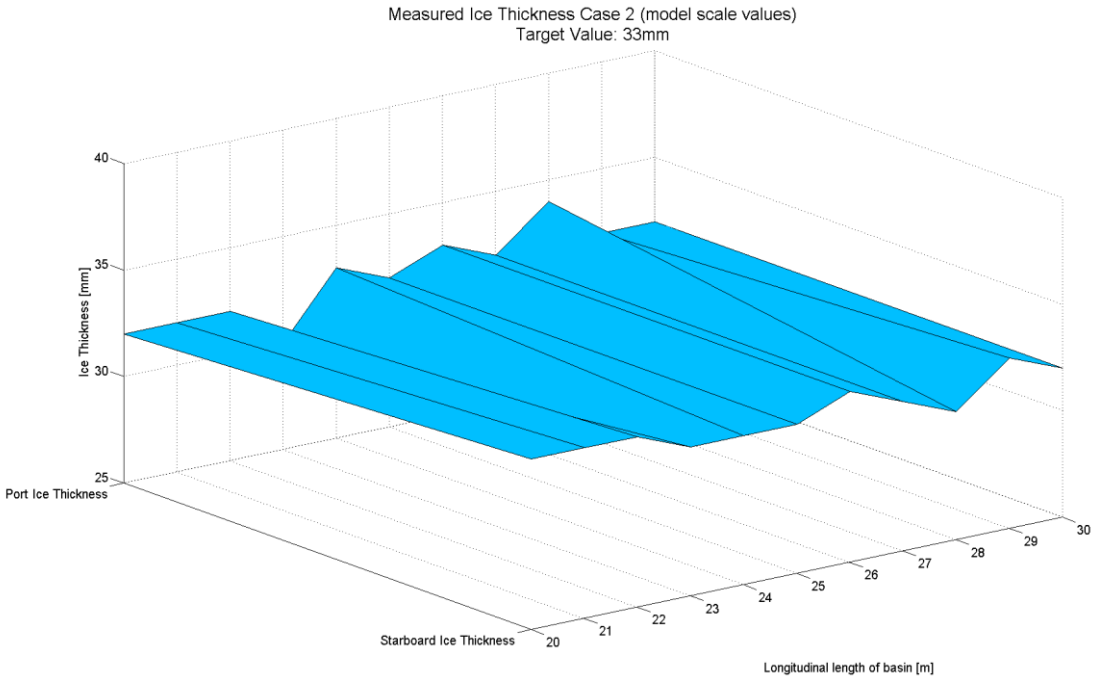

Figure 33 Measured Ice Thickness Case 2

Table 12 Statistics of the Ice Thickness Case 2

	Model Scale [mm]		Full Scale [m]	
	Starboard	Port	Starboard	Port
Average	32.36	32.18	0.97	0.97
Stdev	0.67	0.98	0.02	0.03
Stdev/avg	0.02	0.03	0.02	0.03
Diff. from target	-1.92%	-2.48%	-2.91%	-3.45%

The flexural strength was measured in frame 28 with two cantilever beam tests. The modulus of elasticity was measured with two infinite plate tests with different weights in frame 40. The density of ice was also control measured, and the values obtained are given in Table 13.

Table 13 Measured Ice Properties Case 2

		Model Scale	Full Scale
σ_f	[kPa]	24.21	726.3
E/σ_f	[-]	2847.07	2847.07
ρ_i	[kg/m^3]	925.74	925.74

5.1.2.3 Case 3

The target value of the level ice thickness for this test was 50mm m. sc. (1.5m f. sc.). The test related to Case 3 was run through the first 20 frames of the modeled ice sheet. Figure 34 shows the variation in the level ice thickness over the testing length with starboard and port thickness values for each frame. In [Mattsson, T. 2007] there are no values for the thickness in the first 2 frames. Table 14 gives average values and standard deviation of the ice thickness over the testing length.

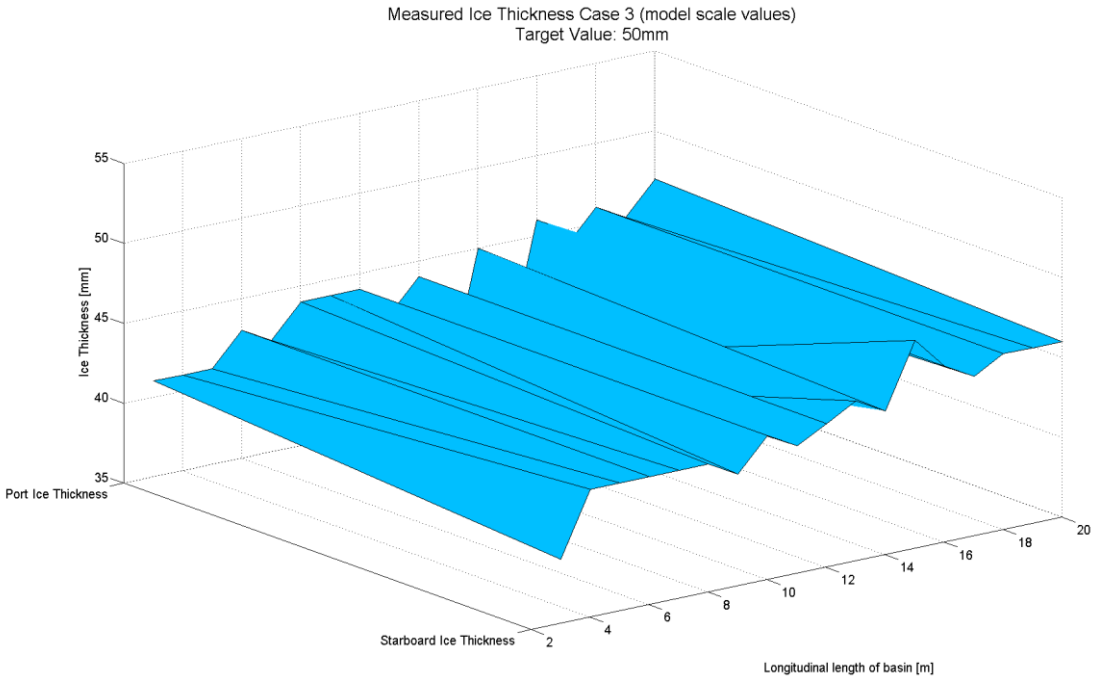

Figure 34 Measured Ice Thickness Case 3

Table 14 Statistics of the Ice Thickness Case 3

	Model Scale [mm]		Full Scale [m]	
	Starboard	Port	Starboard	Port
Average	44.06	43.00	1.32	1.29
Stdev	2.01	2.68	0.06	0.08
Stdev/avg	0.05	0.06	0.05	0.06
Diff. from target	-11.89%	-14.00%	-11.89%	-14.00%

The flexural strength was measured in frame 16 with two cantilever beam tests. The modulus of elasticity was measured with two infinite plate tests with different weights in frame 40. The density of ice was also control measured, and the values obtained are given in Table 15.

Table 15 Measured Ice Properties Case 3

		Model Scale	Full Scale
σ_f	[kPa]	25.28	758.4
E/σ_f	[-]	617.86	617.86
ρ_i	[kg/m^3]	920.22	920.22

5.1.2.4 Case 4

The target value of the level ice thickness for this test was 50mm m. sc. (1.5m f. sc.). The test related to Case 4 was run from frame 20 to frame 30 in the modeled ice sheet. Figure 35 shows the variation in the level ice thickness over the testing length with starboard and port thickness values for each frame. Table 16 gives average values and standard deviation of the ice thickness over the testing length.

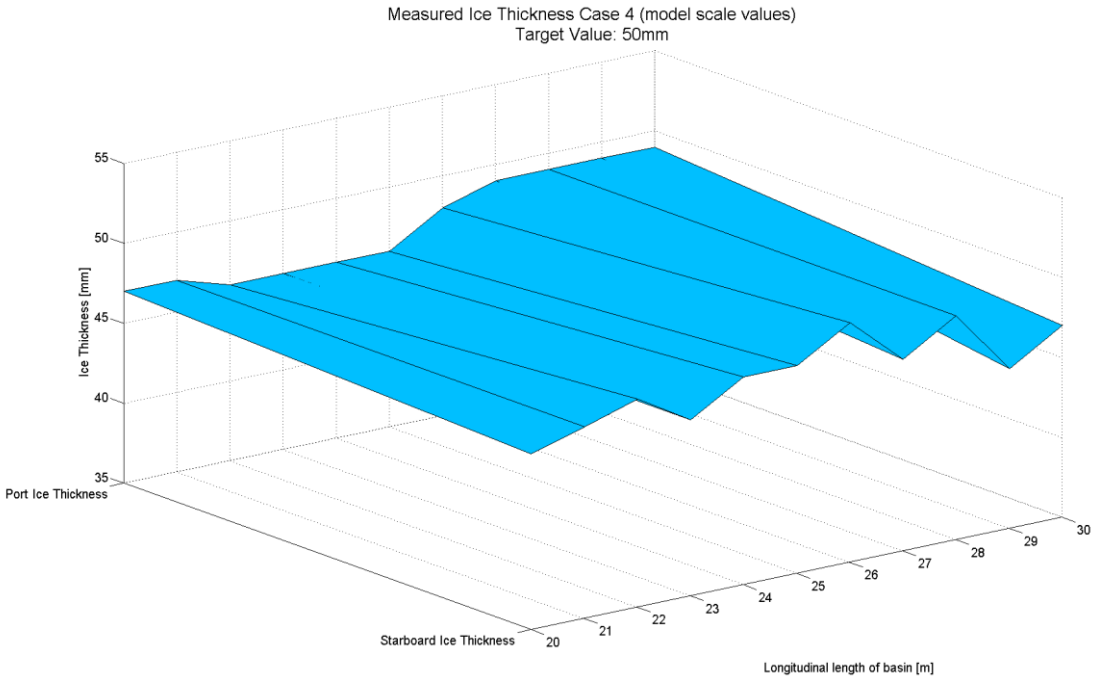

Figure 35 Measured Ice Thickness Case 4

Table 16 Statistics of the Ice Thickness Case 4

	Model Scale [mm]		Full Scale [m]	
	Starboard	Port	Starboard	Port
Average	47.36	47.54	1.42	1.42
Stdev	1.43	1.37	0.04	0.04
Stdev/avg	0.03	0.03	0.03	0.03
Diff. from target	-5.27%	-5.09%	-5.27%	-5.09%

The flexural strength was measured in frame 28 with two cantilever beam tests. The modulus of elasticity was measured with two infinite plate tests with different weights in frame 40. The density of ice was also control measured, and the values obtained are given in Table 17.

Table 17 Measured Ice Properties Case 4

		Model Scale	Full Scale
σ_f	[kPa]	22.67	680.10
E/σ_f	[-]	688.99	688.99
ρ_i	[kg/m^3]	920.22	920.22

5.1.3 Model Testing of Structures in Fixed Mode VS Structures in Moored Mode

When performing model tests of SPAR buoys in ice conditions, there are mainly two different test set-ups that are used. A SPAR buoy designed for Arctic areas will most likely operate in deep waters where a moored solution might be the most feasible. As a result, the model tests are performed with a fixed or a moored model test set-up.

In the fixed set-up the model is suspended from a rigid tow post connected to the towing carriage. The model is towed through a stationary ice feature at a given towing speed. The towing speed represents the ice drift velocity in a real-life situation. In a moored test set-up the model is moored to the bottom of the test basin, and ice is pushed against the structure. The two test set-ups are presented in Figure 36.

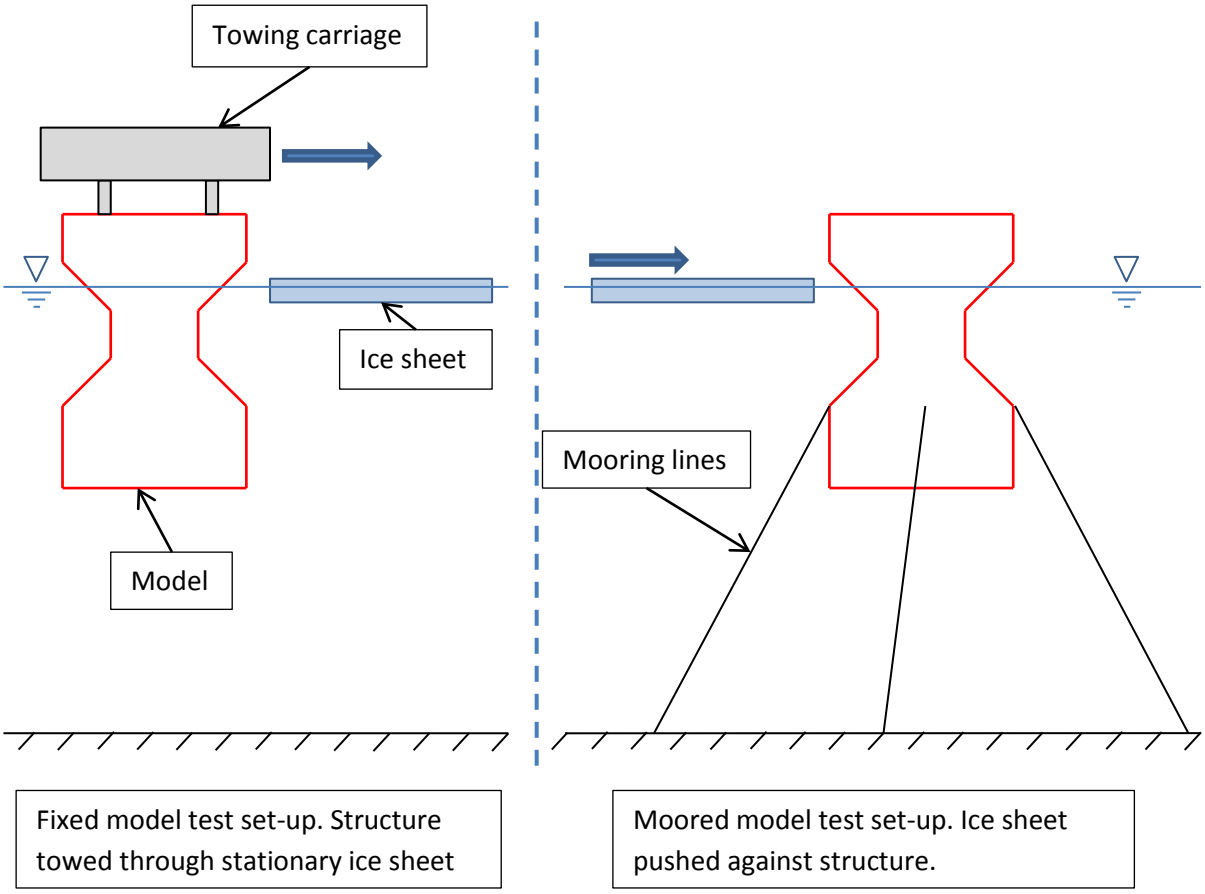

Figure 36 Fixed VS Moored Model Test Set-Up

When performing a fixed model test, the horizontal and vertical load on the structure is measured through force transducers connecting the structure and the towing carriage. The moments can be calculated from these measurements as described in section 5.1. For a moored model test set-up the motions of the model in six degrees of freedom and the velocities and accelerations of the model can be measured. Also the individual mooring line loads and the resulting mooring line restoring loads and moments can be measured in addition to the ice loads against the hull [Bruun, P.K. et.al. 2009].

The ice pressure exerted on the model will differ for a fixed model versus a moored model. The moored model will e.g. experience a surge motion in the ice drift direction before the mooring lines are able to withstand the ice actions. This results in a pitch motion of the model which creates a steeper sloping side that might increase the ice actions. Also a bigger waterline area is obtained from this motion which might increase the loads. Since the fixed model is restrained from moving, results obtained might give a better picture on how different ice configurations affect the pure ice actions. A moored model will on the other hand give a more real-life view of the actual interaction process, but the pure ice loads exerted on the structure might be more difficult to predict as numerous factors influence the interaction scenario.

In this thesis, data from model tests performed on a fixed construction towed through a stationary ice sheet is used to analyze the loads acting on the structure. The model test data is given in accordance with [Mattsson, T. 2007]. In addition, the model tests were filmed with four different cameras. Two cameras shows the model from the top at two different angles, one camera films the

model from below the waterline showing the model from the side and one camera is filming the model from directly underneath. Figure 37 shows an example of the camera views from the test corresponding to Case 1.

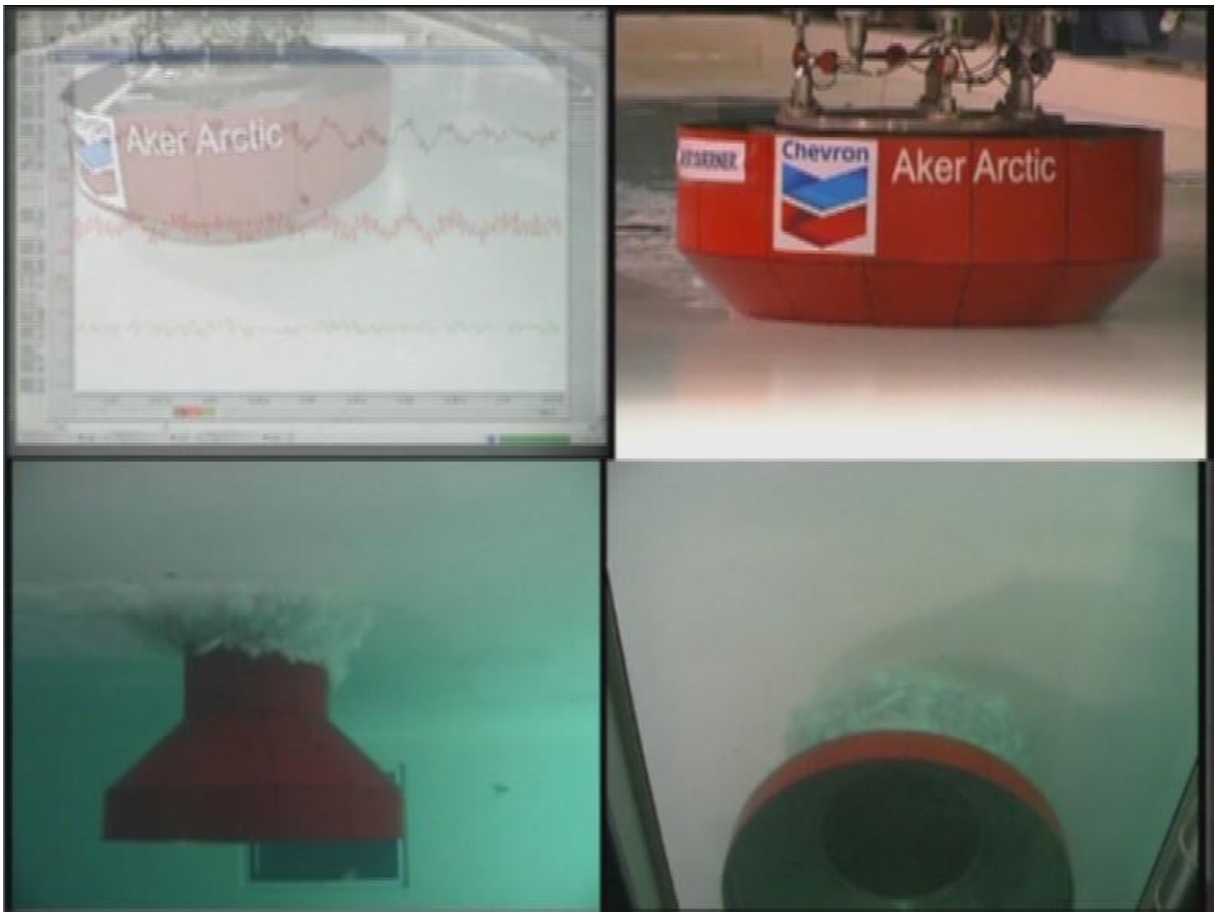

Figure 37 Camera Views in the Model Test Videos

5.2 Analysis of Test Results

In this section an analysis has been performed on the model test data from the four tests performed with the downward breaking structure corresponding to the four interaction cases described in section 4.2.2. The schematics of the downward breaking structure with full scale measurements are given in Figure 38.

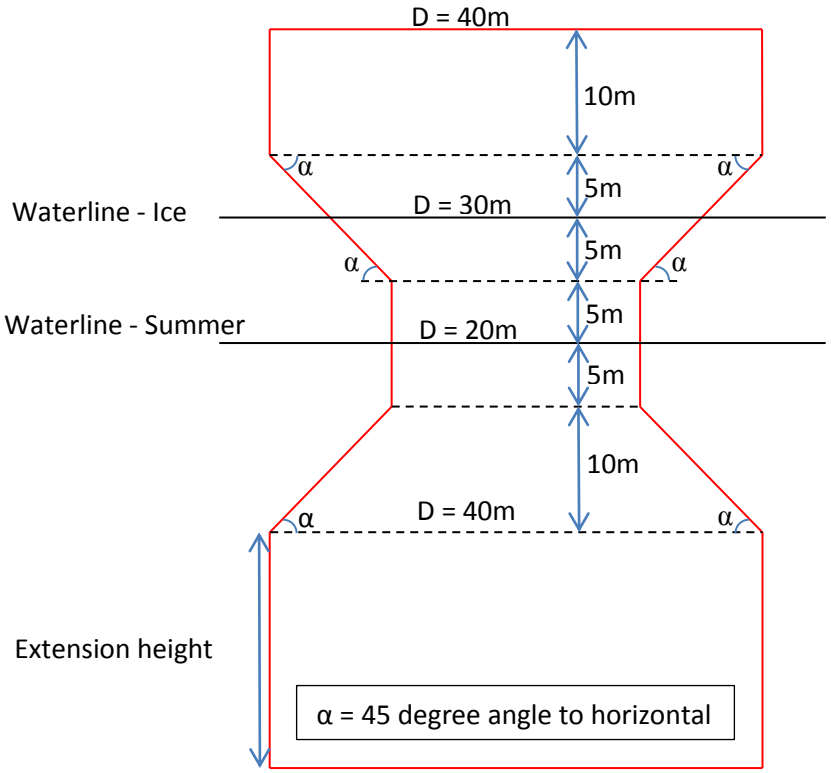

Figure 38 Schematics of the Downward Breaking Structure Analyzed in the Model Tests

The test data have been scaled up to full-scale values. Both the horizontal and vertical loads are analyzed, as well as the resulting load and the angle of attack of the resultant load. The main objective in this section has been to try to describe the rubble geometry, the rubble failing period and the breaking length (*br*) of the ice sheet from visual measurements in the videos. It is assumed that the ice loads will build up from ice impact to a more or less constant level due to rubble accumulation in front of the structure. The loads are assumed to reach a more or less constant level due to rubble transport around the structure (i.e. the rubble volume is kept more or less constant). Further it is assumed that after the rubble volume has reached this relatively constant size it will fail and build up again approximately to this constant level throughout the test. These rubble failures and build ups are then assumed to cause load peaks and low points in the relatively constant load area. As a result, the maximum and minimum ride-down height and maximum and minimum angle of repose of the rubble will be measured from the videos, as well as the average time between each rubble failure. In the following an analyze of each case will be given separately, and this section is ended with a comparison of the tests to establish the differences in ice actions due to varied ice thickness and drift speed. The data from the model tests have been cut to only contain load measurements from the model hits the ice to the model stops through the following steps.

1. The total testing time is found from the videos
2. The time where the model stops is found in the test data where the velocity of the model is starting to decrease
3. The starting point for the test data is found by subtracting the total testing time from the stopping time

This gives data files only containing results from ice impact to the end of the test. The statistics from the tests are chosen to be calculated from the tests when the loads are approximately at a constant level. When the model hits the ice sheet the loads will increase to a certain point and then be kept approximately constant due to rubble transportation around the structure. The time interval for the load statistics is given for each test. There has been established a Matlab script to plot the time series from the different cases, as well as to obtain the most important load statistics. The Matlab script is on the enclosed CD in Appendix E.

5.2.1 Results from Model Test Corresponding to Case 1

The load results from the model test corresponding to Case 1 are given in Figure 39 and the load statistics are given in Table 18. The statistics are taken from t=301.1s to the end of the time series.

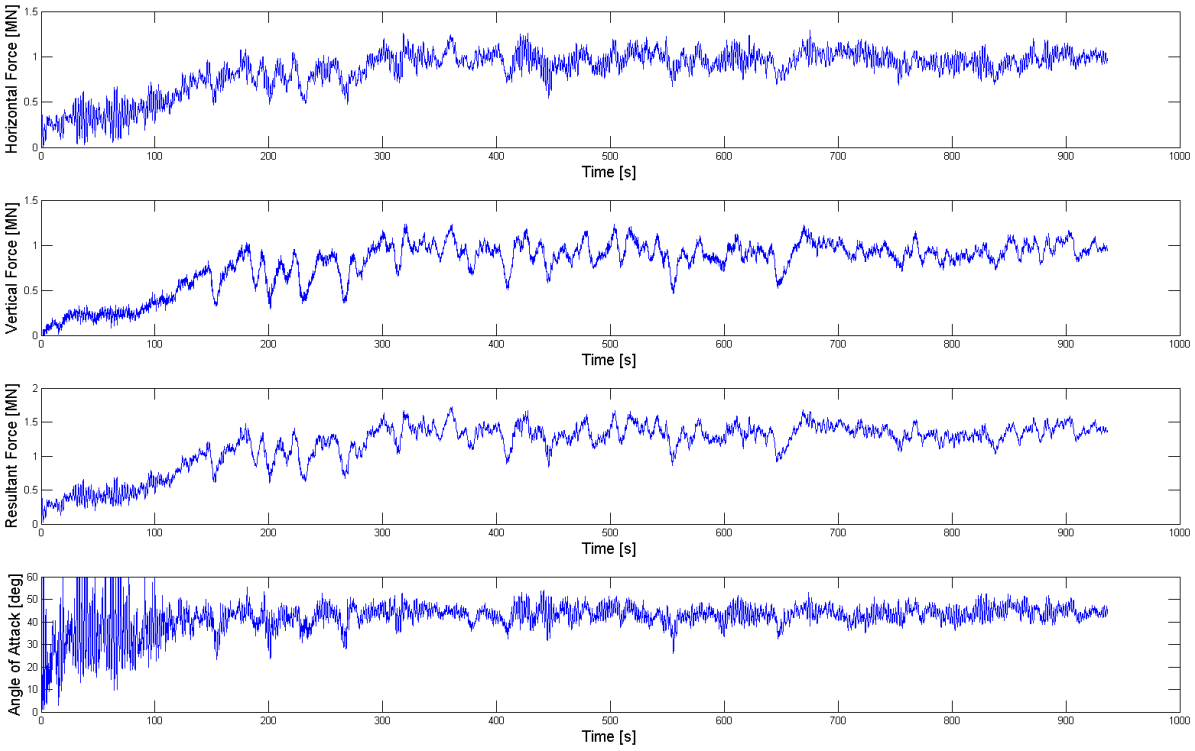

Figure 39 Time Series from the Model Test Corresponding to Case 1

Table 18 Load Statistics for Model Test, Case 1

	F_H [MN]	F_V [MN]	F_R [MN]	θ_{att} [deg]
Max	1.29	1.24	1.72	53.95
Min	0.55	0.46	0.84	25.89
Average	0.97	0.93	1.35	43.65
St. Deviation	0.10	0.12	0.13	3.37

By examining the plots it is seen that the loads are building up from ice impact to approximately *t*=300s. From *t*=300s to the end of the test the loads are kept at relatively constant levels. By examining the test video it is found that this build up sequence corresponds to rubble accumulation in front of the structure. After *t*=300s the volume was found to be kept more or less constant without any significant rubble failures and build-ups. In the relatively constant load area it is seen that the vertical and horizontal load component are following the same trends. The first assumption before examining the video was that the peaks and bottom points throughout the more or less constant load area was due to rubble failure and build up in front of the structure. However, after watching the video, it was found that the rubble volume is kept more or less constant over the entire constant load area without any significant rubble volume increases or decreases.

The breaking length (*br*) of the ice was found to be difficult to determine as there is no good video showing the ice sheet directly in front of the structure. To establish an approximate breaking length for this case, broken off ice pieces was measured and compared to given lengths on the structure multiple times, and the average value of these was calculated. Figure 40 shows an example from the test where a broken off ice piece has been measured. The average value of the broken ice pieces was found to be 5.24m for this test.

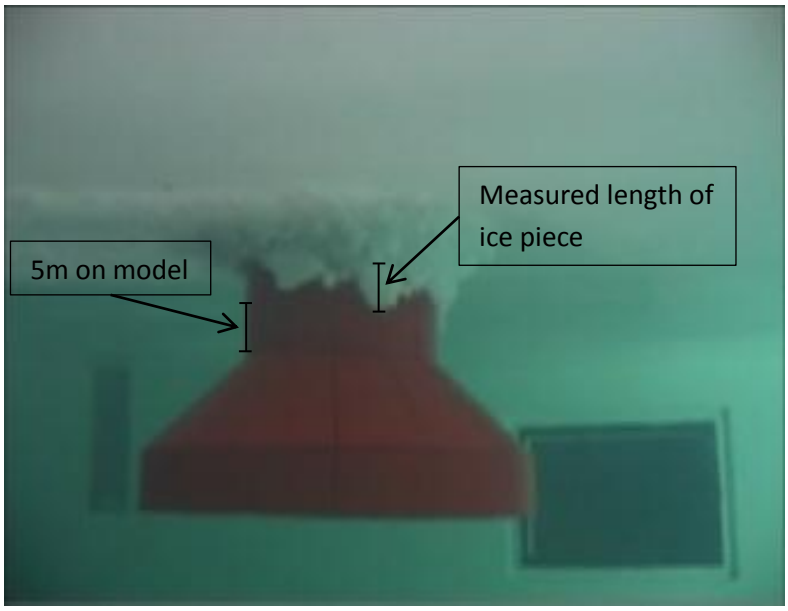

Figure 40 Measurement of Broken Off Ice Piece Case 1

Since there were no clear rubble failures throughout the test, there has not been measured a maximum and minimum rubble ride-down height and rubble angle of repose. An average value for these parameters has been estimated from the videos at two different times. The rubble geometry parameters were measured at times where the camera was directed at the model in an angle of approximately 90 degrees to the towing direction. Figure 41 shows how the ride-down height and rubble angle was measured at one of these points. The average ride-down height and rubble angle were found to be as follows.

- h_r 10 m
- θ 49 degrees

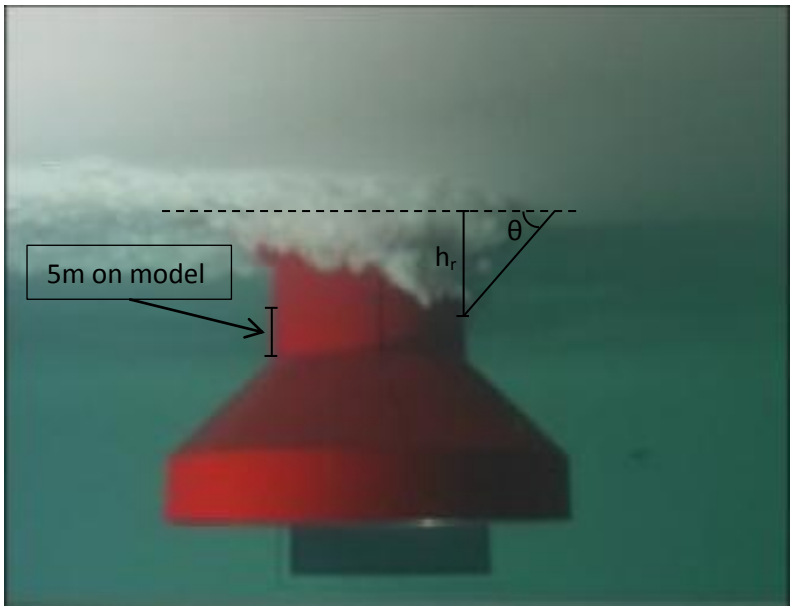

Figure 41 Measurement of Rubble Geometry Case 1

From the model test video it was found that the time it took before the rubble volume had reached a more or less constant volume was approximately 68s, which in full scale is equal to 372.5s. By examining the plot it is seen that this corresponds well with the loads keeping a more or less constant value after this point.

5.2.2 Results from Model Test Corresponding to Case 2

The load results from the model test corresponding to Case 2 are given in Figure 42 and the load statistics are given in Table 19. The statistics are taken from *t*=11.78s to the end of the time series.

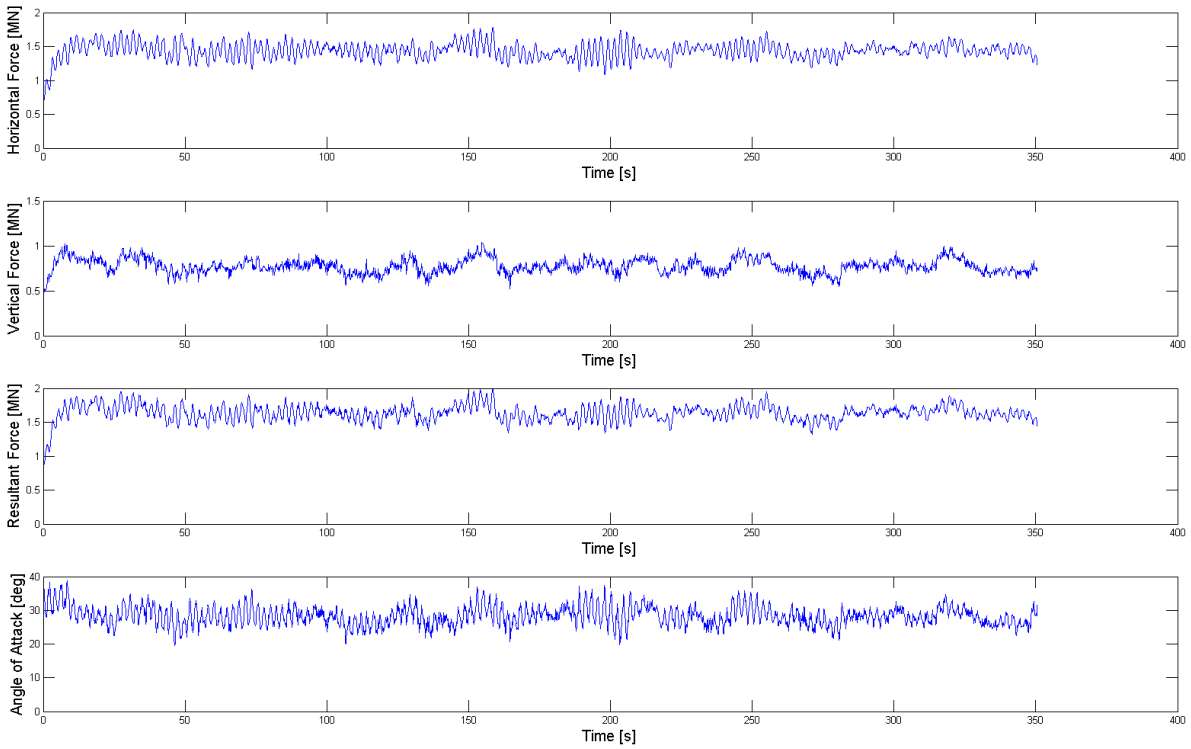

Figure 42 Time Series from the Model Test Corresponding to Case 2

Table 19 Load Statistics for Model Test, Case 2

	F_H [MN]	F_V [MN]	F_R [MN]	θ_{att} [deg]
Max	1.78	1.04	2.00	37.50
Min	1.09	0.52	1.32	19.47
Average	1.44	0.77	1.64	28.21
St. Deviation	0.11	0.08	0.11	2.75

From the plot of the ice loads in Case 2 it is seen that the loads increase rapidly to a more or less constant level in about 12s. After *t*=12s the loads are kept at a more or less constant level throughout the test. As for Case 1 there were no significant rubble failures during this test. The breaking length of the ice and the rubble geometry parameters were found in the similar ways as for Case 1. Figure 43 shows the breaking length measurement at one point and Figure 44 shows one of the rubble geometry measurements.

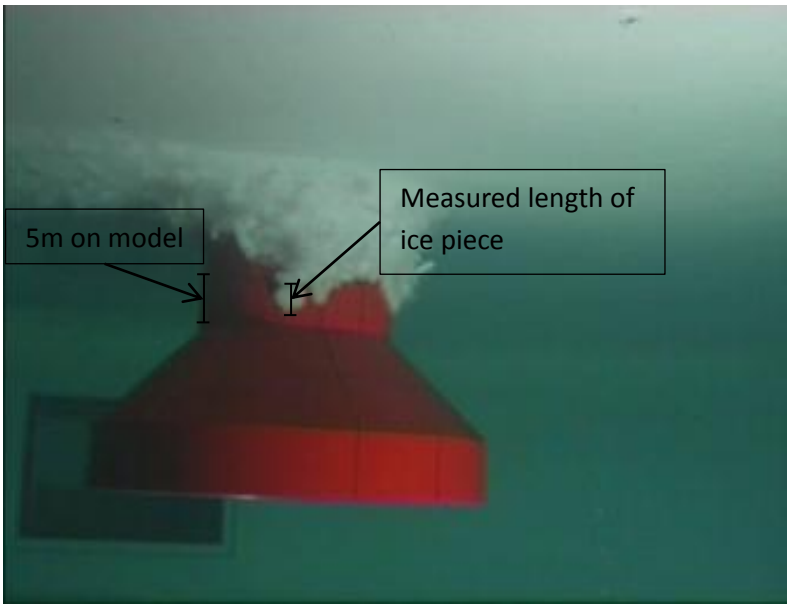

Figure 43 Measurement of Broken Off Ice Piece Case 2

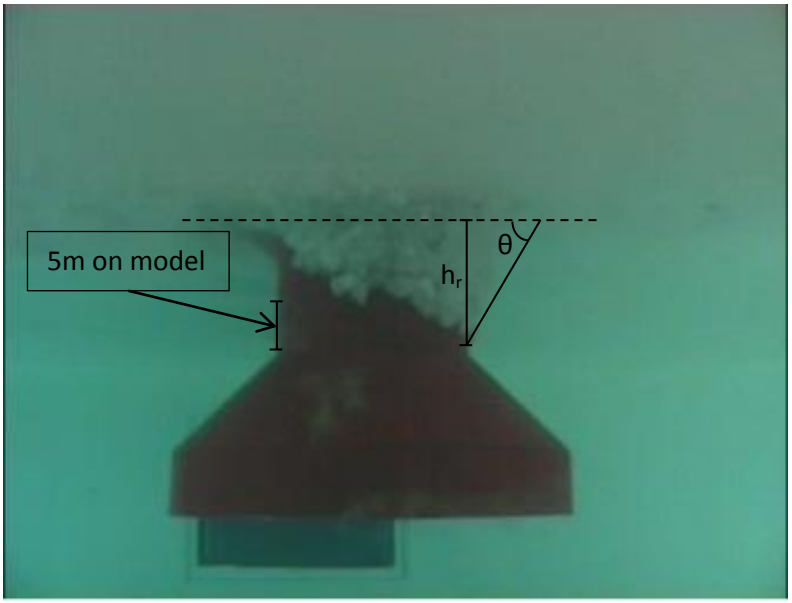

Figure 44 Measurement of Rubble Geometry Case 2

The average breaking length (*br*) and rubble geometry parameters were found to be as follows.

- *br* 3.34 m
- h_r 13.0 m
- θ 57 deg

From the video it was difficult to establish at what time the rubble volume had reached its more or less constant value as the build-up took very little time. It was however observed that the rubble volume experienced very small changes throughout the test.

5.2.3 Results from Model Test Corresponding to Case 3

The load results from the model test corresponding to Case 3 are given in Figure 45 and the load statistics are given in Table 20. The statistics are taken from *t*=211.0s to the end of the time series.

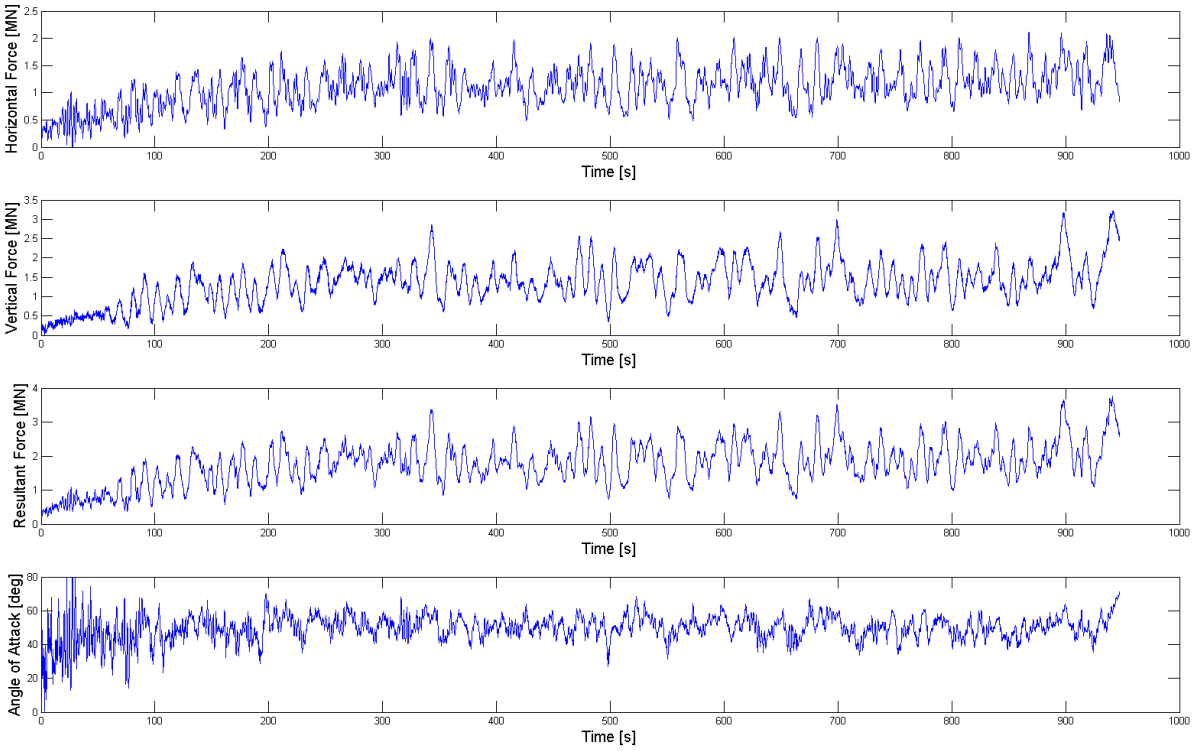

Figure 45 Time Series from the Model Test Corresponding to Case 3

Table 20 Load Statistics for Model Test, Case 3

	F_H [MN]	F_V [MN]	F_R [MN]	θ_{att} [deg]
Max	2.12	3.22	3.75	71.16
Min	0.49	0.35	0.72	26.67
Average	1.20	1.51	1.94	50.96
St. Deviation	0.32	0.47	0.53	6.01

By examining the plot from the model test corresponding to Case 3 it is found that the loads build up to a more or less constant value in approximately 200s. As for the previous tests there were no significant rubble failures throughout the test, but compared to the model test corresponding to Case 2 it was seen that the rubble volume was more dynamic, but still without any clear failures. This might explain the bigger standard deviation for the loads in this case compared to Case 2.

The breaking length of the ice and the rubble geometry parameters were found in the similar ways as for the previous two cases. Figure 46 shows the breaking length measurement at one point and Figure 47 shows the rubble geometry measurement.

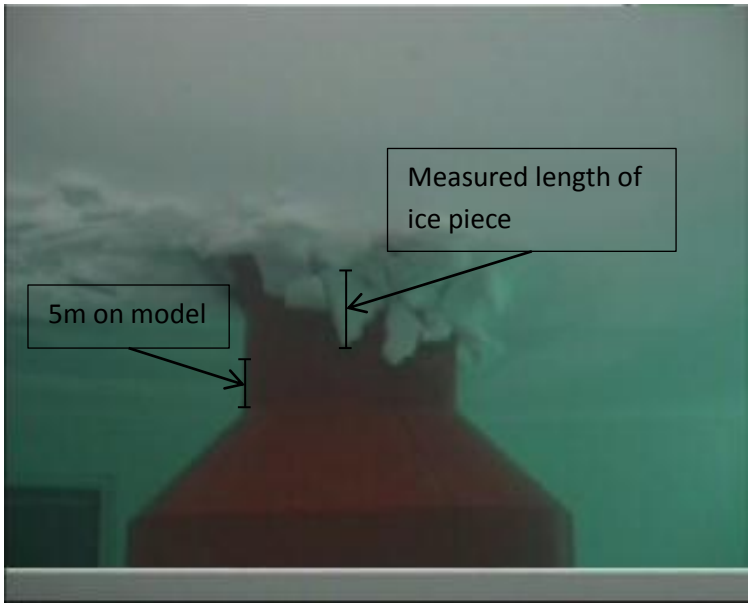

Figure 46 Measurement of Broken Off Ice Piece Case 3

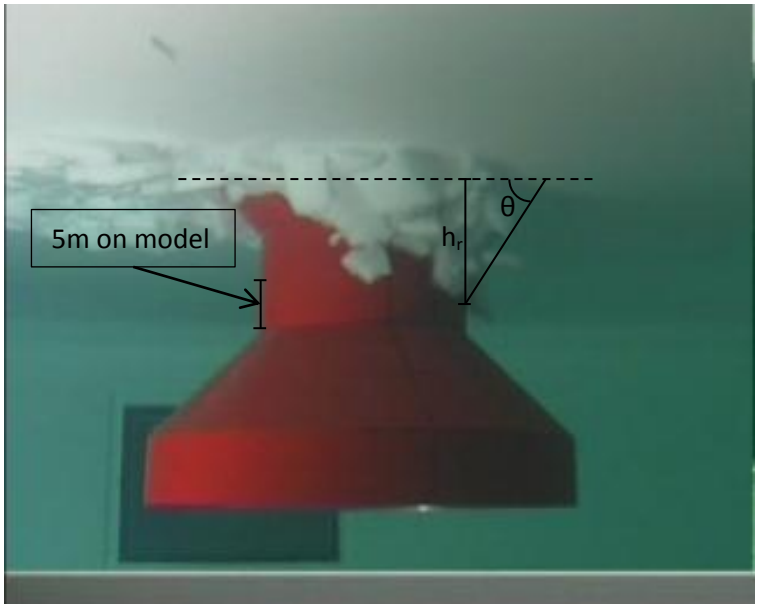

Figure 47 Measurement of Rubble Geometry Case 3

The average breaking length and rubble geometry parameters were found to be as follows.

- *br* 6.07 m
- h_r 12.5 m
- θ 52.5 deg

From the model test video it was difficult to establish the time it took for the rubble volume to reach its more or less constant geometry. The rubble geometry measurements were conducted at two times after the loads were more or less constant.

5.2.4 Results from Model Test Corresponding to Case 4

The load results from the model test corresponding to Case 4 are given in Figure 48 and the load statistics are given in Table 21. The statistics are taken from *t*=0.0s to the end of the time series.

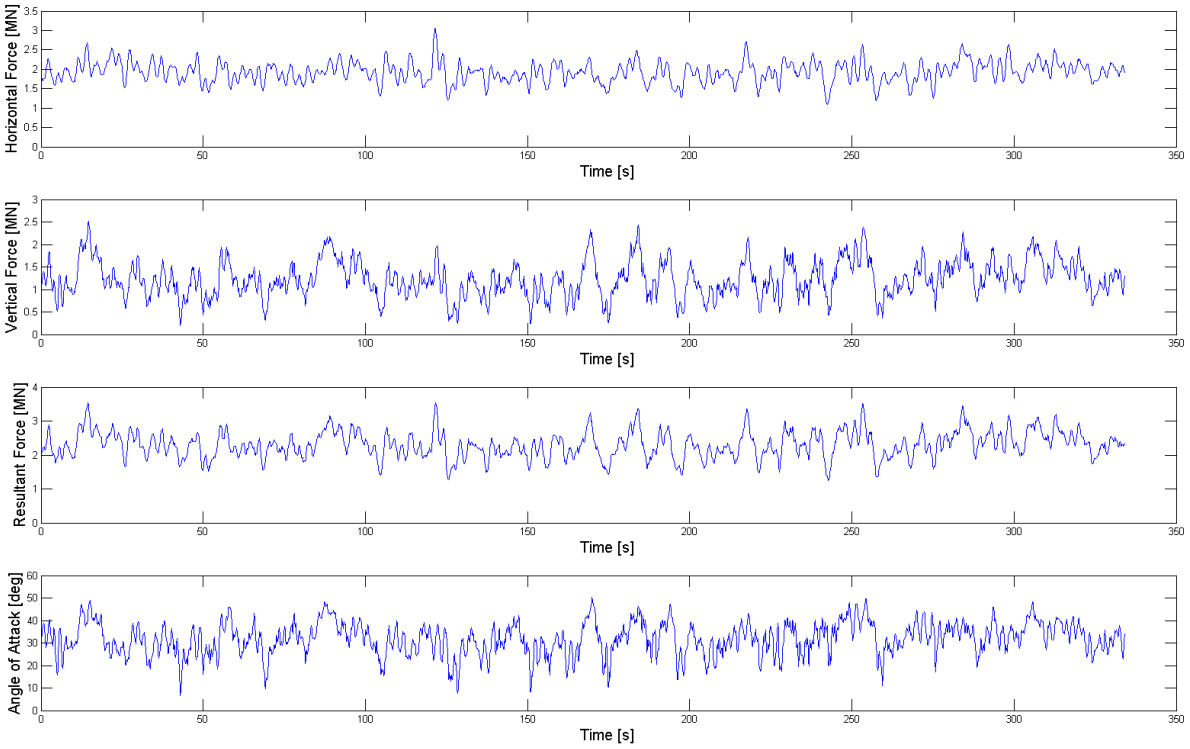

Figure 48 Time Series from the Model Test Corresponding to Case 4

Table 21 Load Statistics for Model Test, Case 4

	F_H [MN]	F_V [MN]	F_R [MN]	θ_{att} [deg]
Max	3.05	2.51	3.55	50.42
Min	1.09	0.19	1.24	6.46
Average	1.93	1.24	2.31	31.92
St. Deviation	0.27	0.40	0.39	7.17

From the plot it is seen that there are no build-up of the loads as was experienced for the previous cases. The reason is that the load measurements for this case commenced after the structure already had hit the ice sheet, and the load measurements from this case starts with an already approximately constant rubble volume. The breaking length and the rubble geometry parameters were found in the same manner as for the previous cases. Figure 49 shows one of the breaking length measurements, and Figure 50 one of the rubble geometry measurements.

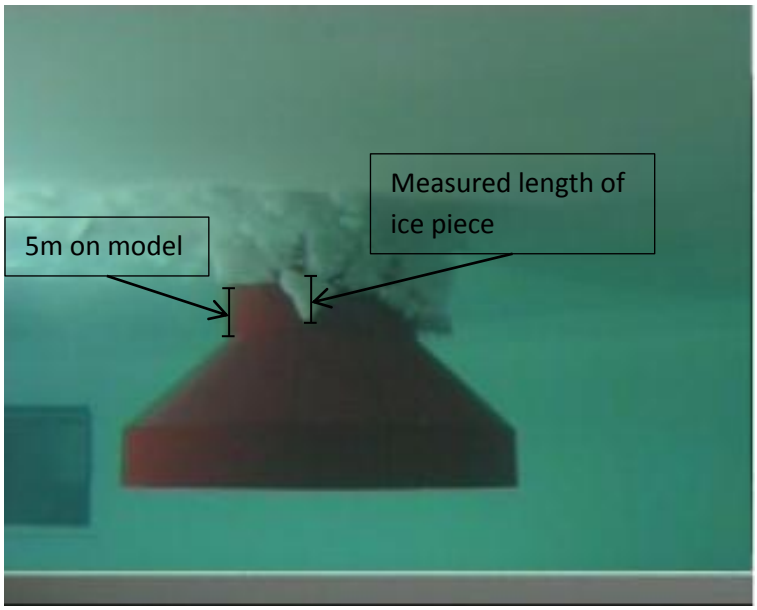

Figure 49 Measurement of Broken Off Ice Piece Case 4

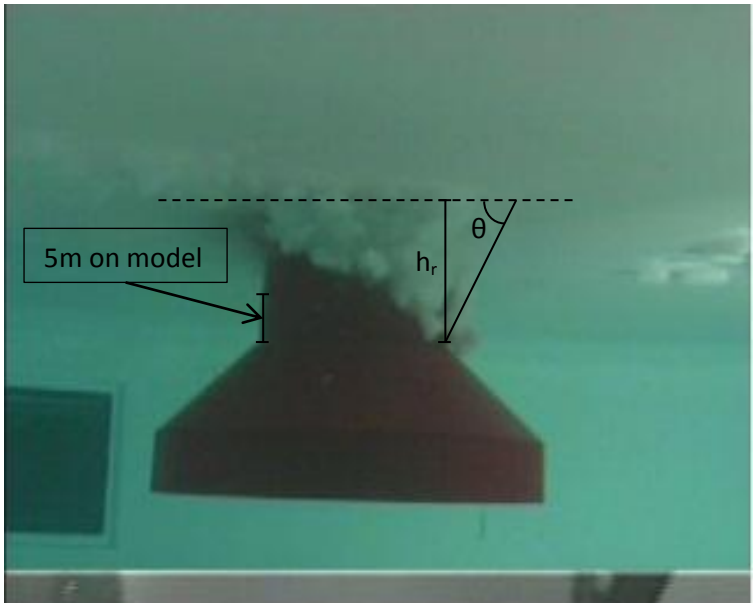

Figure 50 Measurement of Rubble Geometry Case 4

The average breaking length and rubble geometry parameters were found to be as follows.

- *br* 4.38 m
- h_r 13.75 m
- θ 63.5 deg

5.2.5 Comparison of the Four Model Tests

Table 22 shows the main results obtained for the different model tests. The breaking period T_B is calculated from equation (4.1).

Table 22 Main Results from the Model Tests

	Case 1	Case 2	Case 3	Case 4
h [m]	1.0	1.0	1.5	1.5
v [m/s]	0.5	1.0	0.5	1.0
$F_{H,MAX}$ [MN]	1.29	1.78	2.12	3.05
$F_{H,AVG}$ [MN]	0.97	1.44	1.20	1.93
$F_{V,MAX}$ [MN]	1.24	1.04	3.22	2.51
$F_{V,AVG}$ [MN]	0.93	0.77	1.51	1.24
$F_{R,MAX}$ [MN]	1.72	2.00	3.75	3.55
$F_{R,AVG}$ [MN]	1.35	1.64	1.94	2.31
$\theta_{att,AVG}$ [deg]	43.65	28.21	50.96	31.92
br [m]	5.24	3.34	6.07	4.38
T_B [s]	10.48	3.34	12.14	4.38
$h_{r,AVG}$ [m]	10.00	13.00	12.50	13.75
θ_{AVG}[deg]	49.00	57.00	52.50	63.50

The results from the different model tests show some similar trends. The three first cases clearly show that the ice loads are building up from ice impact to a relatively constant load area after a certain time. The time it takes to reach this constant area is dramatically increased when the ice drift speed is increased. For Case 1 with level ice thickness 1.0m and drift speed 0.5m/s it took approximately 300s before this constant load area was reached. For the same ice thickness and double the speed (Case 2), the time was reduced to approximately 12s. For Case 3 (ice thickness of 1.5m and drift speed of 0.5m/s) it took approximately 200s and for Case 4 there are no data to determine this factor. From the three first cases it might seem that the time it takes to reach this relatively constant load area is highly dependent on the ice drift speed, but also on the thickness. This might be explained under the assumption that there has to be accumulated a certain amount of rubble before the rubble transportation around the structure is approximately equal to the rubble accumulation (i.e. the volume of rubble in front of the structure is kept more or less constant). For a higher drift speed and/or an increased ice thickness, this amount is faster obtained and the constant load area is reached sooner.

When comparing Case 1 with Case 2 and Case 3 with Case 4 (h kept constant, v increased) it is clearly seen that the horizontal and resultant load increase. The vertical load component however is decreased. This may be explained by the fact that there will be more crushing of ice when the speed is increased, which results in higher horizontal loads. Since the ice sheet is failed in crushing instead of bending, the vertical load component might be governed by buoyancy forces from the ice rubble more than by failing the ice. The increase in horizontal load and decrease in vertical load also results in a smaller angle of attack of the resultant force. From the videos of the model tests it was also seen that the ice pieces accumulated in front of the structure were of much smaller size for Case 2 and Case 4 compared to Case 1 and Case 3 respectively, which also justify the assumption of more crushing.

When comparing Case 1 with Case 3 and Case 2 with Case 4 (*v* kept constant, *h* increased), there is also a significant load increase. For this comparison, all load components are increasing. When the ice thickness is increased a higher load is required fail the ice. This affects both the horizontal and vertical load component.

By investigating how much the loads differ for either increased ice thickness or increased drift speed, interesting results are found. Table 23 shows the percentage difference of the average loads from Case 1 to Case 3 and from Case 2 to Case 4 (*h* increase) as well as from Case 1 to Case 2 and from Case 3 to Case 4 (*v* increase).

Table 23 Percentage Load Difference Due To Increased *h* and Increased *v*

	Load difference [%] due to increase of *h*		Load difference [%] due to increase of *v*	
	Case 1 to Case 3	Case 2 to Case 4	Case 1 to Case 2	Case 3 to Case 4
$F_{H,AVG}$	23.70	34.00	48.50	60.80
$F_{V,AVG}$	62.40	61.00	-17.20	-17.90
$F_{R,AVG}$	43.70	40.90	21.50	19.10

By first examining the loads for increased ice thickness, it is found that the average resultant load increase with 43.70% from Case 1 to Case 3 (speed equal to 0.5m/s). From Case 2 to Case 4 the increase is 40.90% (speed equal to 1.0m/s). Then, by examining the resultant loads for increased speed, it is found that the average resultant load increase with 21.50% from Case 1 to Case 2 (ice thickness equal to 1.0m). From Case 3 to Case 4 the increase is 19.10% (ice thickness equal to 1.5m). The first conclusion that can be drawn from this is that an increase in ice thickness affect the resultant loads more than an increase in speed. This may be due to the decrease in the vertical load component for the cases where the speed is increased, which will affect the resultant load. Another interesting finding is that the factors are approximately the same for increased ice thickness for both drift speeds. It might seem that the load increase is approximately 40% independent of the drift speed when the ice thickness is increased with 0.5m. The same is found from the results when the ice drift speed is increased and the thickness is kept constant. An increase of about 20% is found when the speed is increased from 0.5m/s to 1.0m/s independent of the ice thickness.

Another important point is that the increase in the horizontal load is bigger for increased drift speed than for increased ice thickness. This builds up under the assumption of more crushing of ice for higher drift speed, which results in a higher horizontal load component. This also affects the vertical load component to decrease when the ice drift speed is increased. The vertical load component follows the same trends as the resultant load component. The vertical load component increases with approximately 60% when the ice thickness is increased, independently of the drift speed. When the drift speed is increased, the vertical load component is decreasing with approximately 17% independently of the ice thickness. These trends are not found for the horizontal load component.

6 Correction of the Numerical Calculation Model

In this section a correction of the Matlab script developed in section 4.2 will be performed by comparing the model test results with the results obtained from this script, for all the four interaction cases. It was found in section 5.1.2 that the measured ice properties from the model tests deviated from the target values. In section 5.2 both the assumed breaking lengths and the assumed rubble geometries were found to deviate from those observed in the model test videos. By implementing the measured ice properties and the observed breaking lengths and rubble geometry parameters in the numerical calculation model, and then comparing the results obtained with the model test results, correction factors for the numerical calculation model can be developed. This exercise has been performed through four correction parts. Table 24 shows the parameters included in the numerical model for each part.

Table 24 Overview of Parameters for the Different Correction Parts

	Mechanical and Physical Ice Properties		Average Breaking Period		Ice Transport and Accumulation	
	Target	Actual	Assumed	Identified	Assumed	Identified
Part 1	X		X		X	
Part 2		X		X	X	
Part 3		X		X		X
Part 4	X			X		X

Part 1 gives results that would have been the first estimate of ice actions in a design phase if no model tests had been run. Part 2 includes the actually obtained ice properties as well as the identified breaking lengths, and Part 3 also includes the identified rubble geometries. Part 3 will then calculate ice actions corrected for the actual conditions found from the model tests. By comparing the results from Part 3 with the model test results, correction factors for the numerical model can be developed. In Part 4, these correction factors are implemented, and ice actions for the target ice properties are calculated. The results from Part 4 will then estimate the ice actions for the target ice properties, where correction factors developed through model testing are implemented.

Mechanical and physical ice properties include the level ice thickness, the flexural strength of the ice, the modulus of elasticity, the density of the ice and the ice-structure friction coefficient. The target values and actually achieved values of these parameters for the different cases are described in section 5.1.2, and also displayed in Table 25 for this section. For the model tests the friction coefficient was equal to 0.05 for all cases. This value has been used as both target and actually achieved value for all cases.

Table 25 Target and Actual Measured Values for the Physical and Mechanical Ice Properties

	Target Values				Actual Values			
	h [m]	σ_f [kPa]	E [GPa]	ρ_i [kg/m^3]	h [m]	σ_f [kPa]	E [GPa]	ρ_i [kg/m^3]
Case 1	1.00	500.00	0.50	900.00	0.95	573.60	2.07	925.74
Case 2	1.00	500.00	0.50	900.00	0.97	726.30	2.07	925,74
Case 3	1.50	500.00	0.50	900.00	1.31	758.40	0.47	920.22
Case 4	1.50	500.00	0.50	900.00	1.42	680.10	0.47	920.22

Ice transport and accumulation includes the rubble ride-down heights and the angle the rubble volumes make with the horizontal. The assumed values and identified values for the rubble geometries and breaking lengths (*br*) of the ice sheet are given in Table 26. The assumed values of the breaking lengths are calculated as the characteristic length l_c given in equation (3.21). The assumed values of the rubble ride-down heights and angles of repose are obtained as described in section 4.2.1.

Table 26 Assumed and Visually Measured Values for Breaking Lengths and Rubble Geometries

	Assumed Values			Measured Values		
	h_r [m]	θ [deg]	br [m]	h_r [m]	θ [deg]	br [m]
Case 1	7.00	35.00	8.21	10.00	49.00	5.24
Case 2	7.00	35.00	8.21	13.00	57.00	3.34
Case 3	9.00	35.00	11.13	12.50	52.50	6.07
Case 4	9.00	35.00	11.13	13.75	63.50	4.38

The rubble build-up period (the time it takes before the loads are at a relatively constant level) was set to be 100s in section 4.2.1. This value was used only to see a load build-up from ice hit to the time where a more or less constant rubble volume has been obtained. For the correction parts described in this section, this build-up period in the calculated time series are taken directly from the model test results to get a visually easier presentation of the loads from the numerical model and the model test results. This period is very difficult to estimate based on ice parameters, and this has not been attempted to accomplish during the work on this thesis. An important point is that this rubble build-up period will not affect the load statistics obtained throughout this section, as all statistics are taken from the area where the loads are stabilized.

The visually measured parameters for the rubble geometries cannot be directly implemented in the Matlab script as the script is based on Croasdale`s method. In this calculation method the angle the rubble makes with the horizontal has to be less than the sloping angle of the structure. If the angle is greater than the sloping angle a negative rubble volume will be calculated which results in a load decrease. Since the structure examined has a vertical section below the sloping section the rubble creates an angle which is steeper than the sloping angle. An approximation has been done where the rubble volume observed from the videos has been transformed into a volume with an angle of 35 degrees (10 degrees less than the sloping angle as explained in section 4.2.1) and a new ride-down height. See Figure 51 for explanation.

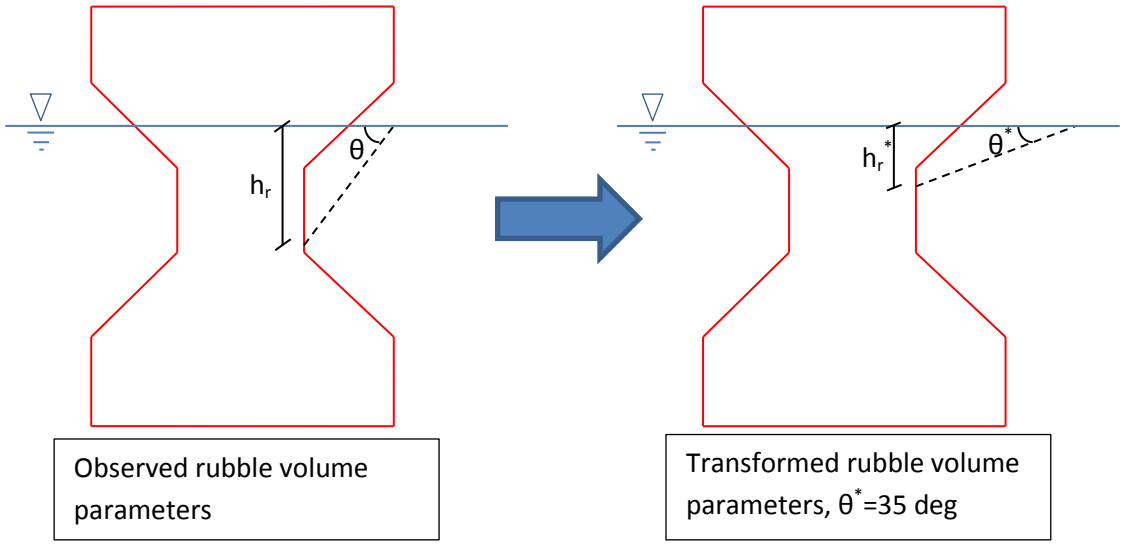

Figure 51 Observed and Transformed Rubble Volume

The new ride-down height, h_r^*, is obtained by demanding that the area from the visually observed parameters is equal to the transformed area where the angle the rubble makes with the horizontal is kept at 35 degrees. From simple geometric considerations, the new ride-down height corresponding to an angle of 35 degrees is given in equation (6.1).

$$h_r^* = h_r \sqrt{\frac{\tan\theta^*}{\tan\theta}} = h_r \sqrt{\frac{\tan 35}{\tan\theta}} \tag{6.1}$$

This should give a correct estimate of the loads as the rubble dependent terms in Croasdale`s method are based on the size of the volume of rubble in front of the structure, and not the shape. The transformed ride-down heights implemented in the Matlab script as the new measured values are given in Table 27.

Table 27 Measured and Transformed Values for Rubble Geometry

	Measured Values		Transformed Values	
	h_r [m]	θ [deg]	h_r^* [m]	θ^* [deg]
Case 1	10.00	49.00	7.80	35.00
Case 2	13.00	57.00	8.77	35.00
Case 3	12.50	52.50	9.16	35.00
Case 4	13.75	63.50	8.12	35.00

In the following, results from each of the four correction parts will be given. The results from the numerical model in Part 1, Part 2 and Part 3 will be compared to the measured results obtained in the model tests. All these parts are compared to the model test results to see how the deviations between the measured and the calculated loads vary when identified parameters are included. From Part 3 the correction factors will be developed, and these are implemented in Part 4. The results from Part 4 are compared to the results from Part 1 to see the difference between the calculated ice actions before and after the correction factors obtained from the model tests are included.

In the four different parts only average values and standard deviations for the loads are given. It has been assumed that a numerical calculation model`s best use is to establish in what range the loads for different interaction cases will be. Maximum and minimum loads in a real-life interaction process can be caused by numerous factors which are beyond what the Matlab script is able to comprehend. Both the horizontal, vertical and resultant loads are plotted for the four interaction cases in the different parts. For the three first parts the calculated loads are plotted together with the measured ones to visually present the differences between the calculated values and the ones measured in the model tests. In Part 4, the results obtained are plotted together with the results obtained in Part 1 to see the effect of the correction factors.

There has been developed a new Matlab script for this section, but the script is based on the one established in section 4.2. The modifications in the new script used in this section is the ability to both calculate ice actions through the numerical model and compare them to the model test results. The Matlab script for this section is given on the enclosed CD in Appendix E.

6.1 Part 1

As Part 1 describes ice actions from target ice properties and assumed breaking lengths and ice accumulations, this part is based on the same assumptions as in the time domain analyze in section 4.2. The only difference is the target values for the ice-structure friction coefficient and the modulus of elasticity. In the model tests the friction coefficient was kept at a constant value of 0.05 and the target value for the modulus of elasticity was 0.5GPa. These parameters are therefore used as the target values in this section.

Figure 52 through Figure 55 shows plots of the horizontal, the vertical and the resultant load for each of the four interaction cases. Both the results obtained from the Matlab script and the results measured in the model tests are plotted together to visually present the deviation between the results. Table 28 shows the main load statistics from the Matlab script compared to the measured values in the model tests, and Table 29 shows the percentage difference between the calculation model and the model tests.

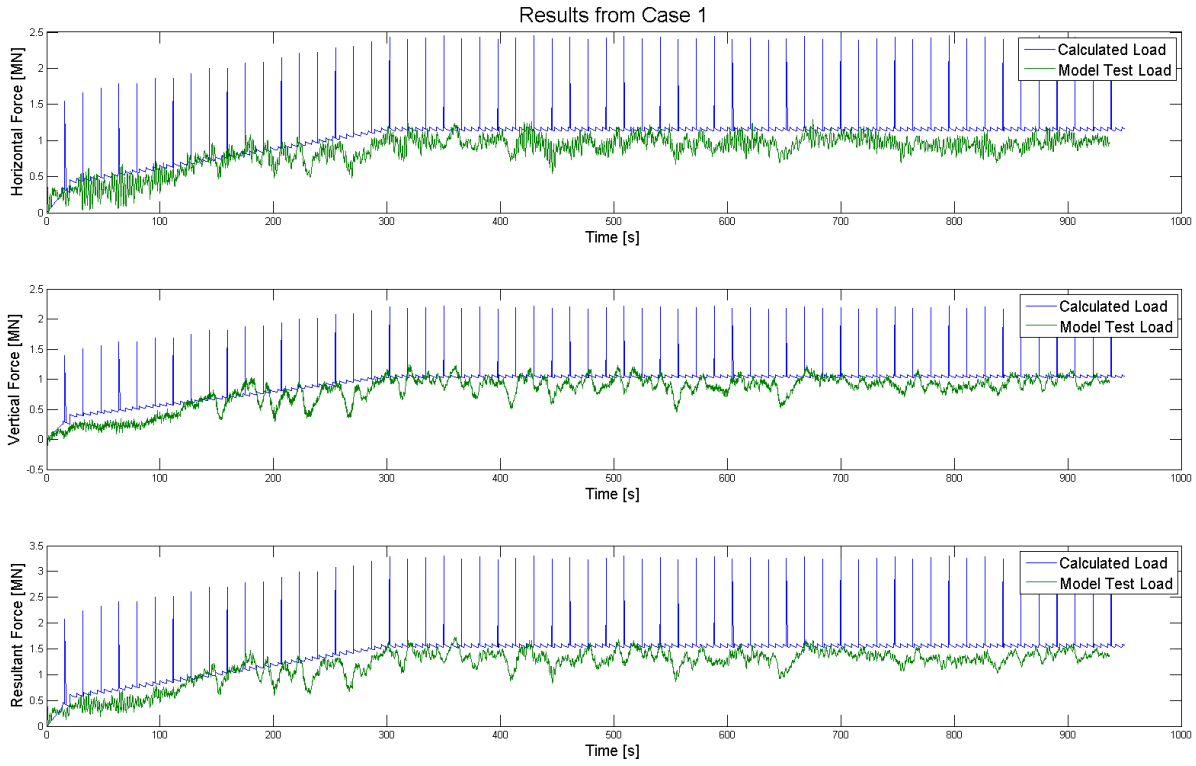

Figure 52 Comparison of Numerical Calculations and Model Test Results, Part 1, Case 1

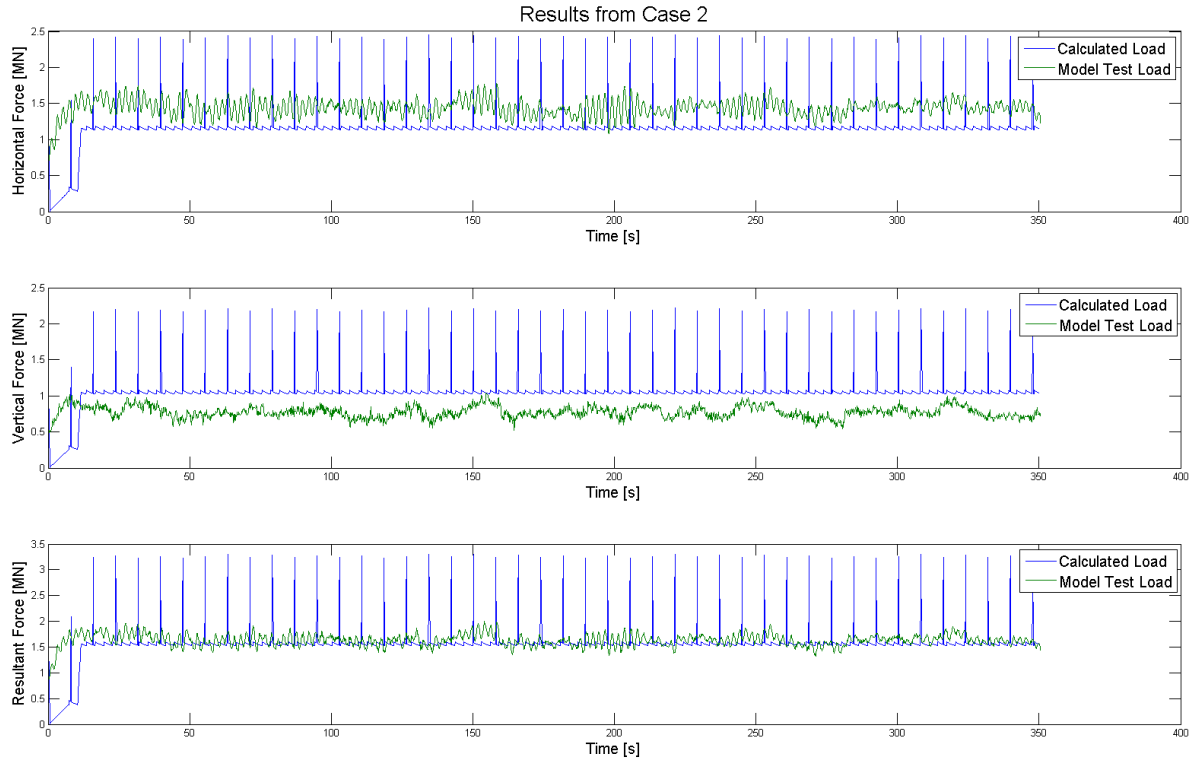

Figure 53 Comparison of Numerical Calculations and Model Test Results, Part 1, Case 2

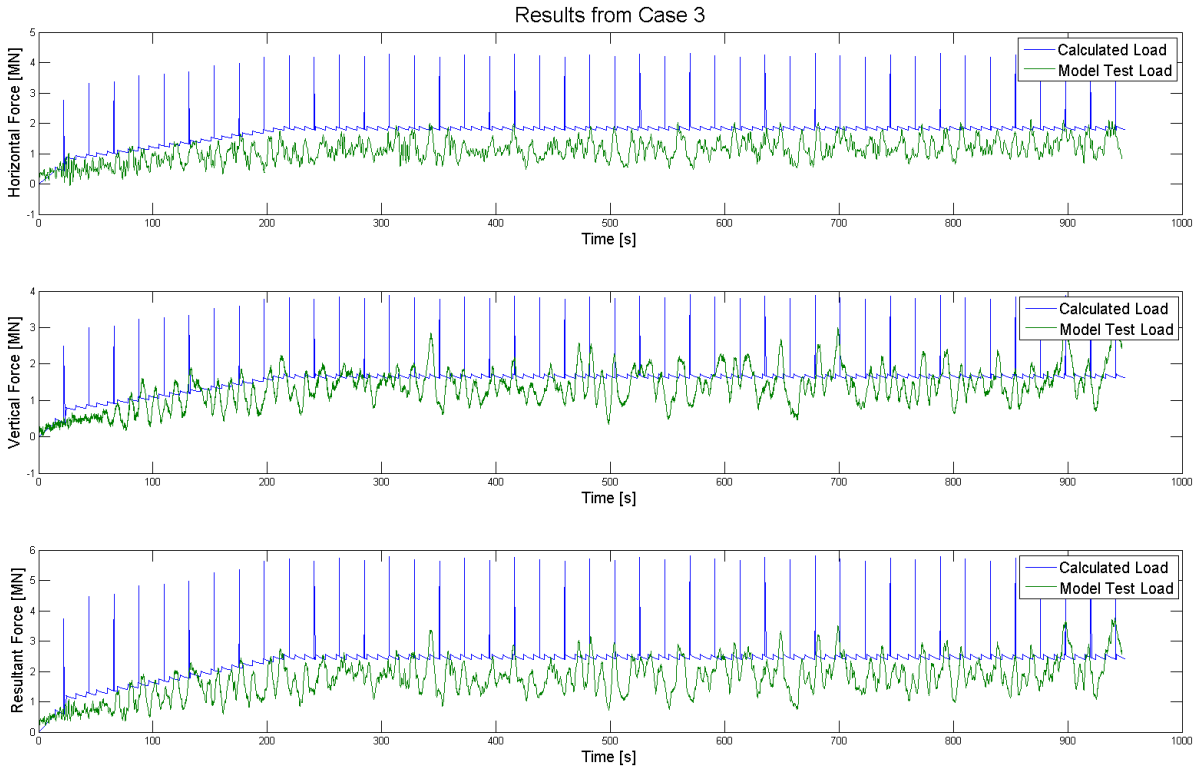

Figure 54 Comparison of Numerical Calculations and Model Test Results, Part 1, Case 3

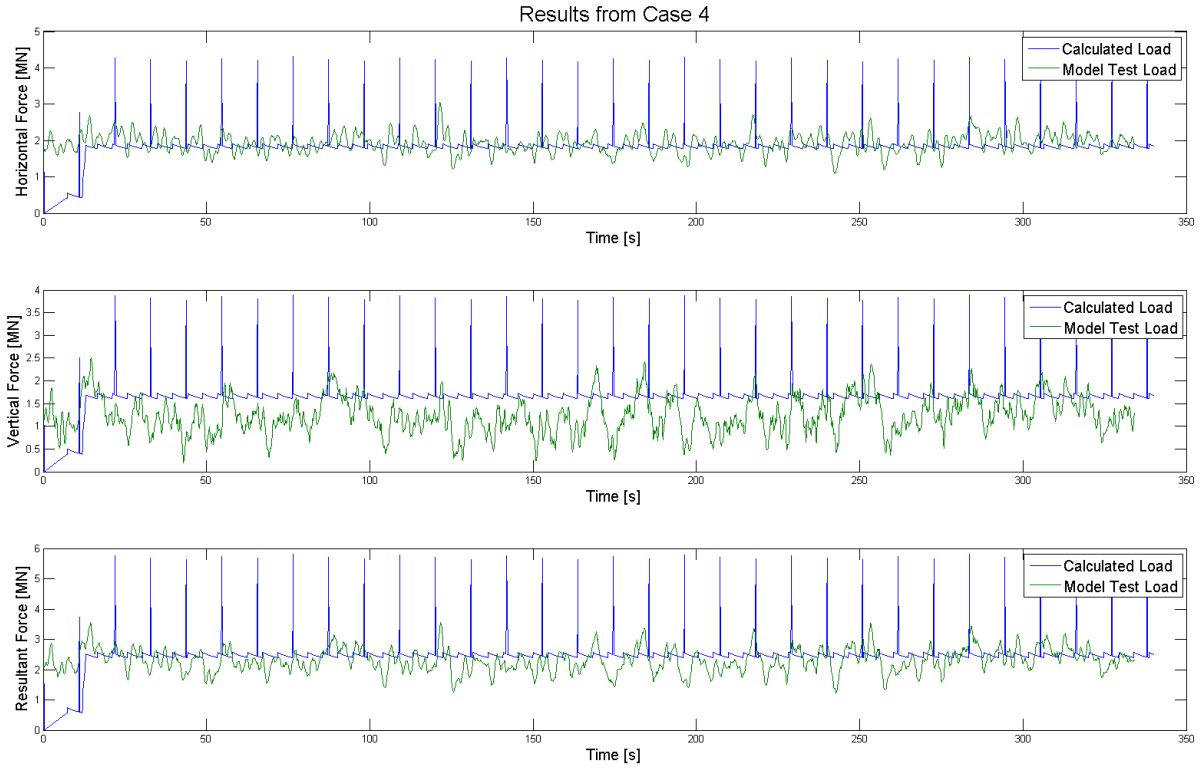

Figure 55 Comparison of Numerical Calculations and Model Test Results, Part 1, Case 4

Table 28 Load Statistics from Numerical Calculations and Model Test Results, Part 1

	Calculated Values						Model Test Values					
	F_H [MN]		F_V [MN]		F_R [MN]		F_H [MN]		F_V [MN]		F_R [MN]	
	Avg	Std	Avg	Std	Avg	Std	Avg	Std	Avg	Std	Avg	Std
Case 1	1.17	0.11	1.06	0.10	1.58	0.15	0.97	0.10	0.93	0.12	1.35	0.13
Case 2	1.18	0.16	1.07	0.14	1.59	0.21	1.44	0.11	0.77	0.08	1.64	0.11
Case 3	1.85	0.18	1.67	0.17	2.50	0.25	1.20	0.32	1.51	0.47	1.94	0.53
Case 4	1.87	0.26	1.69	0.23	2.52	0.35	1.93	0.27	1.24	0.40	2.31	0.39

Table 29 Difference Between Numerical Calculations and Model Test Results, Part 1

	Difference from model test values [%]		
	$F_{H,AVG}$	$F_{V,AVG}$	$F_{R,AVG}$
Case 1	20.62	13.98	17.04
Case 2	-18.06	38.96	-3.05
Case 3	54.17	10.60	28.87
Case 4	-3.11	36.29	9.09

From the results it is seen that there are some deviations between the calculated loads and the loads from the model tests. The vertical load component is a function of the horizontal load component, the sloping angle of the structure and the ice-structure friction coefficient in the numerical model (see equation (3.5)). This means that the vertical load will be a given factor smaller than the horizontal load for all the interaction cases in the numerical model. The vertical load component is approximately 10% smaller than the horizontal load component in the numerical model for all the cases. This factor is not constant for the model test results, which means that even though the

numerical model might correctly calculate either the horizontal or the vertical load component, the resultant load will be off target.

6.2 Part 2

Part 2 describes calculated ice actions with the actually obtained ice properties, the breaking lengths identified from the model test videos and the assumed rubble volume configurations.

Figure 56 through Figure 59 shows plots of the horizontal, the vertical and the resultant load for each of the four interaction cases. Both the results obtained from the Matlab script and the results measured in the model tests are plotted together to visually present the deviation between the results. Table 30 shows the main load statistics from the Matlab script compared to the measured values in the model tests and Table 31 shows the percentage difference between the calculation model and the model tests.

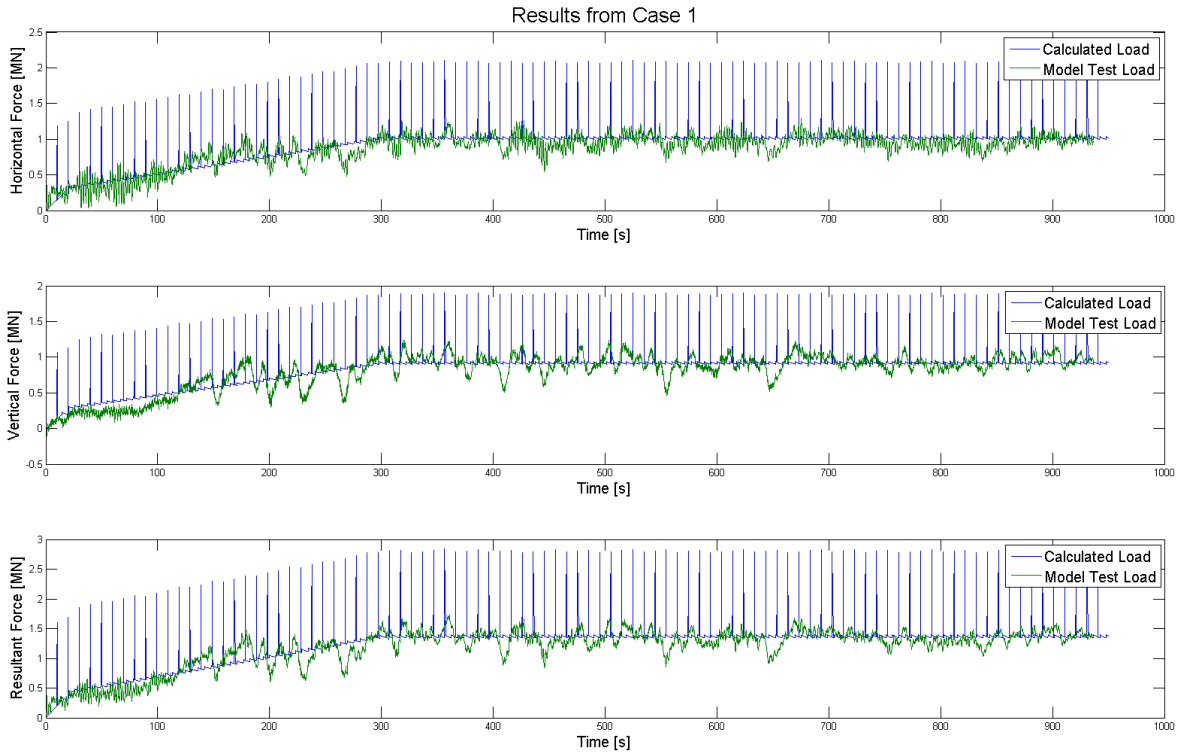

Figure 56 Comparison of Numerical Calculations and Model Test Results, Part 2, Case 1

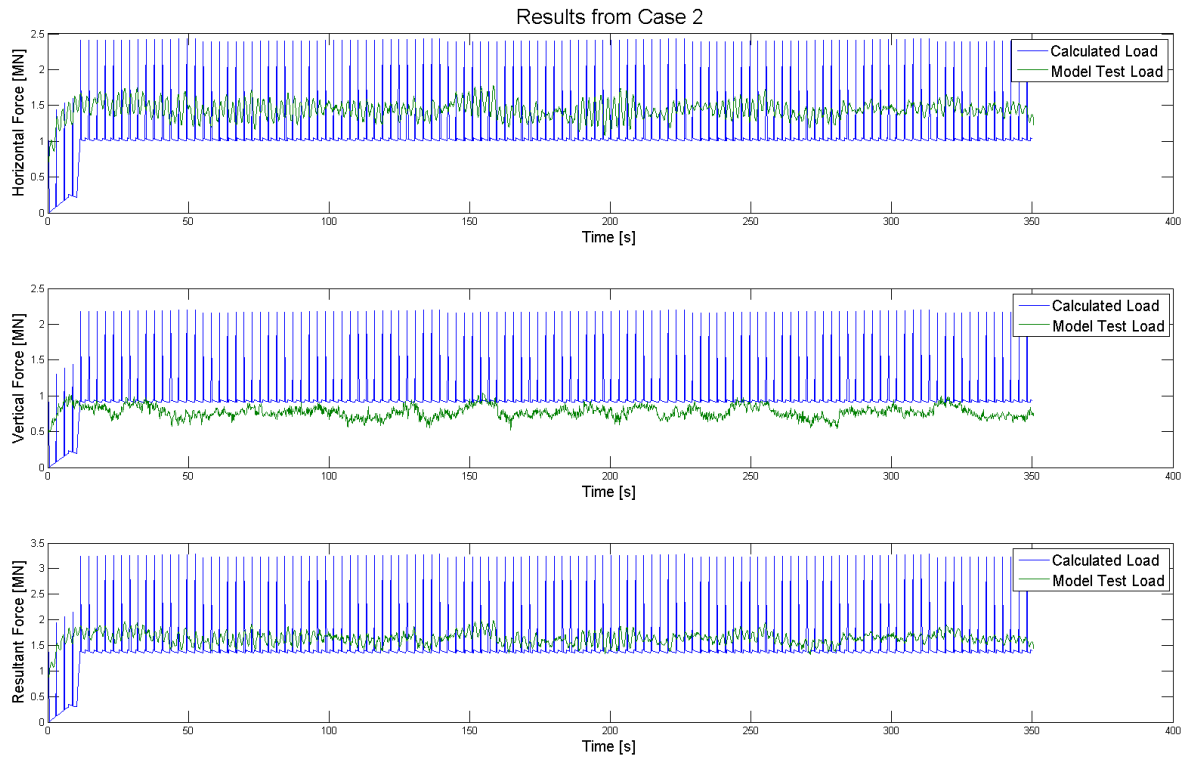

Figure 57 Comparison of Numerical Calculations and Model Test Results, Part 2, Case 2

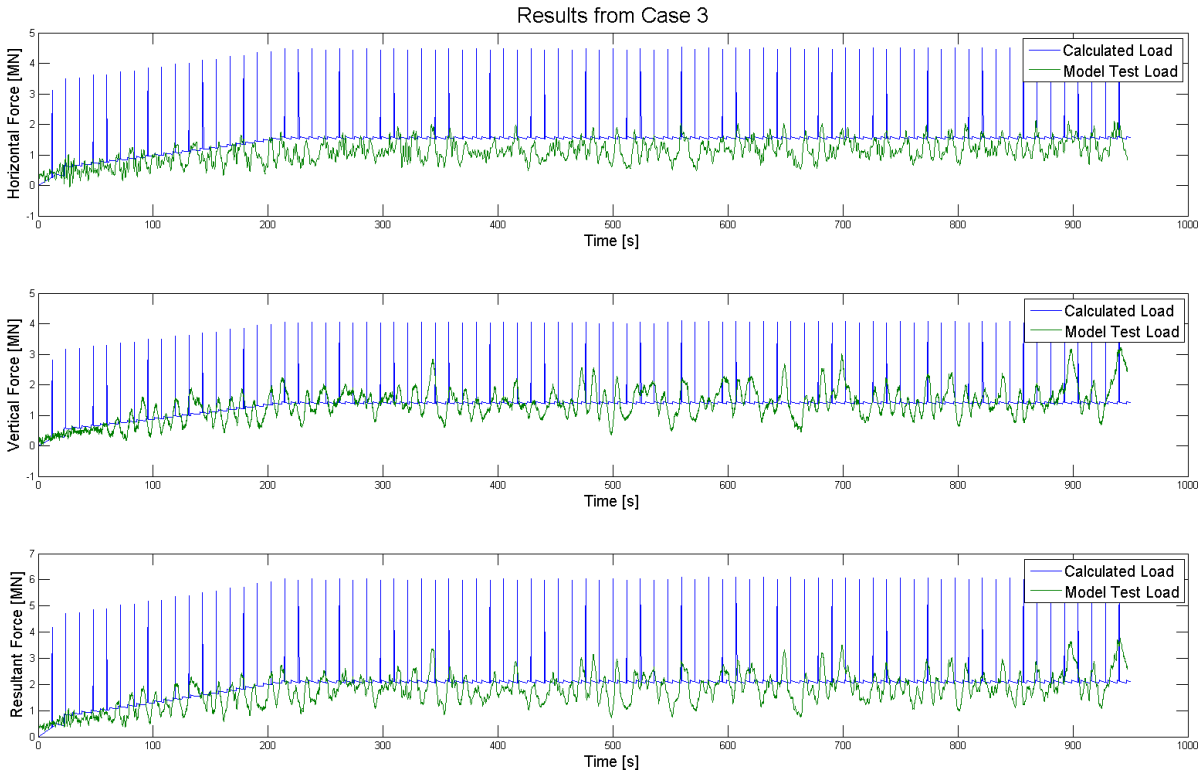

Figure 58 Comparison of Numerical Calculations and Model Test Results, Part 2, Case 3

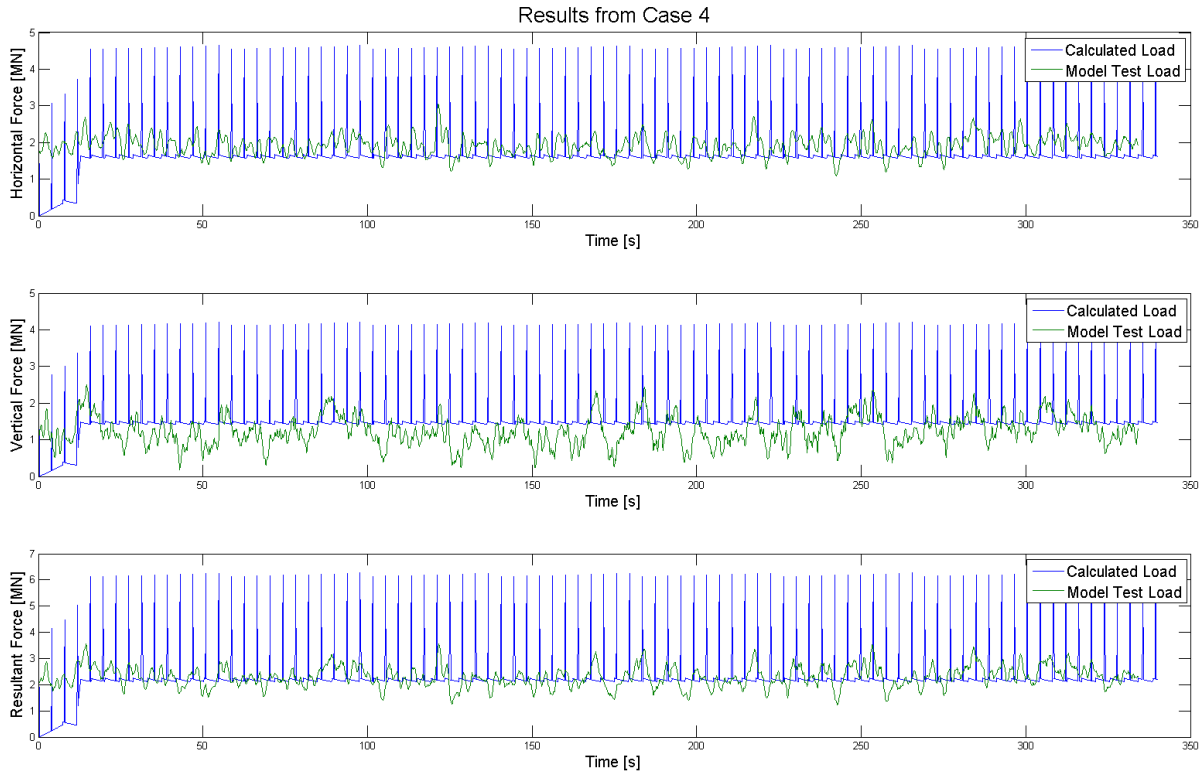

Figure 59 Comparison of Numerical Calculations and Model Test Results, Part 2, Case 4

Table 30 Load Statistics from Numerical Calculations and Model Test Results, Part 2

	Calculated Values						Model Test Values					
	F_H [MN]		F_V [MN]		F_R [MN]		F_H [MN]		F_V [MN]		F_R [MN]	
	Avg	Std	Avg	Std	Avg	Std	Avg	Std	Avg	Std	Avg	Std
Case 1	1.03	0.12	0.93	0.11	1.39	0.16	0.97	0.10	0.93	0.12	1.35	0.13
Case 2	1.09	0.28	0.99	0.25	1.48	0.37	1.44	0.11	0.77	0.08	1.64	0.11
Case 3	1.60	0.29	1.44	0.27	2.15	0.40	1.20	0.32	1.51	0.47	1.94	0.53
Case 4	1.73	0.52	1.56	0.47	2.33	0.70	1.93	0.27	1.24	0.40	2.31	0.39

Table 31 Difference Between Numerical Calculations and Model Test Results, Part 2

	Difference from model test values [%]		
	$F_{H,AVG}$	$F_{V,AVG}$	$F_{R,AVG}$
Case 1	6.19	0.00	2.96
Case 2	-24.31	28.57	-9.76
Case 3	33.33	-4.64	10.82
Case 4	-10.36	25.81	0.87

As was seen in Part 1 there are some deviations between the calculated loads and the ones measured during the model tests, but the difference have dramatically decreased. Especially the values for the resultant loads are very close to the ones measured in the model tests. In this section the actually achieved ice properties have been used which might be the reason for this decrease in the error of the numerical results. The rubble geometry parameters are still assumed in this part, and

might be the reason for the deviations achieved. Also the breaking lengths measured from the videos are used in this part and might include some uncertainties.

6.3 Part 3

Part 3 describes calculated ice actions with the actually obtained ice properties, as well as the breaking lengths and rubble volume configurations identified from the model test videos.

Figure 60 through Figure 63 shows plots of the horizontal, the vertical and the resultant load for each of the four interaction cases. Both the results obtained from the Matlab script and the results measured in the model tests are plotted together to visually present the deviation between the results. Table 32 shows the main load statistics from the Matlab script compared to the measured values in the model tests, and Table 33 shows the percentage difference between the calculation model and the model tests.

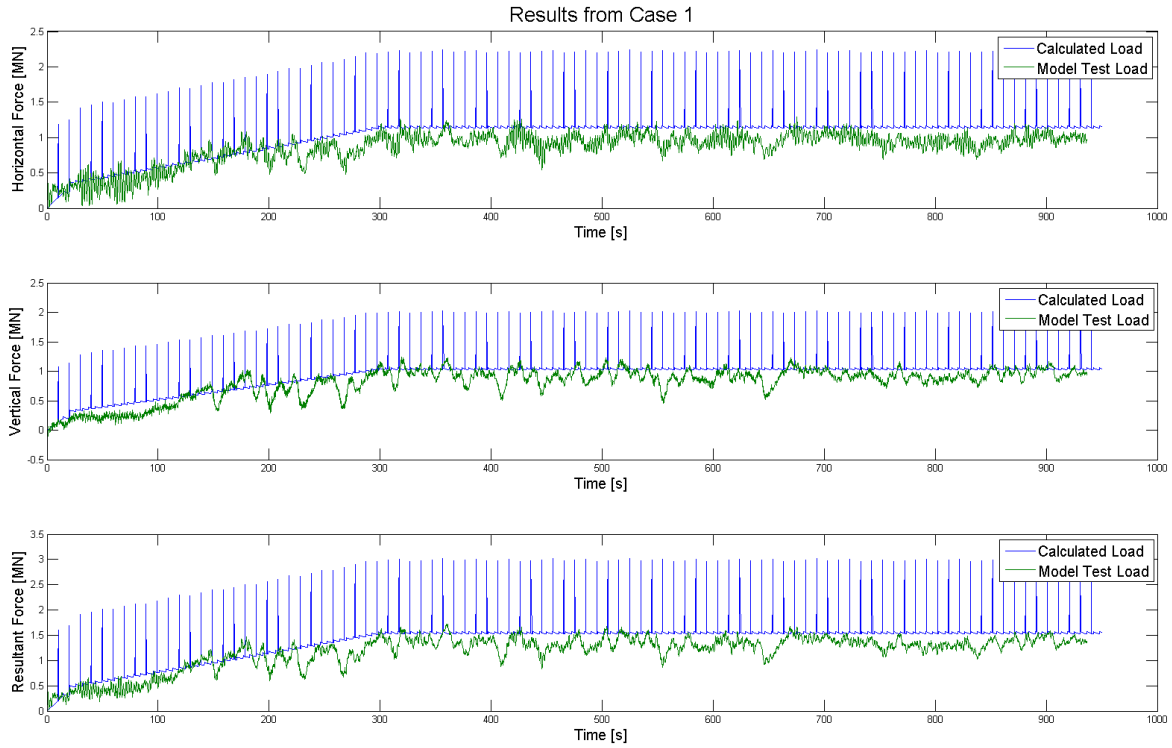

Figure 60 Comparison of Numerical Calculations and Model Test Results, Part 3, Case 1

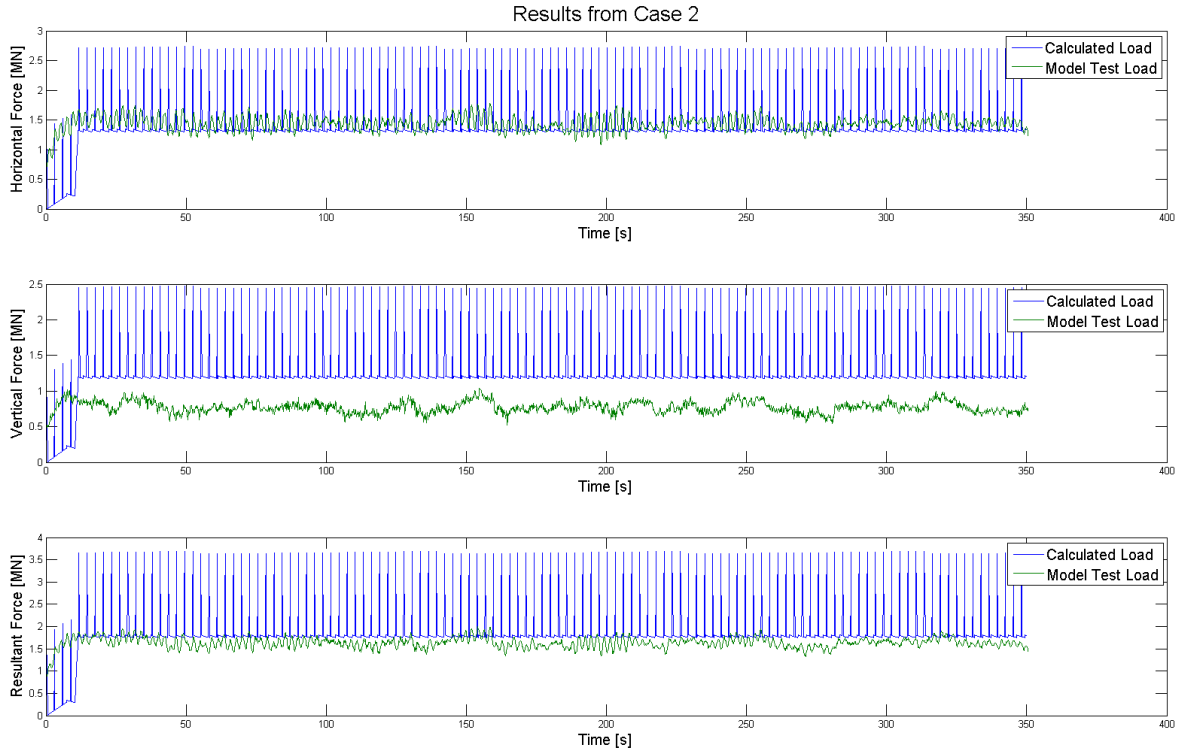

Figure 61 Comparison of Numerical Calculations and Model Test Results, Part 3, Case 2

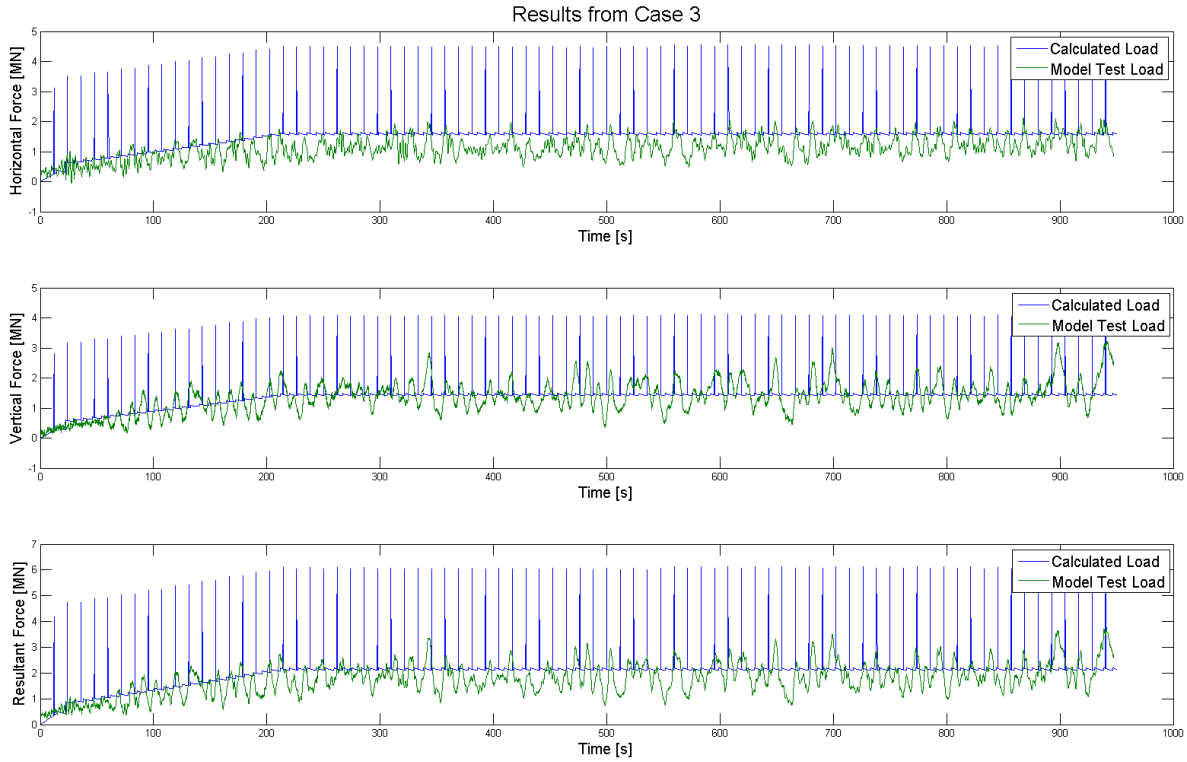

Figure 62 Comparison of Numerical Calculations and Model Test Results, Part 3, Case 3

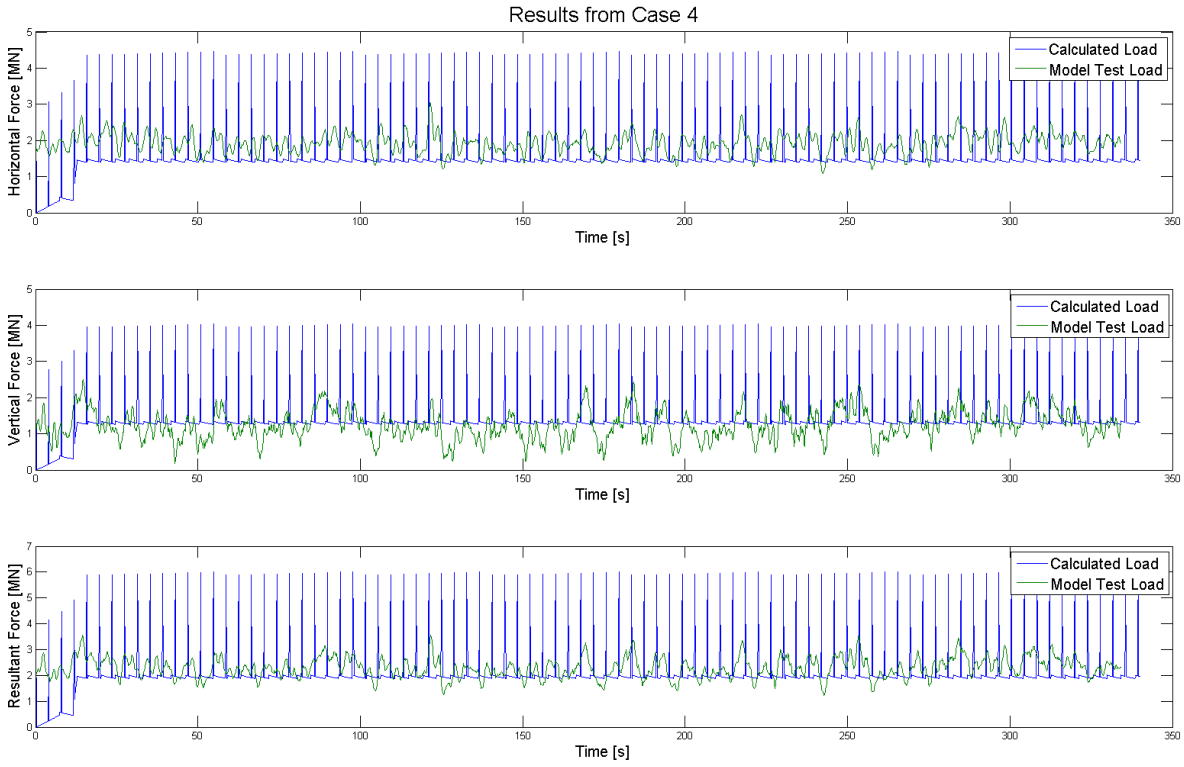

Figure 63 Comparison of Numerical Calculations and Model Test Results, Part 3, Case 4

Table 32 Load Statistics from Numerical Calculations and Model Test Results, Part 3

	Calculated Values						Model Test Values					
	F_H [MN]		F_V [MN]		F_R [MN]		F_H [MN]		F_V [MN]		F_R [MN]	
	Avg	Std	Avg	Std	Avg	Std	Avg	Std	Avg	Std	Avg	Std
Case 1	1.16	0.12	1.05	0.11	1.57	0.16	0.97	0.10	0.93	0.12	1.35	0.13
Case 2	1.39	0.28	1.26	0.25	1.88	0.38	1.44	0.11	0.77	0.08	1.64	0.11
Case 3	1.63	0.29	1.47	0.27	2.19	0.40	1.20	0.32	1.51	0.47	1.94	0.53
Case 4	1.55	0.52	1.40	0.47	2.09	0.70	1.93	0.27	1.24	0.40	2.31	0.39

Table 33 Difference Between Numerical Calculations and Model Test Results, Part 3

	Difference from model test values [%]		
	$F_{H,AVG}$	$F_{V,AVG}$	$F_{R,AVG}$
Case 1	19.59	12.90	16.30
Case 2	-3.47	63.64	14.63
Case 3	35.83	-2.65	12.89
Case 4	-19.69	12.90	-9.52

For this part, the actually achieved mechanical ice parameters, the measured rubble geometries and the identified breaking lengths have been used. The correction factors for the numerical model can be developed by dividing the model test results on the calculated values. Correction factors for the average horizontal loads are found directly from Table 32. Since the vertical load in Croasdale`s method is a function of the horizontal load component, the correction factors for the vertical loads cannot be directly found from the results in Table 32. The correction factors for the vertical loads were manually found through the following three steps.

1. Correction factors for the horizontal loads were found from Table 32.
2. These factors were implemented in the numerical model, and the calculations were run one more time. The new results included horizontal average loads equal to those from the model tests, and new vertical load components had been calculated.
3. The correction factors for the vertical loads were found from the new results.

The correction factors for the horizontal and the vertical load components for all the four interaction cases are given in Table 34.

Table 34 Correction Factors for Horizontal and Vertical Load Components

	Correction Factors	
	$F_{H,AVG}$	$F_{V,AVG}$
Case 1	0.84	1.06
Case 2	1.04	0.59
Case 3	0.74	1.40
Case 4	1.25	0.71

These factors will be implemented in the script in Part 4. The factors will be further discussed in section 6.5.

6.4 Part 4

In this part, the correction factors given in Table 34 are implemented in the numerical model. The ice actions are calculated with the target ice properties, and with breaking lengths and rubble volume configurations identified from the model test videos. The results from this part are compared to the results obtained in Part 1 to see the differences in the calculated ice actions before and after the script has been corrected. Figure 64 through Figure 67 shows plots of the horizontal, the vertical and the resultant load for each of the four interaction cases. The calculated results from Part 1 and Part 4 are plotted together to visually present the deviation between the results. Table 35 shows the main load statistics from the two parts, and Table 36 shows the percentage difference in the results obtained from the two parts.

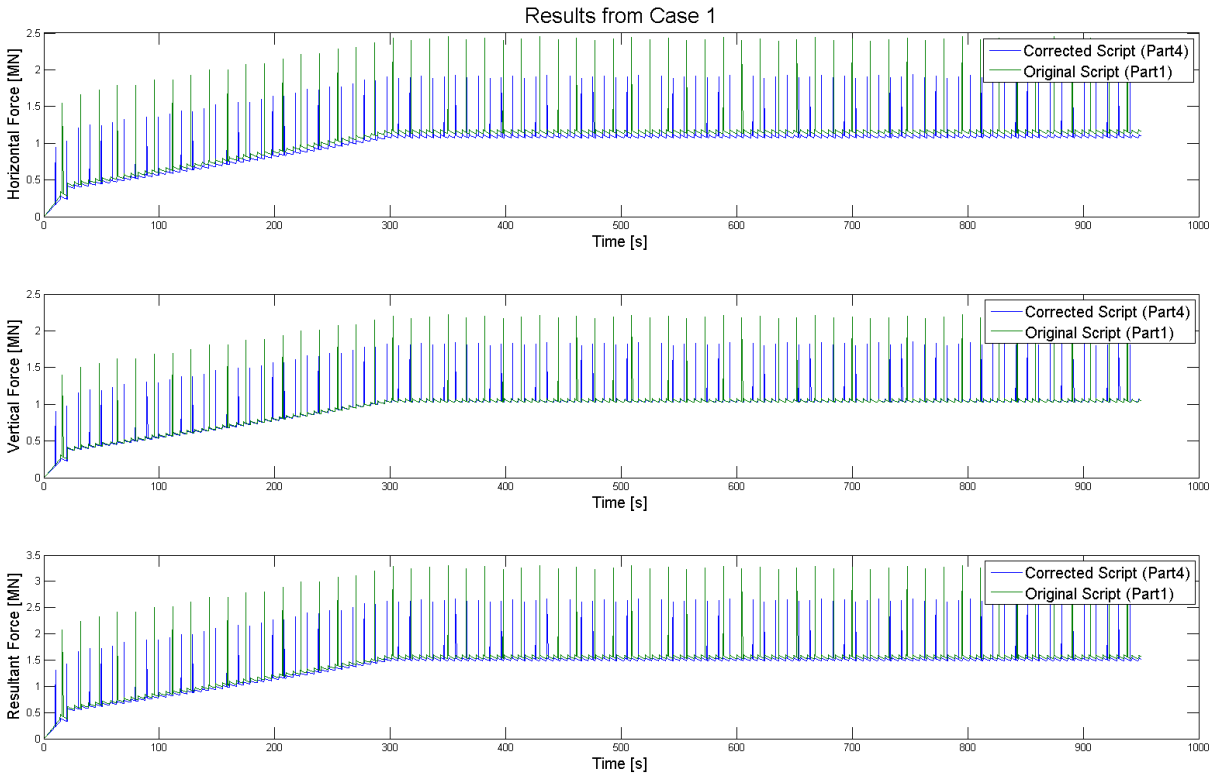

Figure 64 Comparison of Numerical Calculations before and after Correction, Case 1

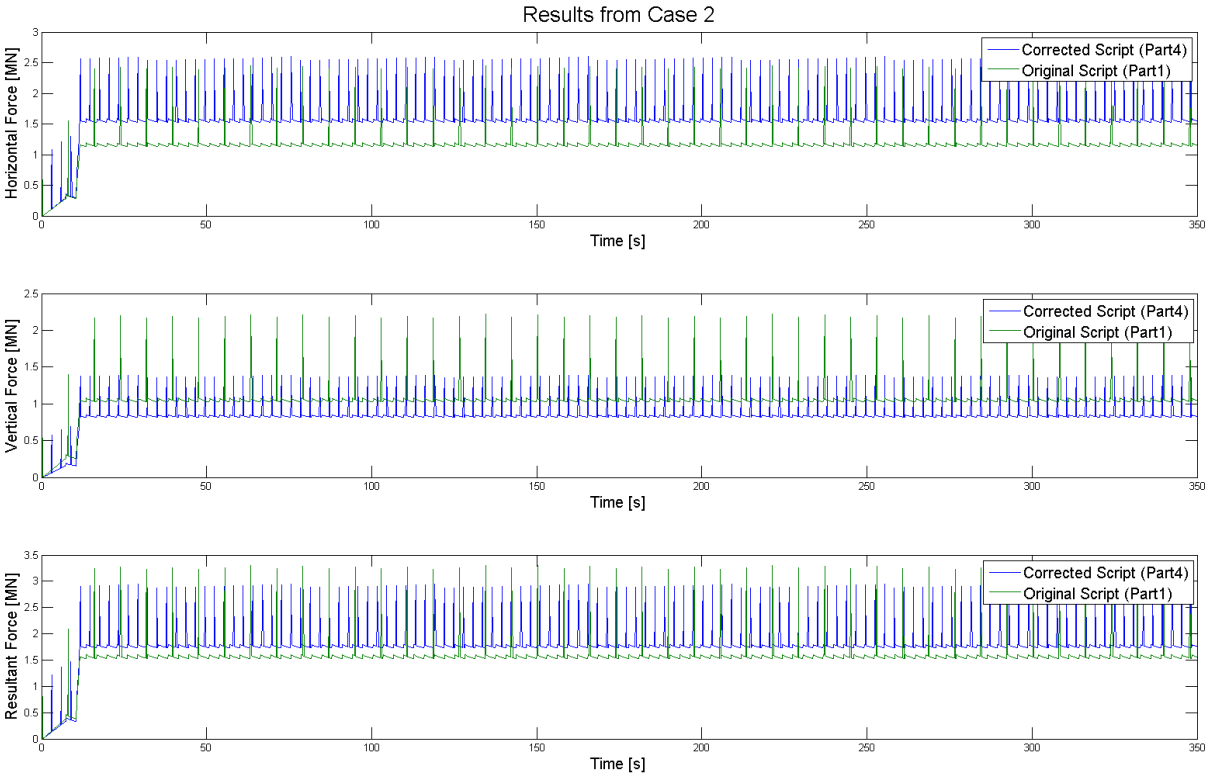

Figure 65 Comparison of Numerical Calculations before and after Correction, Case 2

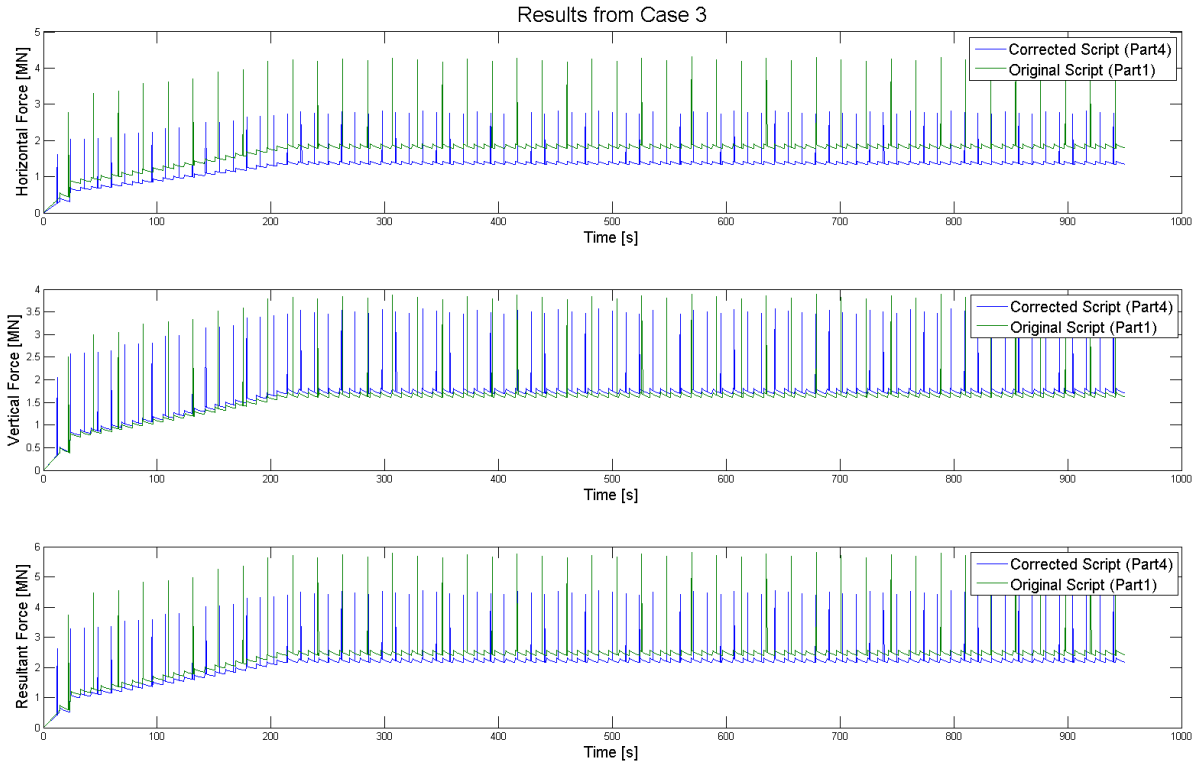

Figure 66 Comparison of Numerical Calculations before and after Correction, Case 3

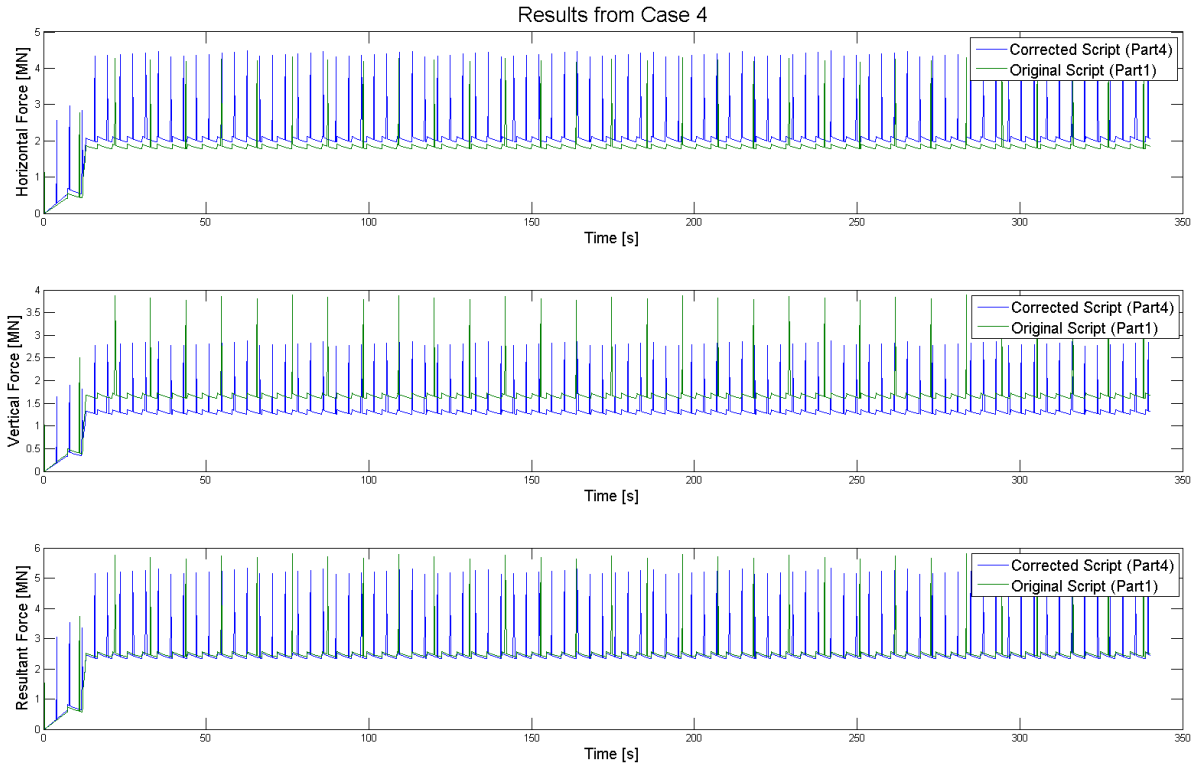

Figure 67 Comparison of Numerical Calculations before and after Correction, Case 4

Table 35 Load Statistics from Original Script (Part 1) and Corrected Script (Part 4)

	Original Script (Part 1)						Corrected Script (Part 4)					
	F_H [MN]		F_V [MN]		F_R [MN]		F_H [MN]		F_V [MN]		F_R [MN]	
	Avg	Std	Avg	Std	Avg	Std	Avg	Std	Avg	Std	Avg	Std
Case 1	1.17	0.11	1.06	0.10	1.58	0.15	1.11	0.09	1.06	0.09	1.53	0.13
Case 2	1.18	0.16	1.07	0.14	1.59	0.21	1.60	0.20	0.86	0.11	1.82	0.23
Case 3	1.85	0.18	1.67	0.17	2.50	0.25	1.39	0.14	1.76	0.18	2.25	0.23
Case 4	1.87	0.26	1.69	0.23	2.52	0.35	2.13	0.41	1.36	0.26	2.53	0.49

Table 36 Difference between Original Script (Part 1) and Corrected Script (Part 4)

	Difference between Original and Corrected Script [%]		
	$F_{H,AVG}$	$F_{V,AVG}$	$F_{R,AVG}$
Case 1	-5.41	0.00	-3.27
Case 2	26.25	-24.42	12.64
Case 3	-33.09	5.11	-11.11
Case 4	12.21	-24.26	0.40

From Table 36 it is seen that there are some deviations between the results obtained from the original script and the results obtained from the corrected script. This will be further discussed in section 6.5.

6.5 Discussion of the Correction Parts

The percentage difference between the calculated loads from the numerical model and the measured loads from the model tests are given for Part 1, Part 2 and Part 3 in Table 37.

Table 37 Percentage Difference between the Calculated Loads and the Measured Loads for the first Three Parts

	Correction Part 1		
	$F_{H,AVG}$	$F_{V,AVG}$	$F_{R,AVG}$
Case 1	20.62	13.98	17.04
Case 2	-18.06	38.96	-3.05
Case 3	54.17	10.60	28.87
Case 4	-3.11	36.29	9.09
	Correction Part 2		
	$F_{H,AVG}$	$F_{V,AVG}$	$F_{R,AVG}$
Case 1	6.19	0.00	2.96
Case 2	-24.31	28.57	-9.76
Case 3	33.33	-4.64	10.82
Case 4	-10.36	25.81	0.87
	Correction Part 3		
	$F_{H,AVG}$	$F_{V,AVG}$	$F_{R,AVG}$
Case 1	19.59	12.90	16.30
Case 2	-3.47	63.64	14.63
Case 3	35.83	-2.65	12.89
Case 4	-19.69	12.90	-9.52

As mentioned in section 6.1, the vertical load component is approximately 10% less than the horizontal load component in the results from the numerical calculation model for all the interaction cases. As this is not the case for the measured loads from the model tests, there will be some

deviations between the calculation model and the model test results even though either the horizontal or the vertical load component is calculated accurately. From Table 37 it is therefore seen that there are no cases where both the horizontal and the vertical load component is calculated accurately. The angle of attack of the resultant load gives a good picture on the difference between the horizontal and vertical load component. In Table 38 the angle of attack is given for the four interaction cases from both the numerical calculations and the measured loads from the model tests.

Table 38 Angle of Attack of the Resultant Load from the Numerical Model and the Model Tests

	θ_{att} Numerical Model [deg]	θ_{att} Model Tests [deg]
Case 1	42.14	43.65
Case 2	42.14	28.21
Case 3	42.14	50.96
Case 4	42.14	31.92

The angle of attack from the calculation model will be unchanged for all cases in all the four parts as the vertical load is a function of the horizontal load component, the sloping angle of the structure and the ice-structure friction coefficient (see equation (3.5)). When comparing the angle of attack from the model test results for the four different cases it is seen that the largest deviations from the numerical model are found in Case 2 and Case 4. In these two cases the drift speed of the ice sheet is 1.0m/s compared to 0.5m/s for Case 1 and Case 3, which results in more crushing of the ice sheet and a higher horizontal load component. The vertical load component in Case 2 and Case 4 is reduced in the model test results compared to Case 1 and Case 3 respectively. The numerical model does not take the speed of the ice sheet into consideration when calculating the vertical load component, which results in deviations. For Case 1 it is seen that the angle of attack is almost the same in the model tests as in the numerical model. From Table 37 it is seen that both the vertical and horizontal load component deviate approximately equally much from the model test results in all the comparison parts for this case.

By visually examining the plots from the first three correction parts, it is seen that the numerical calculation model experiences load peaks that far exceed the measured ice actions in the model tests. These peaks are caused by the breaking load component H_B. As was discussed in section 4.2.3, the breaking load does not affect the average loads significantly due to its short duration. In Appendix C, plots have been given with the same parameters as for Part 1, where the breaking load component has been reduced with 50%. The load statistics are also given, and it is seen that the average loads are slightly reduced for all cases. Visually it looks as though the numerical model is far more accurate, but the deviations for the average loads are insignificantly changed. This might however be a way to determine the maximum loads better with the numerical model, but in this thesis it has been attempted to accurately estimate only the average loads since maximum and minimum loads in a real life interaction scenario can be caused by numerous factors that have not been investigated during this work.

The time between the peaks in the plots from the numerical model is defined by the breaking period given in equation (4.1), and is based on the breaking length of the ice as well as the ice drift speed. In the plots from the model tests it is difficult to find individual peaks due to a lot of noise in the signal, and it is difficult to determine if these peaks are caused by a breaking load. An extensive spectral analysis should be performed in order to determine at what frequency the model test results obtain

the most energy (i.e. the period that the model test loads seem to follow) and see if this coincide with results from the numerical model. This can be performed by establishing the power spectral density (PSD) function for both the numerical results and the model test results and see if the two spectra follow the same trends. This has not been investigated thoroughly throughout this thesis, but in Appendix D the PSD functions from the model tests are plotted together with the PSD functions from the numerical model results for all the interaction cases in both Part 1 and Part 2. In Part 1 the assumed breaking lengths was used in the numerical calculations, and in Part 2 the measured ones were implemented. This comparison was only performed for the horizontal load component, as the vertical and resultant load component seem to follow the same trends as the horizontal component in both the numerical results and the model test results. From the plots in Appendix D it seems that the first peak in the two PSD functions coincides quite well between the numerical model and the model test results both in frequency and in magnitude. The frequency area beyond the first peak is of little interest due to the low energy level compared to the first peak. It might be concluded that the calculated loads follow approximately the same peak period as the measured loads, which might conclude that the individual peaks in the measured time series also occur due to a breaking load. It is difficult to determine if the assumed or the measured breaking lengths give the best results from these plots, but by visually examining the time series plots in section 6.1 and section 6.2, it might seem that the peaks in the numerical calculation model coincides best with the peaks from the model tests in Part 2. It should be noted that this activity is done only to show that the measured loads seem to follow approximately the same peak period as the calculated loads. This is something that should be investigated further before any real conclusions can be made, which is beyond this thesis` scope of work.

When comparing the deviations from Part 2 and Part 3 with the deviations in Part 1 (Table 37), it seems as though the deviations are reduced when the actually measured ice properties and the visually determined breaking lengths and rubble geometries are implemented in the numerical model. The correction factors obtained from Part 3 are given in Table 39 together with the ice drift speed, *v*, and the ice thickness, *h*, for each interaction case.

Table 39 Correction Factors from Part 3, Ice Drift Speed and Ice Thickness for all Interaction Cases

	Ice Properties		Correction Factors	
	v [m/s]	*h* [m]	$F_{H,AVG}$	$F_{V,AVG}$
Case 1	0.5	1.0	0.84	1.06
Case 2	1.0	1.0	1.04	0.59
Case 3	0.5	1.5	0.74	1.40
Case 4	1.0	1.5	1.25	0.71

From the correction factors it is found that the script overestimates the horizontal load component and underestimates the vertical load component in Case 1 and Case 3. For these two cases, the ice drift speed is 0.5m/s. For Case 2 and Case 4, the numerical model underestimates the horizontal load components and overestimates the vertical load component. For these cases the ice drift speed is equal to 1.0m/s. It is also seen that the correction factors vary when the ice thickness is increased (Case 1 to Case 3 and Case 2 to Case 4). From this, it can be concluded that the correction factors depends on both the ice drift speed and the ice thickness.

The average load results obtained from Part 1 and Part 4 are given in Table 40 together with the deviations between the loads in the two parts.

Table 40 Average Load Results from Part 1 and Part 4

	Original Script (Part1) [MN]			Corrected Script(Part4)[MN]			Difference [%]		
	$F_{H,AVG}$	$F_{V,AVG}$	$F_{R,AVG}$	$F_{H,AVG}$	$F_{V,AVG}$	$F_{R,AVG}$	$F_{H,AVG}$	$F_{V,AVG}$	$F_{R,AVG}$
Case 1	1.17	1.06	1.58	1.11	1.06	1.53	-5.41	0.00	-3.27
Case 2	1.18	1.07	1.59	1.60	0.86	1.82	26.25	-24.42	12.64
Case 3	1.85	1.67	2.50	1.39	1.76	2.25	-33.09	5.11	-11.11
Case 4	1.87	1.69	2.52	2.13	1.36	2.53	12.21	-24.26	0.40

From Table 40 it is seen that the horizontal load components calculated in the original script deviates between -33% and 26% from the corrected script. The vertical load components deviates between -24% and 5%, and the resultant load component between -11% and 13%. This means that the original script is able to predict all load components for four different interaction cases within a deviation of approximately ±30%, assuming that the corrected script calculates the loads accurately.

It should be noted that the correction factors obtained throughout section 6 is found based on observed breaking lengths and rubble geometries from the model test videos. As was explained in section 5.2.1, these parameters were difficult to determine as they were measured by hand from rather poor model test videos, and contains some great uncertainties. These parameters were used in both finding the correction factors, and in the correction of the script, which means that the loads estimated in Part 4 should only be relatively accurate compared to a model test where the actually achieved ice properties equaled the target properties. It is seen that there are no specific trend in the correction factors, other than being both ice drift speed and ice thickness dependent. If correction factors were found from several model tests, it might be possible to find some general rules about the correction factors that should be used if either the ice thickness or the ice drift speed were varied.

The original script estimates ice actions for the interaction cases as would have been done without any model testing. As the deviations from the corrected script are approximately ±30%, one should determine whether or not model tests are necessary. When designing an Arctic SPAR for a given project at a given location with known ice properties, the original script might be used to obtain rough ice action estimates in an early design phase on different structures to obtain maybe two or three concepts that seem to experience the lowest ice actions. Model tests can then be performed for only these concepts to determine the best suited one for a specific project. This might prove valuable during a project as model tests are both expensive and time consuming. If no numerical calculations are performed, numerous model tests might be needed to determine the best concept for a given project.

Model tests will probably always be needed to get accurate ice action results for different ice-structure interaction scenarios, but if it is possible to reduce the number of model tests needed by performing numerical calculations, both time and money can be saved.

7 Conclusions

From previous experience with moored floating facilities in Arctic regions, it is important to obtain a good picture on what kind of ice features that are probable to encounter, and how frequent these features are estimated to appear. The hull of the facility and its mooring lines need to be designed to withstand actions from the most probable encountered features. The mooring lines should be protected from direct contact with ice, and the facility should be able to reposition itself due to change in ice drift direction (ship shaped facilities). A conical shaped facility might prove to be a good solution as it obtains an omnidirectional capability to resist ice actions. A ship shaped facility will obtain increased loads for an ice drift direction 90 degrees from the longitudinal direction of the facility. A reliable ice management system should be established to prevent extreme ice features from interacting with the facility. This might include vessels capable of breaking ice in front of the facility as well as towing icebergs away from the structure. In the event of an unmanageable ice feature encroachment, the facility should be able to disconnect from its riser and mooring systems and move off location.

A vertical structure will in general experience much higher ice loads than sloping structures, as the main failure mode of ice against a vertical structure is crushing. Since the flexural strength of ice is less than the compressive strength a sloping structure will reduce the ice actions as the ice will be failed in bending. Sloping structures are preferable over vertical structures if ice is present. An upward breaking structure will experience higher ice actions than a downward breaking one. For a floating facility a downward breaking structure might be the better choice as ice actions are desired as low as possible to not exceed the mooring lines capacity. Due to the direction of the resultant load on an upward breaking structure it might be submerged for high ice actions. For a gravity based structure an upward breaking structure might be preferred as the resultant load from the ice actions point downwards into the ground. This will increase the structure`s stability. A downward breaking structure obtains a resultant load pointing upwards, which might decrease the stability by creating an overturning moment.

From the model tests it was found that during an ice-structure interaction scenario, the ice actions will build up from the time where the model hits the ice to a more or less constant load level. The load build up was found to be caused by rubble accumulation in front of the structure. The rubble volume was after some time kept more or less constant due to rubble transportation around the structure, resulting in a more or less constant load level. The time it took to obtain this relatively constant rubble volume seemed to be affected by both the ice thickness and the ice drift speed.

From the numerical time-domain calculation model it has been found that increased ice thickness will result in higher ice actions. The numerical model does not implement speed effects, and does not obtain any change in loads due to increased ice drift speed. From the model tests analyzed it was found that an increase in drift speed increased both the horizontal and resultant load component, but the vertical load component was reduced due to more crushing of ice. An increase in ice thickness was found to increase all the load components, i.e. it affected the total loads more than an increase in drift speed. From the model test results it seemed that when the ice thickness was increased from 1.0m to 1.5m and the ice drift speed was kept constant at either 0.5m/s or 1.0m/s,

the resultant load would increase equally much. The resultant load would also increase equally much when the ice drift speed was increased from 0.5m/s to 1.0m/s and the ice thickness was kept constant at either 1.0m or 1.5m.

The numerical calculation model was corrected by comparing the calculated ice actions with the measured ice actions from the model tests. By implementing the actually achieved ice properties as well as the identified breaking lengths and rubble geometries in the numerical model, it should give results as accurately as possible compared to the model test results. Correction factors were developed by comparing these calculated results with the ones measured in the model tests. From the correction factors it was found that the numerical model overestimated the horizontal load component and underestimated the vertical load component when the ice drift speed was 0.5m/s. For the cases where the ice drift speed was 1.0m/s, the numerical model underestimated the horizontal load component and overestimated the vertical load component. The correction factors were found to depend on both the ice drift speed and the ice thickness.

The correction factors were implemented in the numerical model, and ice actions were calculated for the target ice properties. Ice actions from the original numerical model were compared to the results from the corrected model, and it was found that all the calculated load components from the original model deviated within a range of approximately ±30% from the corrected model for all the four interaction cases. Model tests should be run in order to obtain as accurate results as possible for target ice properties, but in an early design phase, a well-working numerical model can save both time and money by reducing the model tests needed.

8 Recommendations for Further Work

The numerical calculation model established is based on Croasdale`s method for calculating static ice actions on a sloping structure. To be able to estimate the time varying loads throughout an interaction scenario more accurately, the model should be further developed. An increase in the ice drift speed will increase the horizontal load and decrease the vertical load. The correction factors obtained in this thesis accounts for that change, but the factors will probably vary for other interaction cases. By examining several model tests, it might be possible to determine how these correction factors vary as a function of the ice drift speed and the ice thickness. By obtaining correction factors for several interaction cases, a more accurate numerical model would be achieved. Also the breaking load component should be reduced as this gives maximums that far exceed the maximum loads measured from the model tests. This does not affect the average load estimates that much, as the duration of the breaking load is assumed short.

The rubble volume is in Croasdale`s method calculated as a volume in front of a wedge shaped structure, rather than in front of a cone. A volume of rubble in front of a cone shaped structure will be larger than one in front of a wedge and should be included in the calculation model. A more thorough spectral analysis should be performed on the model test results to better achieve the main trends of the signals. This might also verify the breaking length assumptions made in this thesis.

By performing multiple model tests where only one parameter is varied (e.g. the ice thickness or the ice drift speed), a better view on how much the loads increase could be established. The model tests should also be performed with better filming of the interaction process. The underwater filming in the tests described in this thesis was filmed by hand outside the testing tank. The videos would be much more useful if the cameras had been mounted on a rail inside the testing tank, following the model throughout the test. Also some sort of signal when the model hits the ice and when its speed start to decrease at the end of the test should be implemented in both the model test videos and the result data to easier determine the interesting range of the results.

References

Blanchet, D., 1998, *Ice Loads from First-Year Ice Ridges and Rubble Fields*, Can. J. Civ. Eng., Vol. 25, pp. 206-219

Bruun, P. K., Husvik, J., Le-Guennec, S., Hellmann, J.H., 2009, *Ice Model Test of an Arctic SPAR*, Proc. 20th POAC, Luleå, Sweden, 9-12 June

Croasdale, K. R., 1980, *Ice Forces on Fixed, Rigid Structures,* In CRREL Special Report 80-26, Working Group on ice forces on structures: A State-of-the-Art Report, Int. Association for Hydraulic Research, Section on ice problems, US Army CRREL, Hanover, USA, pp. 34-103

Croasdale, K. R., Cammaert, A. B., Metge, M., 1994, *A Method for the Calculation of Sheet Ice Loads on Sloping Structures,* Proc. IAHR 12th Int. Symp. on Ice, Norwegian Institute of Technology, Trondheim, Norway, 23-26 August, Vol. 2, pp. 874-875

Hetenyi, M., 1946, *Beams on Elastic Foundations*, The University of Michigan Press, Chapter 7

ISO 19906:2010, *Petroleum and Natural Gas Industries – Arctic Offshore Structures*, BSI Standard Publications

Jefferies, M., Kärnä, T. and Løset, S., 2008, *Field Data on the Magnification of Ice Loads on Vertical Structures*, Proc. 1st IAHR Int. Symp. on Ice, Vancouver, 6-11 July, Vol. 2, pp. 1115-1133

Kärnä, T., Qu, Y. and Yue, Q.J., 2006, *Extended Baltic Model of Global Ice Forces*, Proc. 18th IAHR Int. Symp. on Ice, Sapporo, 28-31 August

Le Marechal, G., Anslot, P., Mravak, Z., Liferov, P., Le Guennec, S., 2011, *Design of a Floating Platform Hull for Arctic Conditions in the Barents Sea*, paper ATC 22161, Houston, Texas, USA, 7-9 February

Lever, G. V., Dunsmore, B., Kean, J. R., 2001, *Terra Nova Development: Challenges and Lessons Learned*, paper OTC 13025, Houston, Texas, USA, 30 April-3 May

Liferov, P., Metge, M., 2009, *Challenges with ice-related design and operating philosophy of the Shtokman Floating Production Unit*, Proc. 20th POAC, Luleå, Sweden

Løset, S., Shkhinek, K. N., Gudmestad, O. T., Høyland, K. V., 2006, *Actions from Ice on Arctic Offshore and Coastal Structures: Student`s Book for Institutes of Higher Education*, -St. Petersburg: Publisher "LAN"

Määttänen, M., Hoikkanen, A.N., Avis, J., 1996, *Ice Failure and Ice Loads on a Conical Structure: Kemi-I Cone Full Scale Ice Force Measurement Data Analysis*, Proc. 13th IAHR Int. Symp. on Ice, Beijing, Vol. 1, pp. 8-16

MARC Report, 2001, *Standard Model Tests With Offshore Structures, Ice Conditions and Analysis At Masa-Yards Arctic Research Centre*, MARC REPORT D-115

Mattsson, T., 2007, *Model Tests In Ice With Two SPAR Concepts For AKET*, AARC REPORT A-371

Paterson, R., Edwards, R., Glen, I., 2000, *A Conceptual Study for Measuring Global Loads on the Terra Nova FPSO*, Report for PERD/CHC 20-57

Ralston, T. D., 1977, *Ice Force Design Considerations for Conical Offshore Structures*, Exxon Production Research Company Houston, Texas

Serway, R. A., *Physics for Scientists & Engineers*, Fourth Edition p. 126

Timco, G. and Johnston, M., 2004, *Ice Loads on the Caisson Structures in the Canadian Beaufort Sea*, Cold Regions Science & Tech., 38, pp. 185-209

Wright, B., 1998, *Insights from Molikpaq Ice Loading Data: Validation of Low Level Ice Forces on Coastal Structures*, LOLEIF Report No. 1, EU Project, Contract MAS3-CT 97-0098, p. 88

Wright, B., 1999, *Evaluation of Full Scale Data for Moored Vessel Stationkeeping in Pack Ice (With Reference to Grand Banks Development)*, Report for PERD/CHC 26-200

Wright, B., 2000, *Full Scale Experience with Kulluk Stationkeeping Operations in Pack Ice*, Report for PERD/CHC 25-44

www.oilpubs.com/oso, 2000, *Terra Nova FPSO Sets Sail for Newfoundland*, Online Article

Appendices

Appendix A. Schematics of the Models

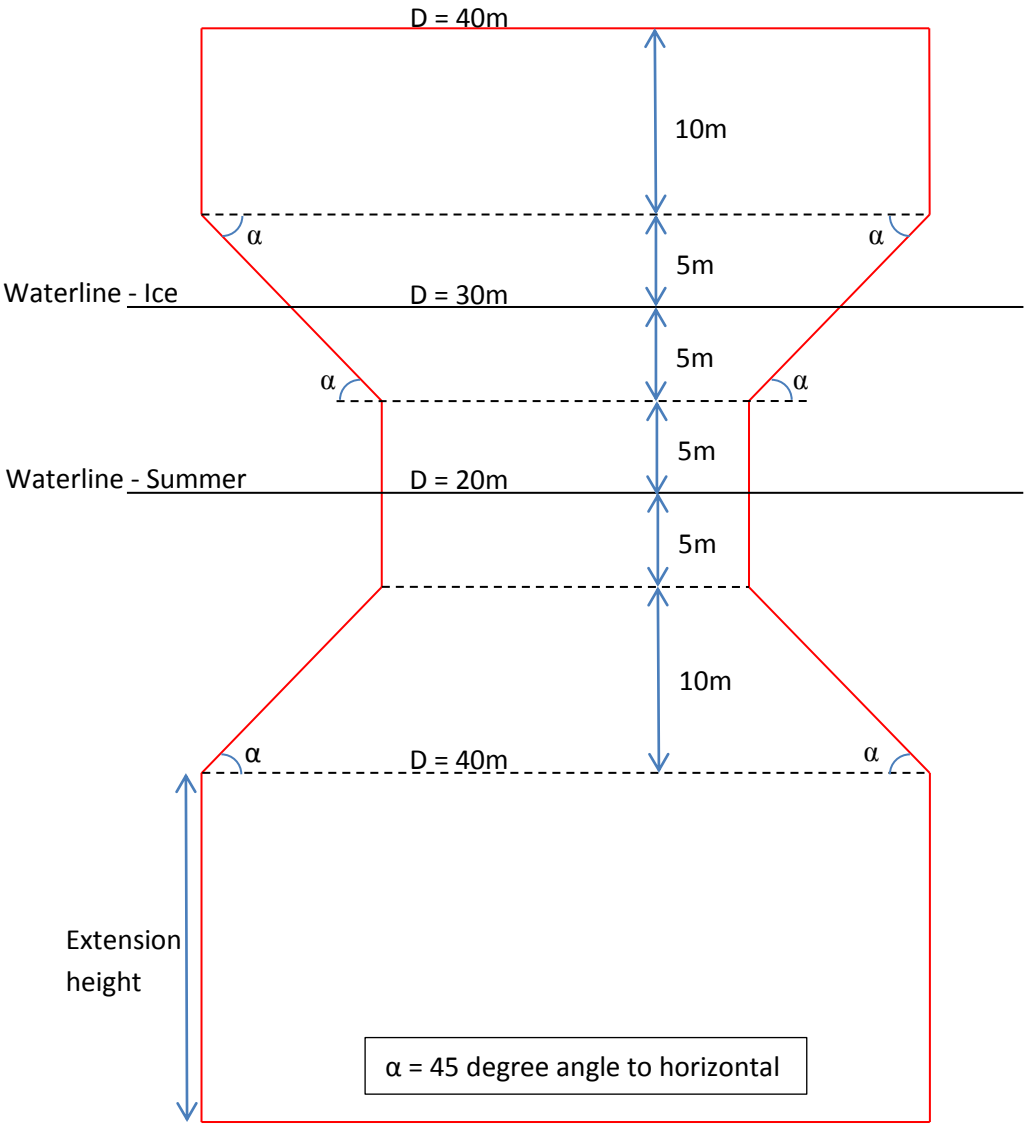

Figure A-1 Downward Breaking Structure

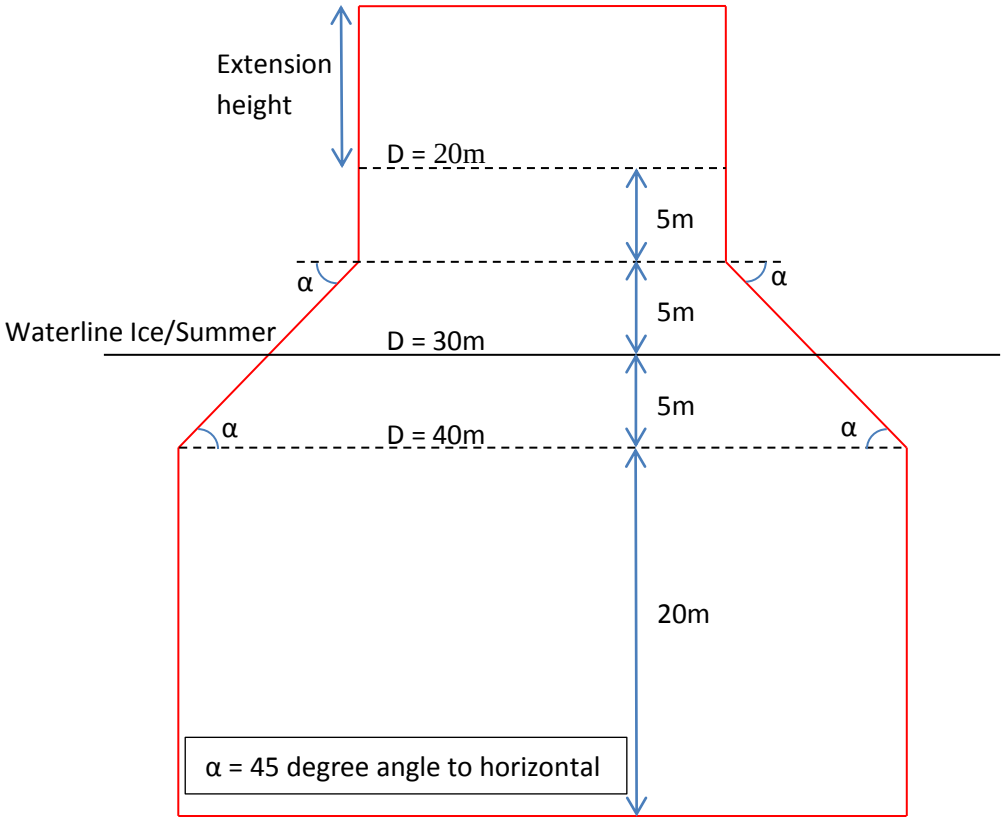

Figure A-2 Upward Breaking Structure

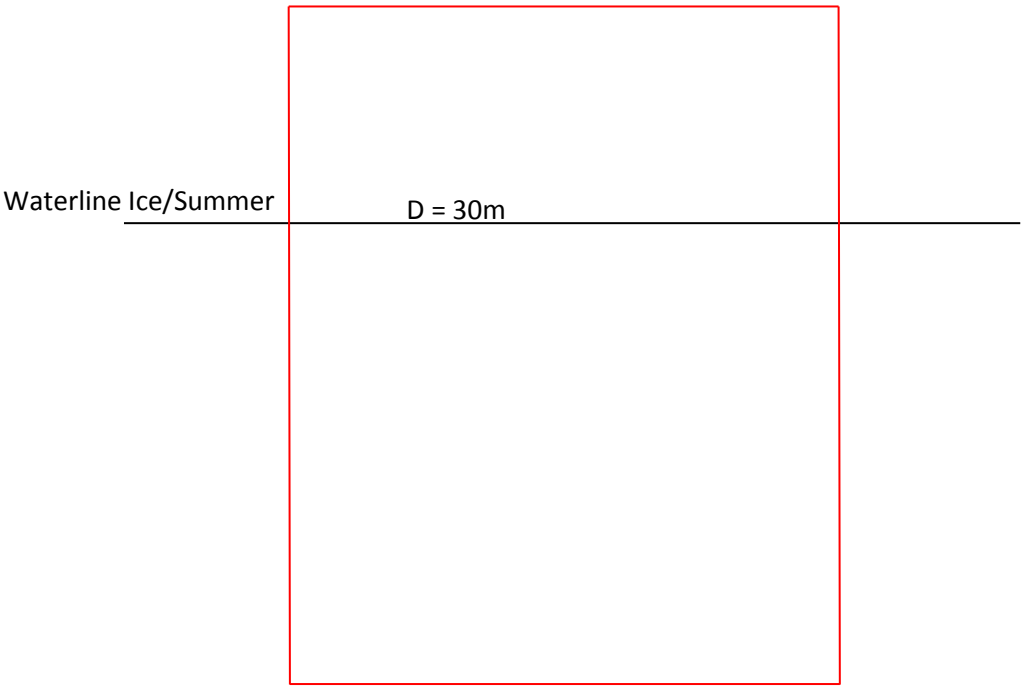

Figure A-3 Structure with Vertical Sides

Appendix B. Deflection Analysis of an Ice Beam

As sheet ice interacts with the structure it is bent downwards by a vertical force from the structure. When this force reaches a limit value, the ice sheet will fail in bending. The horizontal component of this force is the bending force H_B given in equation (3.23), and its corresponding vertical load can be found from equation (3.5). Through simple calculations using the unit load method the deflection of the ice sheet caused by this vertical force can be found. By using this deflection and the slope angle of the structure we can obtain the length in the sloping direction the sheet ice needs to be pushed before H_B is reached. If we then introduce the ice drift speed we can find the time it takes from the sheet ice hits the structure until it is bent down far enough to fail in bending. This time period is introduced in the time-domain Matlab script as a "build-up period" H_B needs to obtain its value. The reason why this period is introduced is to be able to see the bending load as a time varying force instead of an impulse load. The time it takes for the bending force to obtain its value will be further analyzed in the model test videos.

The vertical load component of H_B (V_B) is found to be as follows.

$$V_B = 0.68\sigma_f \left(\frac{\rho_w g h^5}{E}\right)^{0.25} \left(D + \frac{\pi^2 l_c}{4}\right) \tag{B.1}$$

The ice sheet is modeled as a beam fixed in one end with length equal to l_c given in equation (3.21) as shown in B-1.

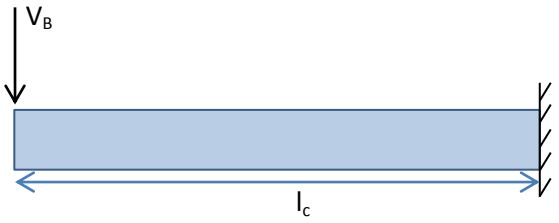

Figure B-1 Ice Sheet Modeled as a Fixed Beam

To find the deflection, δ, under V_B through the unit load method we need two moment diagrams, one for V_B and one for a unit load at the same point. The moment diagrams are shown in Figure B-2.

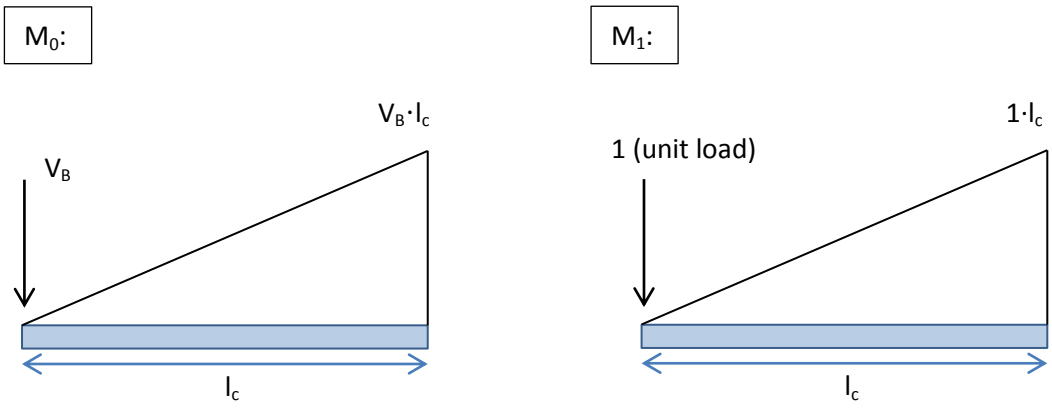

Figure B-2 Moment Diagrams in the Unit Load Method

By using these moment diagrams we can find the deflection through the following formula.

$$\delta = \int_0^L \frac{M_0 M_1}{EI} dx = k \frac{M_0 M_1}{EI} L \tag{B.2}$$

L is the length of the beam, equal to l_c and k is an integration coefficient equal to 1/3 as both the moment diagrams are triangular. If the width of the beam is equal to the diameter of the structure, D, we can find the moment of inertia, I, as $Dh^3/12$. When the deflection is determined we can find the length in the sloping direction the ice sheet has been pushed, x, and the time it takes for the ice sheet to reach this depth is given by x/v, where v is the ice drift velocity. The relationship between the deflection δ and x is shown in Figure B-3.

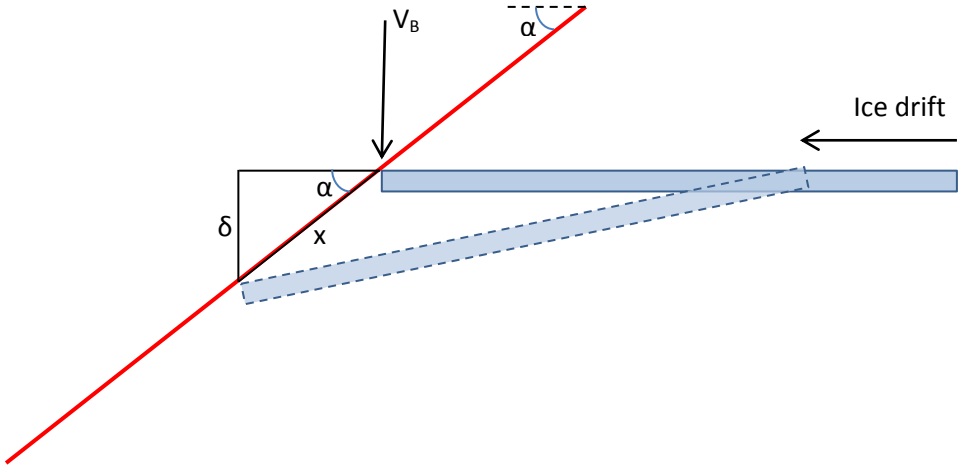

Figure B-3 Relationship between Deflection and Sloping Length *x*

From the figure it is found that x can be found by using the sloping angle α of the structure as follows.

$$x = \frac{\delta}{\sin \alpha} \tag{B.3}$$

These equations have been used with ice parameters as given in Table 1 to obtain the following results of the time it takes for H_B to obtain its value, T_{break}, for the four different cases described in section 4.2.

Table B-1 Breaking Period for the Four interaction Cases

		Case 1	Case 2	Case 3	Case 4
h	[m]	1.00	1.00	1.50	1.50
δ	[m]	0.08	0.08	0.12	0.12
x	[m]	0.12	0.12	0.17	0.17
v	[m/s]	0.50	1.00	0.50	1.00
T_{break}	[s]	0.24	0.12	0.35	0.17

The average period is 0.22 seconds, and this is the period used in the time-domain script. As mentioned before this period is found to see the breaking load as a time varying load rather than an

impulse load, and it will be verified through model test videos whether this is a good approximation or not.

Appendix C. Comparison Part 1 with 50% reduced H_B

In this appendix the numerical calculation model results and the ice actions measured in the model tests are compared when the breaking load component H_B is reduced with 50% in the numerical model. Plots of the four different cases as well as tables showing the average load values and the deviation between the numerical model and the model test results are given. The reader is encouraged to compare the results in this section with the ones obtained in section 6.1. The values obtained differ very little from section 6.1, but the plots look visually more correct. The standard deviations will be approximately reduced with 50% as a result of reducing the peaks with 50%. The conclusion meant to be drawn from this section is that the breaking load component H_B affects the average loads very little, but by reducing it, it might seem that maximum loads can be calculated more accurately.

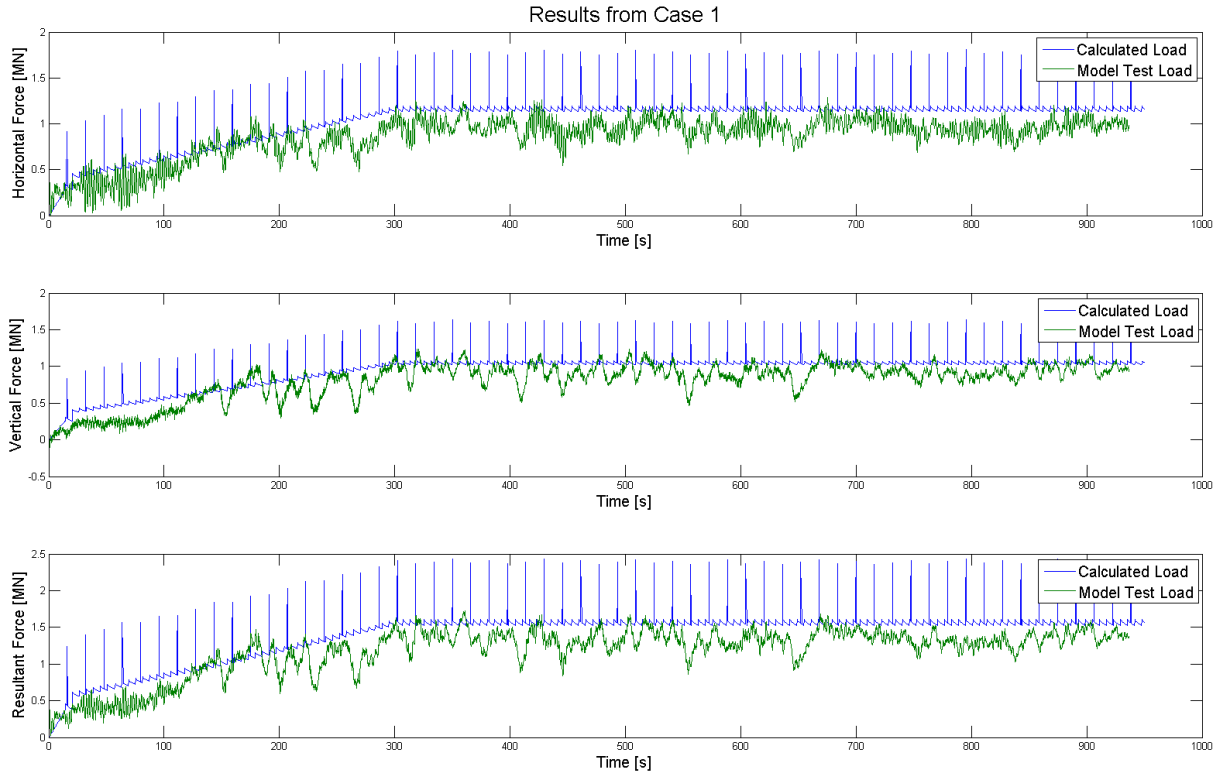

Figure C-1 Part 1, Case 1, Reduced Breaking Load

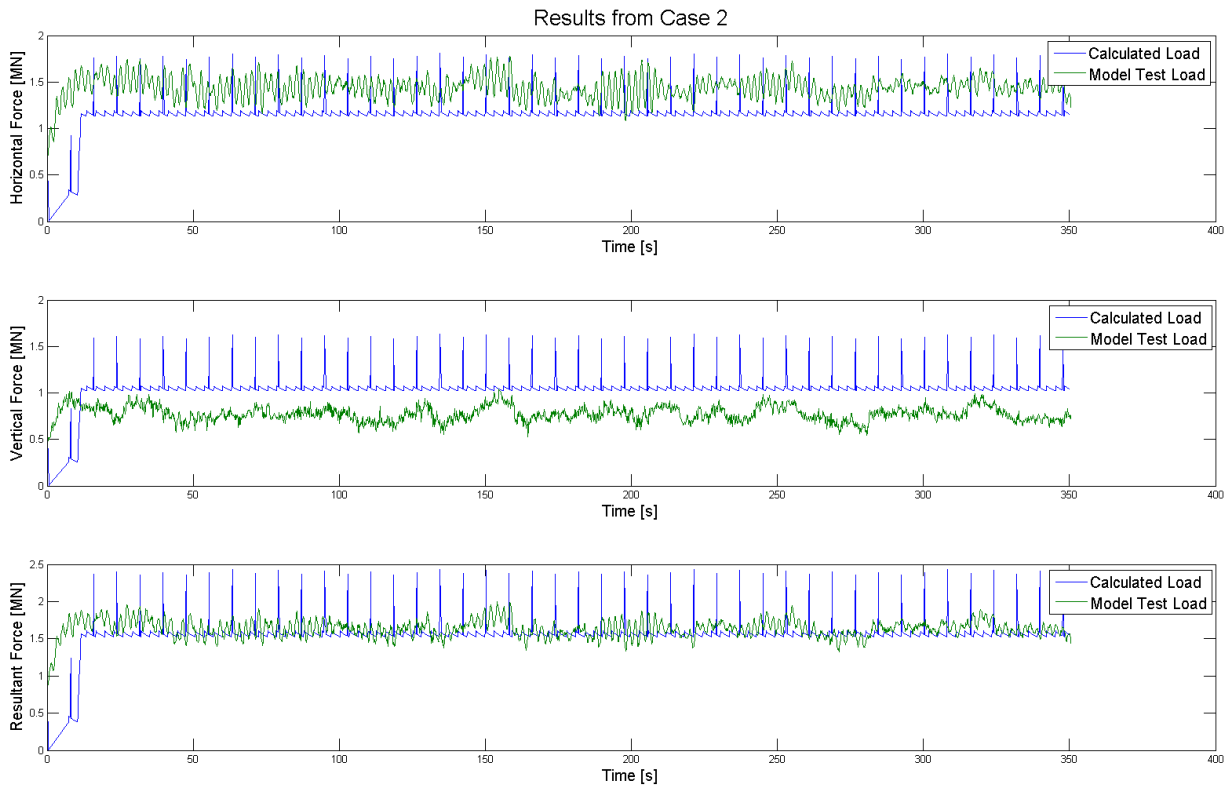

Figure C-2 Part 1, Case 2, Reduced Breaking Load

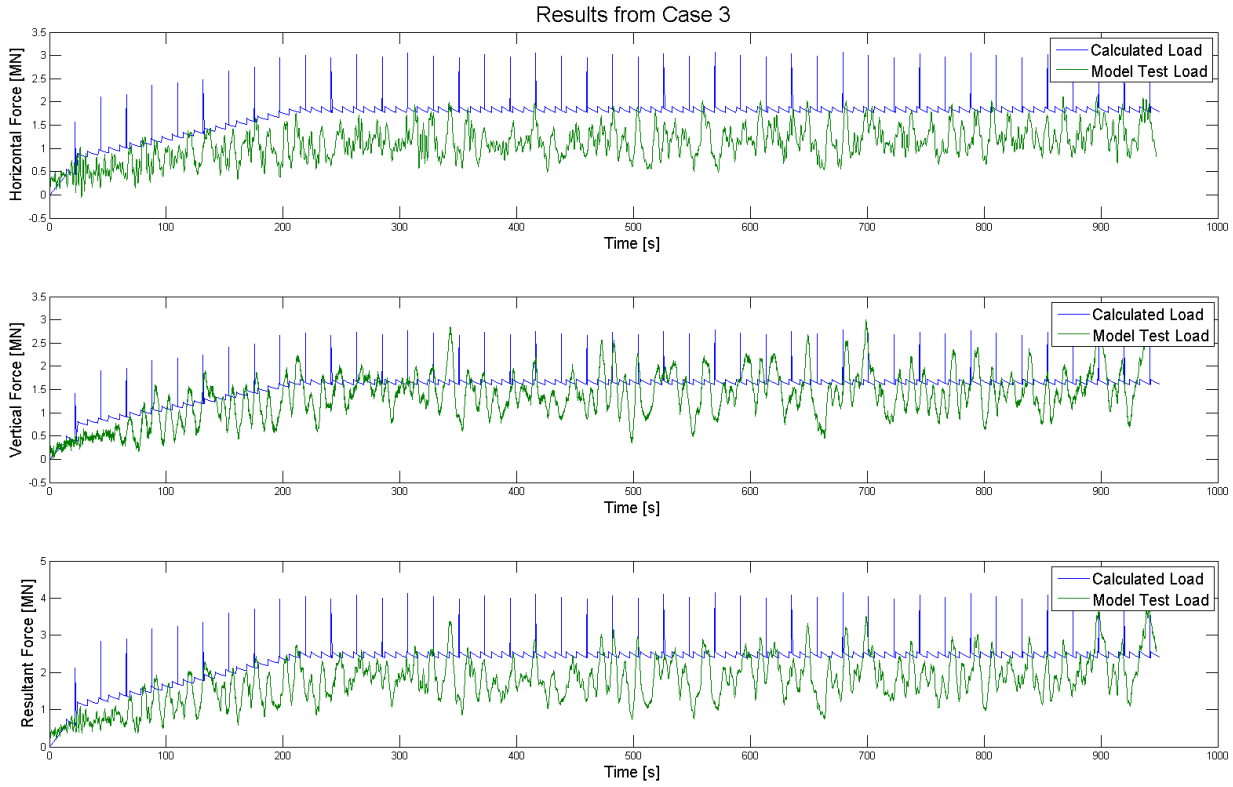

Figure C-3 Part 1, Case 3, Reduced Breaking Load

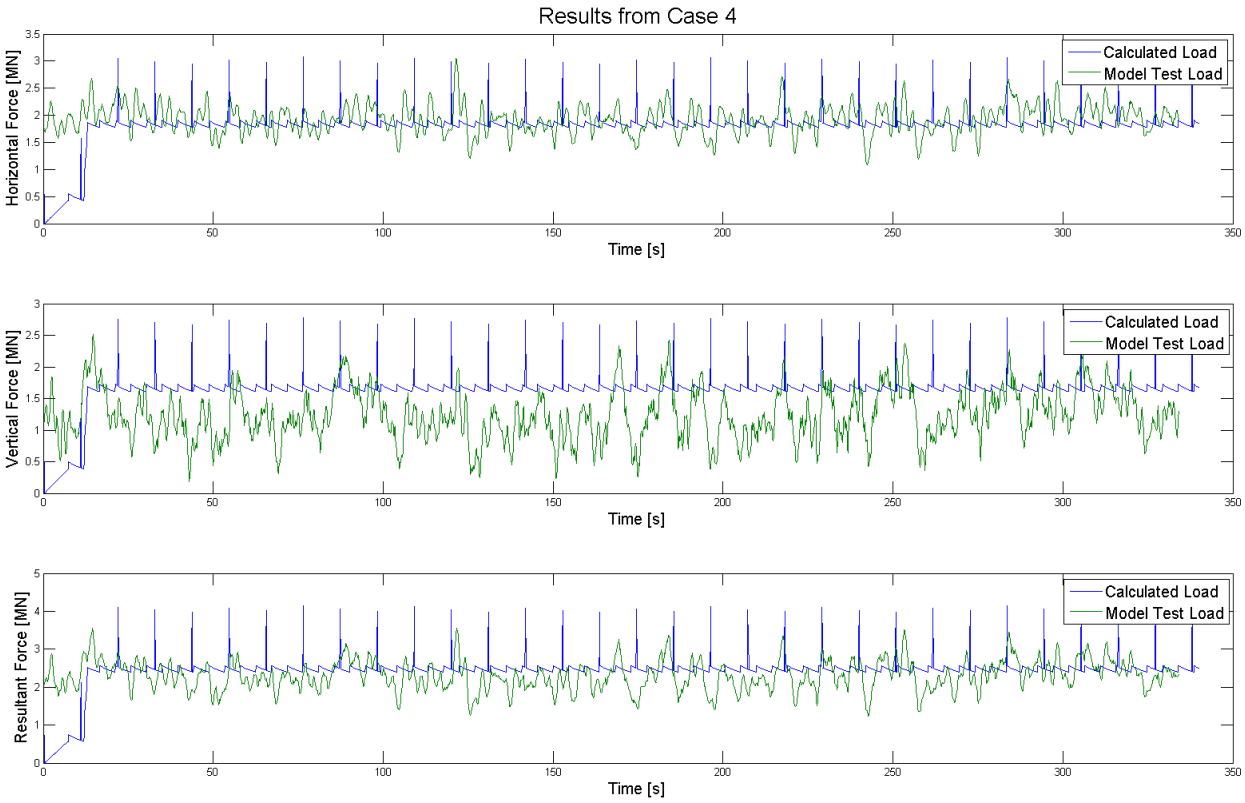

Figure C-4 Part 1, Case 4, Reduced Breaking Load

Table C-1 Load Statistics Part 1, Reduced Breaking Load

	Calculated Values						Model Test Values					
	F_H [MN]		F_V [MN]		F_R [MN]		F_H [MN]		F_V [MN]		F_R [MN]	
	Avg	Std	Avg	Std	Avg	Std	Avg	Std	Avg	Std	Avg	Std
Case 1	1.16	0.06	1.05	0.05	1.57	0.08	0.97	0.10	0.93	0.12	1.35	0.13
Case 2	1.17	0.08	1.06	0.07	1.58	0.11	1.44	0.11	0.77	0.08	1.64	0.11
Case 3	1.84	0.10	1.67	0.09	2.48	0.13	1.20	0.32	1.51	0.47	1.94	0.53
Case 4	1.85	0.13	1.67	0.12	2.50	0.17	1.93	0.27	1.24	0.40	2.31	0.39

Table C-2 Difference between Numerical Calculations and Model Test Results, Part 1, Reduced Breaking Load

	Difference from model test values [%]		
	$F_{H,AVG}$	$F_{V,AVG}$	$F_{R,AVG}$
Case 1	19.59	12.90	16.30
Case 2	-18.75	37.66	-3.66
Case 3	53.33	10.60	27.84
Case 4	-4.15	34.68	8.23

Appendix D. PSD plots for Part 1 and Part 2

This section is established to enlighten the similarity between the PSD functions for both the numerical calculations and the model test results. Due to this similarity it might seem that the measured loads follow approximately the same peak period as the numerical model, which might conclude that the individual peaks in the model test results are due to a breaking load, as is the fact for the numerical model peaks. This section is meant as a brief introduction to the importance of a spectral analysis when analyzing model test results. Figure D-1 shows the PSD for both the numerical model and the model test results for all the interaction cases from Part 1, and Figure D-2 shows the PSD functions from Part 2.

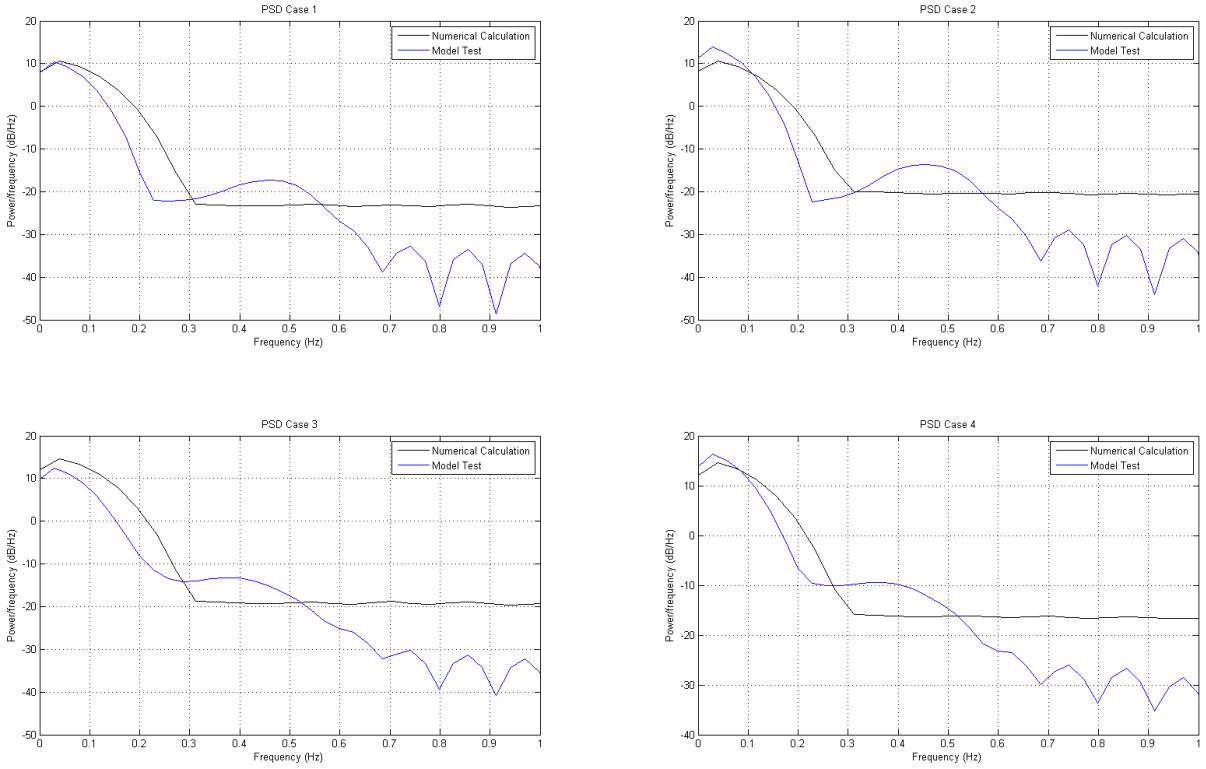

Figure D-1 PSD Plots Part 1

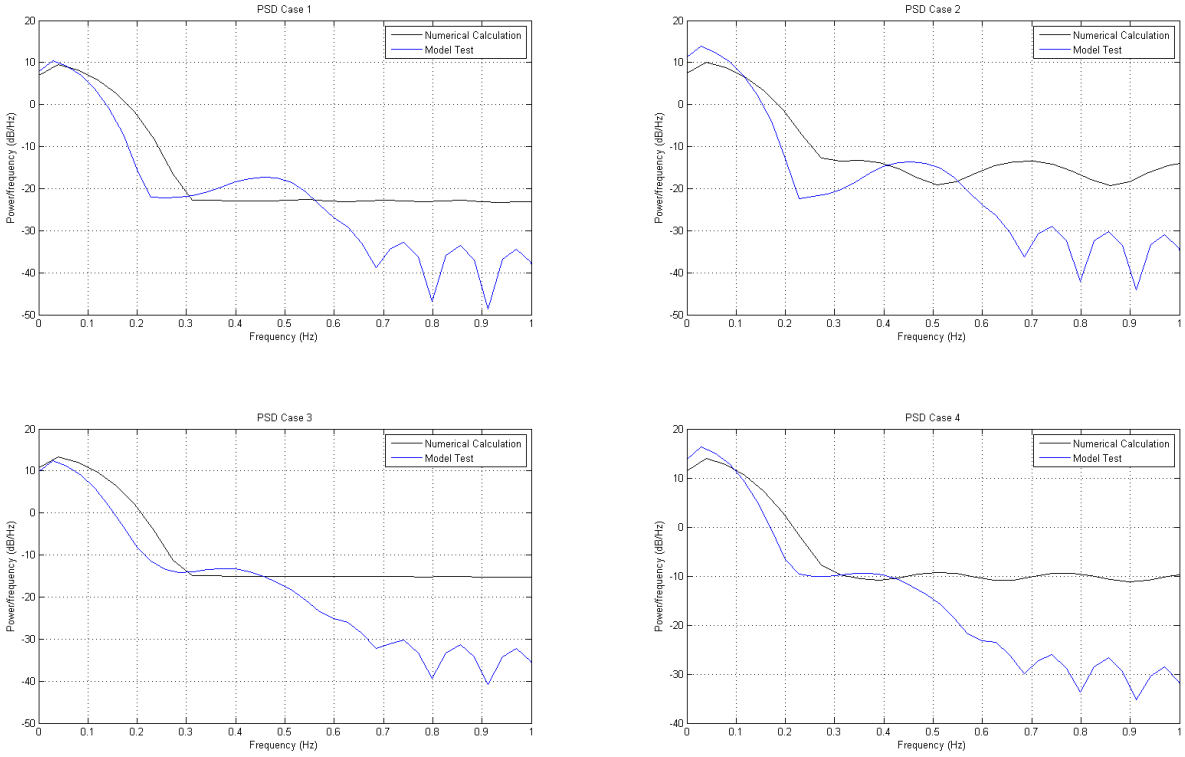

Figure D-2 PSD Plots part 2

Appendix E. Matlab Scripts

The enclosed CD contains all the Matlab scripts established for calculations throughout this thesis. The different scripts with all required files are placed in separate folders, and each folder contains a readme.txt file for information about the different programs. The following folders are included on the CD.

- *Static Analysis* — Contains the script used to calculate static ice actions on both sloping and vertical structures in section 4.1.
- *Time Domain* — Contains the script used to calculate the time varying ice actions on a downward sloping structure using Croasdale`s method in section 4.2.
- *Ice Plots* — Contains the script used to plot the level ice configurations measured in the model tests. The plots are displayed in section 5.1.2.
- *Model Test Results* — Contains the script used to plot the time series from the different model tests as well as obtaining the most important load statistics from the tests. The results obtained are given in section 5.2.
- *Correction* — Contains the script used to correct the numerical calculation model established in section 4.2. This script is based on the script in the *Time Domain* folder, but with modifications to be able to run the four correction cases described in section 6. All the results from this script are displayed throughout section 6.
  If this script is run directly from the CD, you will get a warning message when running Part 1 as the program attempts to write a result file to the CD. To avoid this warning message, copy this folder to a computer before running the program. The warning message can be ignored as the result file the program attempts to write is found on the CD, and all results presented in this thesis can be obtained directly from the CD. Please see the readme file in this folder for more information.

The CD also contains the complete Master thesis in a pdf format.